Alma Mater Studiorum – Università di Bologna

DOTTORATO DI RICERCA IN
CHIMICA

Ciclo XXVI

Settore Concorsuale di afferenza: A3/01

Settore Scientifico disciplinare: CHIM/02

Electrochemical surface modification of Single walled carbon nanotubes and Graphene-based electrodes for (bio) sensing applications

Presentata da: SANDRA ENRIQUEZ SANSALONI

Coordinatore Dottorato

Aldo RODA

Relatori

Francesco PAOLUCCI
Alain PENICAUD

Esame finale anno 2014

THÈSE

PRÉSENTÉE A

L'UNIVERSITÉ BORDEAUX 1

ÉCOLE DOCTORALE DES SCIENCES CHIMIQUES

Par

SANDRA ENRIQUEZ SANSALONI

POUR OBTENIR LE GRADE DE

DOCTEUR

SPÉCIALITÉ : Chimie-Physique

Electrochemical surface modification of Single walled carbon nanotubes and Graphene-based electrodes for (bio) sensing applications

Directeur de recherche : Alain Pénicaud
Francesco Paolucci

Soutenue le : 11 Juillet 2014
Devant la commission d'examen formée de:

M. Alain PENICAUD	Directeur de recherche, CNRS	Directeur de thèse
M. Francesco PAOLUCCI	Professeur, Université Bologna	Directeur de thèse
Mme. Patrizia MUSSINI	Professeur, Université Milano	Rapporteaur
M. Stéphane CAMPIDELLI	Chercheur, CEA-SACLAY	Rapporteaur
M. Maurizio PRATO	Professeur, Université Trieste	Examinateur
M. Neso SOJIC	Professeur, ENSCPB, Bordeaux	Examinateur

Abstract

Sensors are devices that have shown widespread use, from the detection of gas molecules to the tracking of chemical signals in biological cells. In general, a sensor is made of an active sensing element and a signal transducer producing an electrical, optical, thermal or magnetic output signal. Single walled carbon nanotube (SWCNT) and graphene based electrodes have demonstrated to be an excellent material for the development of electrochemical biosensors as they display remarkable electronic properties and the ability to act as individual nanoelectrodes, display an excellent low-dimensional charge carrier transport, and promote surface electrocatalysis.

The present work aims at the preparation and investigation of electrochemically modified SWCNT and graphene-based electrodes for applications in the field of biosensors. We initially studied SWCNT films and focused on their topography and surface composition, electrical and optical properties. We show that these films are homogeneous with thickness around ~60-70 nm, resistance values around ~200-300 Ω/□, and transparency around ~40%. Parallel to SWCNTs, graphene films were investigated. Higher resistance values were obtained in comparison with nanotubes films.

The electrochemical surface modification of both electrodes was investigated following two routes (i) the electrografting of aryl diazonium salts, and (ii) the electrophylic addition of 1, 3-benzodithiolylium tetrafluoroborate (BDYT). Both the qualitative and quantitative characteristics of the modified electrode surfaces were studied such as the degree of functionalization and their surface composition. The combination of Raman, X-ray photoelectron spectroscopy, atomic force microscopy, electrochemistry and other techniques, has demonstrated that selected precursors could be covalently anchored to the

nanotubes and graphene-based electrode surfaces through novel carbon-carbon formation.

In route (i), their post-modification by click-chemistry reactions finally leads to the immobilization at the electrode surface of desired functional groups, such as redox probes/shuttles (e.g., a ferrocenyl group) or catalytic moieties (e.g., an enzyme). HRP has been for instance immobilized on SWCNT-aryl-modified surfaces, and its voltammetric study showed catalytic response with the increasing concentration of hydrogen peroxide in solution upon monitoring the redox shuttle hydroquinone/benzoquinone at the electrode surface.

In route (ii), the electrophylic addition of electrogenerated BDYT radicals was investigated for the first time at either SWCNT- or graphene-based electrodes. The combination of different techniques has demonstrated the covalent attachment of BDYT to SWCNT-based electrodes. Such modification leads to the formation of twisted ropes observed and analyzed by AFM and scanning electron microscopy. No evidence of twisted ropes formation was instead observed for modified graphene-based electrodes.

Abstract

I sensori sono dispositivi che presentano innumerevoli applicazioni, dalla rilevazione di molecole gassose fino al tracciamento di segnali chimici in sistemi biologici. In generale, un sensore è constituito da un elemento attivo (sensibile) e da un transduttore in grado di produrre un segnale elettrico , ottico, termico, o magnetico.

Elettrodi costituiti da nanotubi di carbonio a parete singola (SWCNTs) e/o grafene hanno dimostrato di essere eccelenti materiali per lo svilupo di biosensori elettrochimici; essi mostrano ottime proprietà elettroniche ed eccellente trasporto di carica (mono-bidimensionale), possono essere utilizzati direttamente come nanoelettrodi, e possono promuovere elettrocatalisi alla superficie.

Questo lavoro di tesi è focalizzato sulla preparazione e caratterizzazione di elettrodi a base di SWCNT e grafene, opportunamente funzionalizzati elettrochimicamente, per applicazioni nel campo della sensoristica.

Inizialmente è stata studiata la topografia, composizione superficiale, proprietà elettriche e ottiche di elettrodi a base di nanotubi di carbonio. Questi film, mostrano proprietà superficiali omogenee, resistenza di circa 200-300 ohm/□, e trasparenza di circa 40%. La stessa caratterizzazione è stata effettuata su film a base di grafene che mostrano valori di resistenza più elevati rispetto ai film di nanotubi.

La funzionalizzazione elettrochimica delle superfici elettrodiche è stata condotta seguendo due strategie (i) l´elettrografting di sali di aril-diazonio, e (ii) la addizione elettrofilica di 1,3- benzoditiolilio tetrafluoroborate (BDYT). Le modifiche delle superfici elettrodiche sono state studiate dal punto di vista sia qualitativo che quantitativo, al fine di valutare come il grado di

funzionalizzazione e la loro composizione superficiale. L´utilizzo di tecniche quali la spettroscopia Raman, diffrazione di raggi X, microscopia a forza atomica (AFM), e altre tecniche elettrochimiche confermano la formazione di nuovi legami covalenti carbonio-carbonio tra i precursori e la superficie elettrodica.

Nell caso (i), l´ulteriore modifica superficiale tramite reazione di cicloaddizione (click-chemistry) permette l´immobilizzazione di specifici mediatori redox, ad esempio gruppi ferrocene, o unità catalitiche (enzimi). Ad esempio, l'enzima HRP è stato immobilizzato sulla superficie elettrodica di SWCNT; la risposta elettrochimica del mediatore idrochinone/benzochinone ha permesso l'osservazione di una risposta catalitica nei confronti di perossido di idrogeno in soluzione.

Nell secondo caso (ii), è stata studiata, per la prima volta, l´addizione elettrofilica di radicali BDYT elettrogenerati su elettrodi di nanotubi e/o grafene. Anche in questo caso, l´utilizzo di varie tecniche di caratterizzazione ha confermato la formazione di legami covalenti fra superficie elettrodiche e precursore. Analisi di microscopia di forza atomica (AFM) e la microscopia a scansione elettronica (SEM) mostrano diverse conformazioni superficiali a seconda della natura della superficie elettrodica; infatti, nel caso di BDYT ancorato alla superficie di SWCNT si osservano fibre polimeriche attorcigliate, mentre niente di simile è stato osservato nel caso di elettrodi a base di grafene.

Résumé

Les capteurs sont des dispositifs ayant montré une utilisation répandue, allant de la détection des molécules en phase gazeuse au suivi de signaux chimiques dans les cellules biologiques. En général, un capteur est réalisé à partir d'un élément actif de détection et d'un signal transducteur produisant un signal de sortie qui peut être électrique, optique, thermique ou magnétique. Les électrodes à base de nanotubes de carbone à simple paroi et les électrodes à base de graphène se sont révélées être un matériau excellent pour le développement des biocapteurs électrochimiques, puisqu'ils montrent des propriétés électroniques remarquables et la capacité de se comporter en tant que nano-électrodes individuelles, un excellent transport de porteur de charge à faible dimension, et permettent de l'électrocatalyse de surface.

Le travail présenté vise à la préparation et à l'étude d'électrodes de nanotubes de carbone à simple paroi et d'électrodes de graphène modifiées par voie électrochimique pour des applications dans le domaine des biocapteurs. Nous avons d'abord étudié les films de nanotubes de carbone à simple paroi et nous nous sommes intéressés à leur topographie, à leur composition de surface, et leurs propriétés électriques et optiques. Nous montrons que ces films sont homogènes avec une conductivité d'environ 200-300 Ω/□, et une transparence d'environ 40%. En parallèle aux nanotubes de carbone à simple paroi, des films de graphène ont été étudiés. Des valeurs de résistance plus élevées en comparaison avec les films de nanotubes ont été obtenues. La modification de surface par voie électrochimique des deux types d'électrodes a été étudiée en suivant deux voies, (i) l'électro-greffage de sels d'aryl diazonium, et (ii) l'addition électrophile de 1, 3- benzodithiolilyum tetrafluoroborate (BDYT). Les caractéristiques qualitatives et quantitatives de la surface modifiée des électrodes ont été étudiées, comme le degré de fonctionnalisation et la

composition de surface. La combinaison de spectroscopie Raman, et de photoelectrons X- (XPS) de microscopie à force atomique (AFM), d'électrochimie et d'autres techniques, a montré que des précurseurs particuliers peuvent être ancrés de façon covalente à la surface des électrodes de nanotubes et de graphène, grâce à la formation de nouvelles liaisons carbone-carbone.

Dans le premier cas (i), leur post-modification par des réactions de « click-chemistry » mène finalement à l'immobilisation sur la surface de l'électrode des groupes fonctionnels souhaités, comme des sondes/shuttles redox (e.g., un groupe ferrocenyl) ou des groupements catalytiques (e.g., une enzyme). L'enzyme HRP (horse-radish peroxidase) a été, par exemple, immobilisée sur des surfaces de nanotubes de carbones à simple paroi modifiées par un groupe aryl, et l'étude voltammétrique a montré une réponse catalytique avec l'augmentation de la concentration de peroxyde d'hydrogène en solution, en suivant le « shuttle » redox hydroquinone/benzoquinone à la surface de l'électrode.

Dans le second cas (ii), l'addition électrophile de radicaux BDYT électro-générés a été étudiée pour la première fois sur des électrodes de nanotubes de carbone à simple paroi ou sur les électrodes de graphène. La combinaison de différentes techniques complémentaires a montré l'attachement covalent de BDYT aux électrodes de nanotubes de carbone à paroi simple. Une telle modification mène à la formation de rubans torsadés qui ont pu être observés et analysés par AFM et par microscopie électronique à balayage. Aucune preuve de la formation de rubans torsadés n'a pu être mise en évidence pour les électrodes modifiées à base de graphène.

Acronyms

ACN: Acetonitrile

AFM: Atomic Force Microscopy

BDYT: Benzodithiolilyum tetrafluoroborate

BQ: Benzoquinone

BSE: Back scattered electrons

CNRS: Centre National de la Recherche Scientifique

CNTs: Carbon nanotubes

CoMoCAT: Cobalt molybdenum catalyst

CPME: Cyclopentyl methyl ether

CRPP: Centre de Recherche Paul Pascal

C-SWCNTs: CoMoCAT-single walled carbon nanotubes

CV: Cyclic Voltammetry

CVD: Chemical Vapour deposition

DB-TTF: Dibenzo tetrathiafulvalene

DLS: Dynamic Light scattering

DMSO: Dimethyl sulfoxide

DWCNTs: Double walled carbon nanotubes

ED: Electron diffraction

Acronyms

EDA: Ethylenedianiline

EG: Epitaxial graphene

FEG: Field emission gun

FETs: Field-effect transistors

FT-IR: Fourier-transformed infrared spectroscopy

GC: Glassy carbon

GICs: Graphite intercalation compounds

NHS: N-hydroxysuccinimide

HIPCO: High-pressure carbon monoxide

HOPG: Highly-oriented pirrolitic graphite

HQ: Hydroquinone

HRP: Horse-radish Peroxidase

HR-SEM: High-resolution scanning electron microscopy

H-SWCNTs: HiPCO-single walled carbon nanotubes

ITO: Indium-Tin Oxide

MeOH: Methanol

MALDI-TOF: Matrix-assisted desorption ionization-time of flight

M-THF: Methyl- tetrahydrofurane

Acronyms

OCP: Open circuit potential

OFETs: Organic field-effect transistors

PBS: Phosphate buffered solution

PET: Polyethylene terephthalate

P-PhDA: Para-phenylenediamine

PS: Polystyrene

RBM: Radial breathing mode

SAM: Self-assembled monolayers

SEM: Scanning electron microscopy

STM: Scanning tunneling microscopy

SWCNTs: Single-walled carbon nanotubes

TEM: Transmission electron microscopy

THF: Tetrahydrofurane

TMS: 4-[(Trimethylsilyl) ethynyl] aniline

TTF: Tetrathiafulvalene

XRD: X-Ray diffraction

XPS: X-Ray photoelectron spectroscopy

Table of contents

CHAPTER 1: INTRODUCTION **3**

1.1. Carbon Nanotubes and Graphene **5**

1.2. Graphite Intercalation Compounds (GIC_s) **12**

1.3. Electrochemical surface modification of SWCNTs: the state of the art **15**

1.3.1. Diazonium chemistry 15

1.3.2. Azide-alkyne Cu (I)-cycloaddition reaction: Click-Chemistry 21

1.3.3. Electrophylic additions: 1, 3-Benzodithiolilyum tetrafluoroborate 25

CHAPTER 2: CHARACTERIZATION TECHNIQUES **29**

2.1. Atomic Force Microscopy (AFM) **30**

2.2. Scanning Electron Microscopy (SEM) **34**

2.3. Surface Resistivity measurements **37**

van der Pauw and Four-point methods 37

2.4. Contact Angle **39**

2.5. X- Ray Photoelectron Spectroscopy (XPS) **41**

2.6. Raman Spectroscopy **44**

Characteristic Features of SWCNTs Raman spectroscopy and Variation of the intensities upon functionalization 47

2.7. Electrochemical Techniques **51**
Electrode Processes 53
Cyclic Voltammetry 58
Impedance spectroscopy 61

CHAPTER 3: SWCNT TRANSPARENT CONDUCTIVE FILMS **63**

3.1. Introduction of the study **64**
3.1.1. Solutions of $SWCNT_s$ 65

3.3. SWCNT FILMS CHARACTERIZATION **74**

3.4. CONCLUSIONS **82**

CHAPTER 4: ELECTROCHEMICAL SURFACE MODIFICATION OF SWCNT-BASED ELECTRODES **83**

4.1.2. Transformation of the remaining active moieties 95
4.1.3. Azide-alkyne Cu (I) cycloaddition reaction: click-chemistry 99
4.1.4. Immobilization of a redox enzyme: Horseradish Peroxidase (HRP) 104

4.2. Electrochemical surface modification with 1, 3-Benzodithiolilyum tetrafluoroborate **108**

4.3. Conclusions **130**

CHAPTER 5: TRANSPARENT CONDUCTIVE FILMS FROM GRAPHITE INTERCALATION COMPOUNDS (GICs) 133

5.1. Synthesis and solutions of KC8 compounds 135

5.2. From solutions to graphene films 137

5.3. Graphene-based electrodes 140

5.3.1. Surface modification upon Electrografting with aryl diazonium salts 146

5.3.2. Surface modification through Electrophylic addition of 1, 3- BDYT 152

5.4. Conclusions 158

BIBLIOGRAPHY 161

SUMMARY 177

Table of contents

Thesis description

The thesis is made up of 5 chapters.

Chapter 1 gives a general introduction about latest literature in the field of carbon nanotechnology and carbon nanomaterials. The state of the art aims at the electrochemical surface modification of SWCNT and graphene-based electrodes through two different approaches: the diazonium chemistry reaction and the covalent surface modification of SWCNT with BDYT.

Chapter 2 introduces the characterization techniques used during this work. It will sum up important aspects in our field; i.e. Raman spectroscopy as an important key when working with carbon nanotubes and graphene.

Chapter 3 explains the preparation of SWCNT-based electrodes starting from solutions of HiPCO and CoMoCAT-SWCNTs. Preparation of solutions and films, selection of substrates and characterization are described.

Chapter 4 describes *the state of the art* on this thesis work and will show the results obtained for the electrochemical surface modification of SWCNT-based electrodes via covalent surface modification by: (a) diazonium chemistry (followed by click chemistry reaction) and (b) the electrophylic addition of 1, 3-BDYT molecules.

Chapter 5 is dedicated to GICs and graphene-based electrodes. Synthesis of graphite intercalation compounds (GICs) with particular stoichiometry, GIC solutions, deposition on glass are explained along the chapter. Graphene films are tested as electrode material. Its performance for surface modification is described.

CHAPTER 1: INTRODUCTION

The early understanding and manipulation of nanostructured materials, as the colloidal ruby gold discovered by M. Faraday, demonstrated that gold nanoparticles produce different color light under different lighting conditions. The physicist R. Feynman, Nobel Prize in 1965, gave what is considered to be the first lecture based on the atomic scale under the title: *There is a plenty of room at the bottom* in a meeting of the American Physical Society.[1] The lecture provided inspiration for the field of nanotechnology with an emergence in the 80s where the convergence of experimental advances, as the invention of the scanning tunneling microscope (STM), took off. Along with the years the concept has shifted, up to now, where nanotechnology gives rise to lots of contributions in the field.

Nature has always attracted attention and it is a fact that the majority of biological processes occurs at the nanometer scale. DNA chains, building blocks of the human life are only 2 nm in diameter. Proteins, enzymes, and other biomolecules in charge of important processes in the human body are only 5 nm in diameter.

Carbon, being an inexpensive raw material, has shown to be an ideal candidate as a source of fantastic nanomaterials with noticeable properties. The use of

such unique nanomaterials for the investigation of biological processes is an exciting challenge in the field of nanotechnology.

H. W. Kroto, O' Brien, Curl, and Smalley are credited with the discovery of the Buckminsterfullerene in 1985[2] upon study of vaporized graphite by laser irradiation producing stable C_{60} clusters observed by TOF spectroscopy (see figure 1).

Fig. 1: Time-of-flight mass spectrometry (TOF) of C_{60} cluster from Smalley and coworkers[2] (left). First representation of carbon nanotube (CNT) reported by Iijima[3] in 1991 (right).

They are commonly named buckyball or fullerene. They are soccer ball in shape and are entirely composed of carbon, like other carbon allotropes as graphite, diamond or nanotubes.

1.1. CARBON NANOTUBES AND GRAPHENE

Carbon Nanotubes

The discovery of carbon nanotubes is credited to S. Iijima back in 1991,[3] where he described the preparation of a new type of finite carbon structures (later named carbon nanotubes) consisting in needle-shape tubes obtained by arc-discharge evaporation (similar to that used for fullerenes).

Carbon nanotubes, here-after CNTs, are tubular shape structures composed mainly of carbon atoms in sp^2 hybridation upon hexagonal honey-comb lattices as it is showed in figure 2.

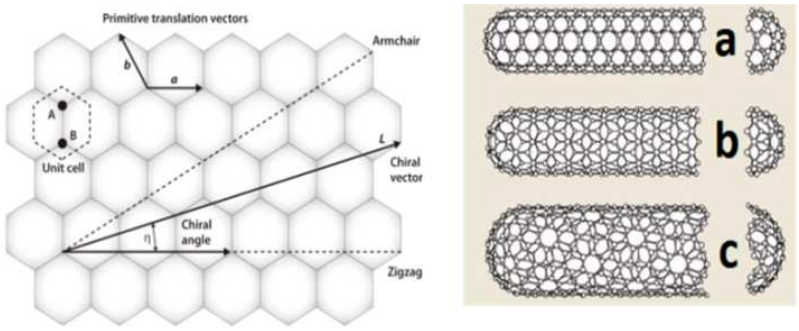

Fig. 2: Graphite sheet (left) showing possible chiral angles for wrapping up resulting in (a) arm-chair, (b) zig-zag, and (c) intermediate conformations of CNTs (right)[a].

They are described as individual graphite sheets that have been wrapped into themselves forming a tube. These tubes are closed defining two regions, the

[a] *Picture from Internet.*

nanotube body and the cap, being this last half-fullerene with topological defects as pentagons.[4]

Structure and properties associated to CNTs have been shown to be the most diverse and rich among nanomaterials.[5] Carbon nanotubes can be classified into single-walled nanotubes (SWCNTs) and multi-walled carbon nanotubes (MWCNTs). The difference between them remains in the number of sheets of carbon forming the final tube. MWCNTs are concentric single graphitic tubes, while a SWCNT is a single graphitic layer rolled forming a cylinder of 1-2 nm in diameter. The way to roll up is defined by specific chiral angles, resulting in a specific nanotube electronic behavior (metallic or semiconducting) upon definition of the n and m indices. Being n and m two natural numbers, and a and b two primitive translation vectors (see figure 2) where the chiral vector of a specific CNT can be describe as,

$$\vec{\eta} = n\vec{a} + m\vec{b}$$

Kataura and co-workers published in 1999, SWCNT characterization upon the study of the optical absorption spectra and transmission electron microscopy observations (TEM) obtaining what is known as Kataura's plot showed in figure 3.[6]

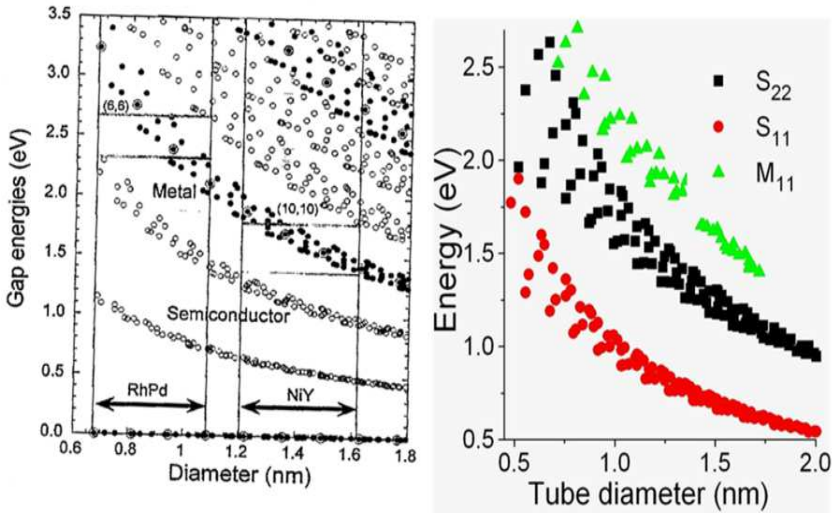

Fig. 3: Kataura's plot showing specific resonant nanotubes (metallic or semiconducting) when excited at specific laser energy. From: Optical properties of single-walled carbon nanotubes.[6]

This plot helps to individualize precise (n, m) SWCNT under specific excitation energy. Many efforts have been done in CNT synthesis controlling the CNT growth resulting in specific nanotubes with desired (n, m) indices. Pure metallic or pure semiconducting CNT samples are very important in many electronic applications, but unfortunately synthesis methods used up to now, produce mixtures of CNTs with random indices.[7]

SWCNTs are produced mainly by arc-discharge, laser ablation, and chemical vapor deposition (CVD) methods. CVD was described to be a method for potential industrial scale up on CNT synthesis upon controlled morphology and structure of the produced SWCNTs.

- High-pressure carbon monoxide (HiPCO) is a SWCNT synthesis process where high-pressure carbon monoxide is used as carbon source. The iron catalyst formed in the reactor form clusters upon decomposition where the SWCNTs undergo nucleation and grow. This was originally developed by Smalley's group in Rice University.[8]

- Cobalt-Molybdenum catalyst process (CoMoCAT) is attributed to Resasco group in Oklahoma University,[9] being an important advance on scale up synthesis of SWCNTs.

The work by R.E. Smalley and coworkers in 1997 showed a STM study to explore the local electrical characteristics of SWCNTs. It was the first publication for a nanotube nanodevice.[10] SWCNTs are interesting materials to be used in electrochemical devices from the point of view of surface area availability, as well as high conductivity and excellent mechanical properties.[11] The electroactivity of SWCNTs has been widely studied and some works concluded by the attribution of electroactivity to reacting groups on the tube's surface. Later ab-inito calculations have demonstrated that this observed improvement in the electron transfer was due to the inherent curvature of the CNTs.[7]

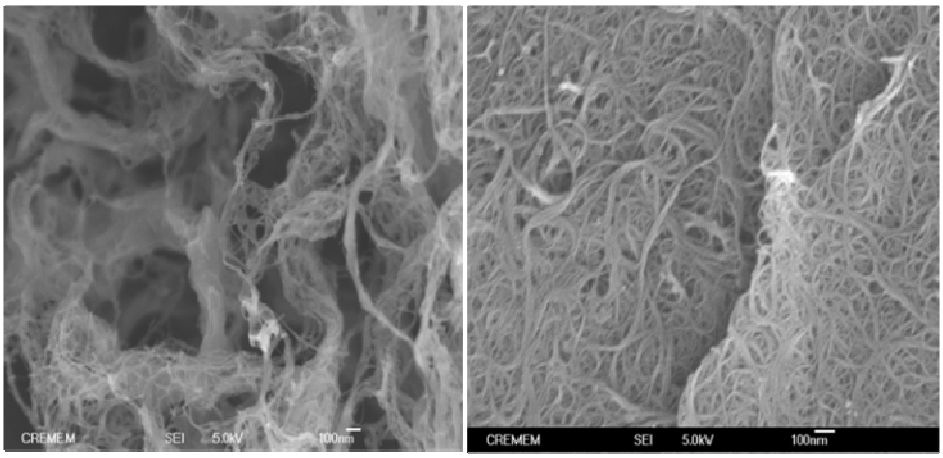

Fig. 5: SEM images for HiPCO (left) and CoMoCAT (right) SWCNT raw powders.

In the present study, two different sources of SWCNTs were studied, HiPCO and CoMoCAT, as starting materials for the preparation of SWCNT-based electrode devices. Specific characteristics at their final state will be shown along with the redaction. Here it is shown (see above, figure 5) SEM images for raw powder material of HiPCO and CoMoCAT SWCNTs.

Graphene

The concept of graphene appears for the first time in 1947 but the scientific community of carbon was relatively small and they worked separately. [12] The first International Conference on Intercalation Compounds was in France, in 1977. It was the first important event in which carbon researchers were brought together. In the 80s Materials Research Society (MRS) meetings and other conferences started including carbon nanostructure sessions.

Graphene it is defined as a single sheet of sp^2 hybridation carbon atoms forming a net of hexagons. An infinite number of graphene layers stabilized upon π-π stacking interactions, as it is showed in figure 6, results in graphite structures.

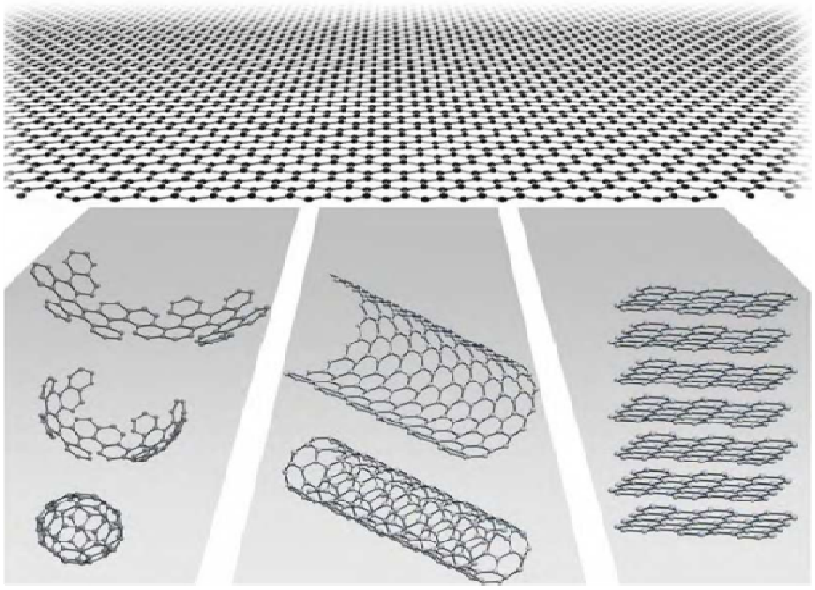

Fig. 6: Graphene sheet and derivate structures. From: Geim and Novoselov, 2004.[13]

The synthesis of a monolayer graphene was published in 2004 by Geim and Novoselov,[13] and many experimental efforts were done for the understanding of this new material. Since then, an exponential growth of experimental contributions in the field occured.[14,15,16] In 2010, the Nobel prize in Physics was awarded to Geim and Novoselov for their innovative experiments on these 2D materials.[17] Graphene was announced to be an interesting material for nanoelectronic devices.

In 2006, the group of R. Haddon from the University of California Riverside, made a contribution regarding properties of graphite and graphene solutions[18] highlighting graphene as a novel promise of electronic material.

The dissolutions or dispersions of SWCNT and Graphene are critical for further applications. A Nature review in chemical methods for the production of graphene by S. Park and R. S. Ruoff[19] in 2009, sums up latter contributions over the years. In 2010, R. S. Ruoff published a roadmap for the preparation of high quality graphene with R. Gengler and K. Spyrou.[20] Up to then, the most explored route to obtain large quantities of soluble or dispersed graphene was upon reduction of graphene oxide.[21]

The reactivity of graphene is described to be reduced compared to the reactivity of SWCNTs because of a lack of local strain or misalignment of the π orbitals.[22]

In 2008, E.R. Margine showed a theoretical paper for the study of the thermal stability of covalently functionalized graphene and CNTs.[23] Haddon and co-workers communicated experimental data of modified epitaxial graphene (EG) with aryl diazonium salts as shown in figure 7.[24]

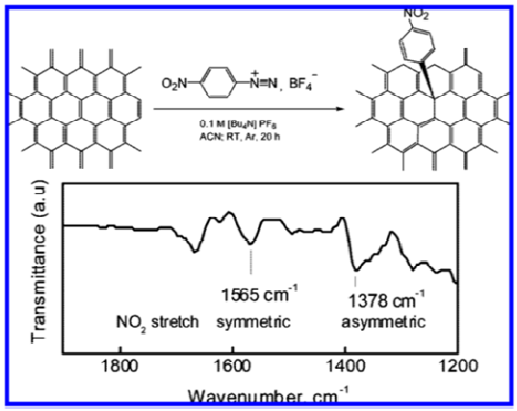

Fig. 7: EG surface modification upon spontaneous grafting of aryl diazonium salts.

Here it is shown an example of using the spontaneous grafting of aryl diazonium salts. It will be introduced later on as one of the reactions selected in this work for the functionalization of carbon materials as SWCNTs and graphite intercalation compounds (GICs). A nice review on chemical functionalization of graphene and its further applications was published by J. H. Lee in 2012.[25]

1.2. GRAPHITE INTERCALATION COMPOUNDS (GICS)

The CNT group at CRPP-CNRS, Pessac, developed in 2004 an original method for the reductive dissolution of CNTs: by electrostatically charging nanotube bundles polyelectrolytes are formed that spontaneously dissolve in organic solvents.[26] Graphene solutions were analogously[27] prepared by mild spontaneous dissolution of a graphite intercalation compound (KC_8) in NMP (see figure 8).

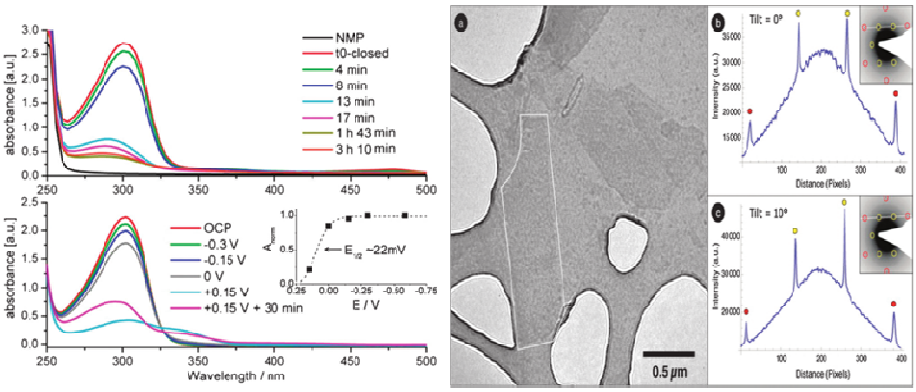

Fig. 8: Left: Spectroelectrochemical experiment showing the absorption spectra of GICs in NMP upon air exposure (above) and electrochemical oxidation (below). Right: TEM images of graphene flakes obtained in NMP.[27]

This approach was recently reviewed in ref.[28] The availability of real solutions of pristine nanocarbon opens a roadmap to SWCNT/graphene-based devices for many applications.

GICs were firstly synthesized in 1841 by Schaffäutl, but it was the introduction of X-ray diffraction techniques which showed the stage index of these compounds in the 30s. This stage index is determined by the number of layers of graphite between the intercalate species set. Mildred Dresselhaus and coworkers determined in the 70s the related properties of GICs (see figure 9).[29]

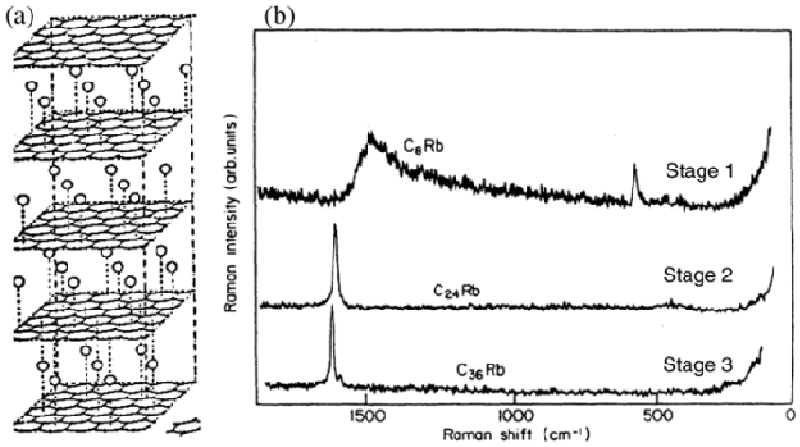

Fig. 9: GIC representation (left) and Raman spectra (right) obtained for different stage index GICs in 1970s. From: Physica scripta,2012.[29]

Nowadays GICs is a field with intense activity, and our laboratory in CRPP is an example.[28]

Alkali metals are the most widely studied intercalating species used for the intercalation of graphite. The preparation of those compounds usually needs to be done under encapsulation due to air-instability of many of them.[30] Ferrari and coworkers in 2010 had investigated the Fermi level of a group of GICs upon intercalation with anhydrous ferric chloride by Raman spectroscopy.[31]

The present thesis work will focus on the study of the electrochemical surface modification of electrodes made from solutions of pristine SWCNTs and GICs. The functionalization of nanoscale material surface (addition of specific moieties for specific purposes) is well reported and some of the applications go from drug delivery to electronic devices. In the present work we describe the

electrochemical surface modification of electrodes made entirely of SWCNTs or graphene, aimed to the obtainment of bio-sensing devices.

1.3. ELECTROCHEMICAL SURFACE MODIFICATION OF SWCNTS: THE STATE OF THE ART

1.3.1. DIAZONIUM CHEMISTRY

The modification of CNT surfaces upon electrochemical or spontaneous grafting is one of the most studied coupling methods for nanotube-surface functionalization. It can be a solution for derivatizing CNTs, and also can give functionalities that could improve properties, as for example, in composites. The modification of electrode surfaces for analytical or catalytic purposes has attracted much attention along the years. In this section, some literature about diazonium chemistry and carbon surface modification will be introduced remarking pros and cons on using this functionalization chemistry.

J. Pinson, J.M. Savéant and co-workers showed in 1992 a first approach for carbon surface modification upon the reduction of diazonium salts. Until this time, the modification of carbon surfaces underwent upon surface oxidation with formation of oxygenated species on the surface like ketones, hydroxilic groups, and so on, that would react with selected molecules to be attached. The resulting oxygenated functional groups were difficult to control and besides, the corrosion of the carbon surface was often observed.

Instead, the covalent attachment of aryl radicals precursors onto carbon surfaces upon electrochemical reduction of diazonium salts[32] leads to non

corrosive covalent attachment upon one-electron reduction of diazonium salt through (see figure 10) *Meerwein arylation reactions*.

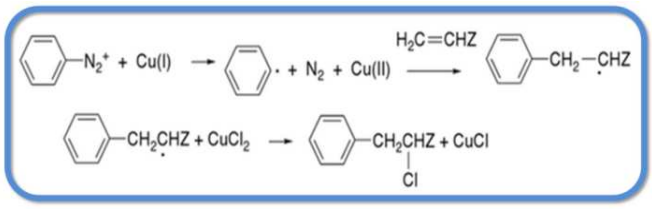

Fig. 10: Arylation reaction: Meerwein Arylation.

5 *mM* diazonium salt was reported to be the best concentration to obtain a compact layer, or close-packed monolayer on glassy carbon electrode (GC). In 1997, they published the covalent attachment of aryl radicals onto glassy carbon and HOPG surfaces upon electrochemical reduction of diazonium salts with diazonium precursors (see figure 11).[33]

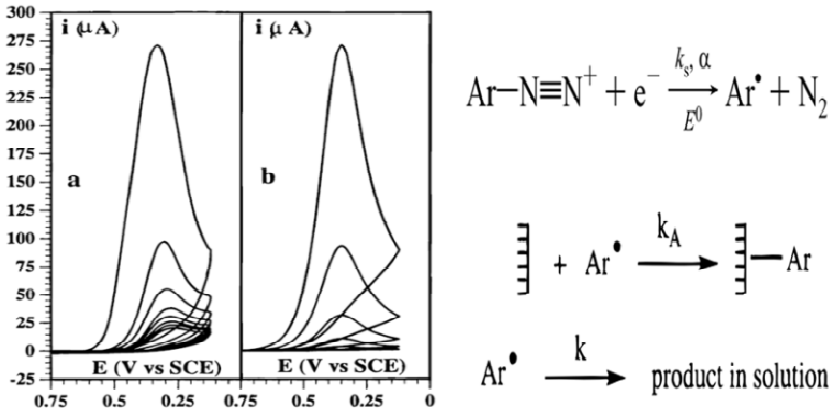

Fig. 11: Cyclic voltammetry for the surface modification of HOPG with aryl diazonium salts (left), and mechanism proposed for the covalent attachment (right).[33]

The modified surfaces were analyzed by Raman spectroscopy, X-ray photoelectron spectroscopy (XPS) and electrochemical techniques for the detection of nitro groups. They noticed that the film formed in GC surface was difficult to remove upon rinsing and sonication.

The surface coverage can be controlled upon controlling the diazonium concentration in solution and/or controlling the electrolysis time. The electrolysis time can be extended until obtaining surface saturation. Such conditions were also used in our study.

Electrochemical reduction of a variety of aryl diazonium salts leads to derivatization of SWCNTs. The work of J. Tour and co-workers in 2001 shows the preferential derivatization of small diameter SWCNTs for the enhanced reactivity of these tubes (0.7 nm) for aryl diazonium compounds.[34] The absorption spectra of pristine and derivatized tubes show clear differences (in terms of loss of structure) consistent with a covalent functionalization rather than a strong adsorption (see figure 12).

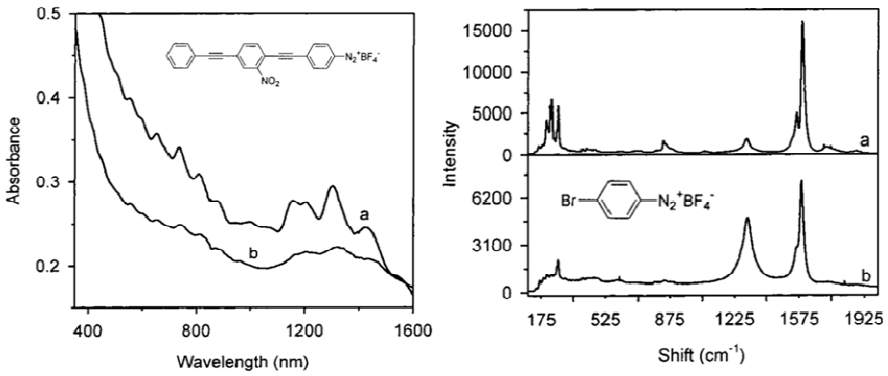

Fig. 12: Absorption and Raman spectra of pristine (a) and surface modified-SWCNTs (b). From: JACS, (2001), 123, 6536.

During our study, Raman spectroscopy has been an important tool of characterization in our systems. In order to investigate covalent or non-covalent surface functionalization of SWCNTs and GICs we will measure changes in the D-band. Derivatization of CNTs in solid state presents an advantage with respect to the solution-phase method by the fact that radicals are generated at the surface of the CNTs where the reaction is desired. Those radicals are able to react with the CNT surface, but also on any other aromatic ring, like for example, those of the already bonded aryl moieties.

In 2004, P. Marcoux, J. Pinson and co-workers[35] published the electrochemical surface modification of SWCNTs (see figure 13), remarking that clear evidences exist for the growth of aryl chains and multilayers of aryl moieties on the surface of SWCNTs.

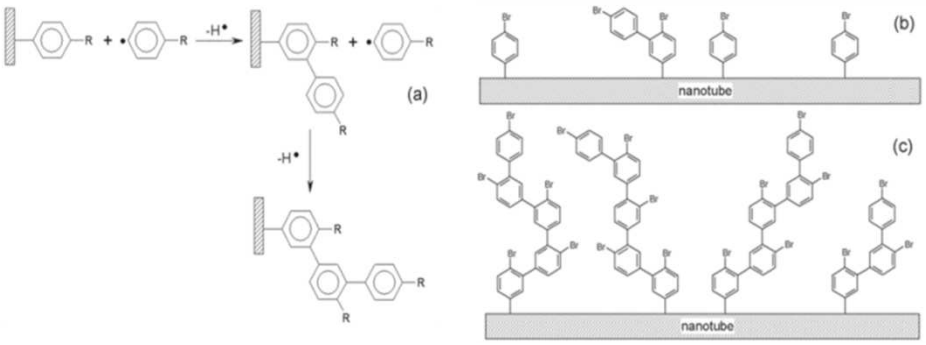

Fig. 13: Electrochemical surface modification of SWCNTs with aryl radicals showing polymeric growth. From: New. J. Chem., 2004, 302.[35]

Control or/and limit the polymerization reactions is still an important issue to study. The electrogeneration of radical species at the SWCNT surface shows advantages compared to other techniques resulting in a clean and non-

destructive process for surface modification where an alternative method for controlling polymerization thus obtaining mono-to-few layers through diazonium reaction at the electrode surface was described in 2012 by S. U. Pedersen, K. Daasbjerg and coworkers.[36]

In 2009, Joyeux, Mangiagalli, and Pinson showed an approach (see figure 14), to place CNTs in trenches through chemical attachment using ethylene dianiline (EDA) as a linker.[37]

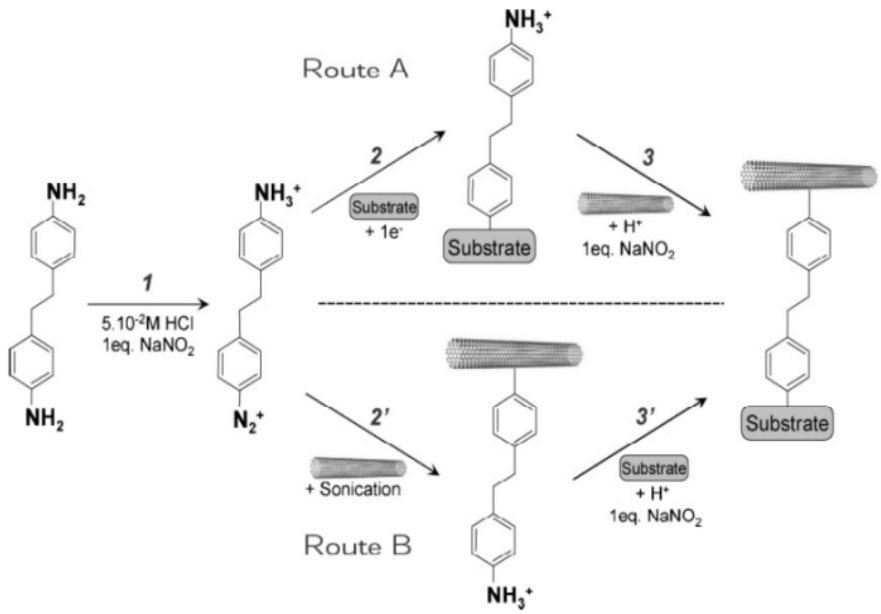

Fig. 14: Route selected for the covalent immobilization of EDA molecules on SWCNT- and graphene-based electrodes. From: Adv. Matter., 2009, 21, 4404.

This EDA molecule possesses, after CNT-surface modification, another free amine group able to react with the substrate. Two routes are described for the

covalent surface modification of SWCNTs. Both are described to occur upon formation of the mono-diazonium salt of the EDA moiety.

Route **A,** describes the electrografting of EDA on the surface of a selected substrate followed by the transformation of the remaining amino group in a second diazonium moiety which grafted spontaneously to the SWCNT-surface. Route **B**, follows the opposite approach binding firstly to the SWCNT surface followed by the transformation of the amino free groups which bind to the selected substrate.

The in-situ formation of the diazonium salt was already shown in 2006 by D. Bélanger and J. Lyskawa,[38] where the electrochemical surface modification of gold substrates with p-Phenylenediamine (PhDA) moieties was reported. They remarked that one equivalent of sodium nitrate was the optimal amount to obtain a compact layer of aryl groups; above that value the amount of moieties grafted was diminished.

In the present study following the same strategy EDA moieties were used for the electrochemical surface modification of SWCNT-based electrodes. SWCNT devices were prepared from a spontaneous dissolution of a SWCNT salt.[26] The process will be explained in detail in chapter 3: SWCNT-transparent conductive films. Likewise 4-[(Trimethylsilyl) ethynyl] aniline (TMS) and p-Phenylenediamine (PhDA) (Figure 15) were selected as precursors for the present study.[39,40,41]

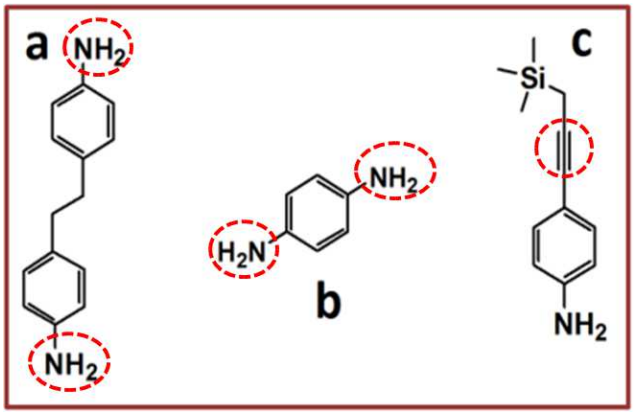

Fig. 15: Precursors selected for the electrochemical surface modification of SWCNT and graphene-based electrodes. (A) 4, 4'- Ethylene dianiline (EDA), (B) p-Phenylenediamine (p-PhDA), and (C) 4-[(Trimethylsilyl) ethynyl] aniline (TMS).

The remaining reactive groups after the grafting process (amines and internal azides) are suitable to anchor electroactive probes and set up a bioconjugation protocol for the final preparation of bio-sensing surfaces based on carbon materials. Among the chemical methods for post-functionalization of CNTs and graphene films, bio-conjugation amidation and copper catalyzed cycloaddition (click) reaction have been widely used. [4,42,43,44]

1.3.2. AZIDE-ALKYNE CU (I)-CYCLOADDITION REACTION: CLICK-CHEMISTRY

The copper (I)-catalyzed azide-alkyne cycloaddition reactions, named click-chemistry" due to facility of conditions for high-yield reactions by simply "clicking" the two reactive groups[45] is expected to provide in the future years excellent opportunities for the construction at the nano-scale. This concept

was introduced in 2001 by Sharpless and coworkers opening a new pathway for versatile chemical reactions in synthetic chemistry.[46,47]

The mechanism of the in situ reaction was studied by V. O. Rodionov, V. V. Fokin and M.G. Finn[48] with the objective of developing new ligands and autocatalytic systems. At that time, the precise nature of the binuclear copper system responsible for an efficient catalysis was not resolved.[49 50] In 2013, B.T. Worrell, J.A. Malik, and V.V. Fokin[51] showed evidence of an involvement of a dinuclear copper intermediate solving issues present at that time in the mechanism (see figure 16).

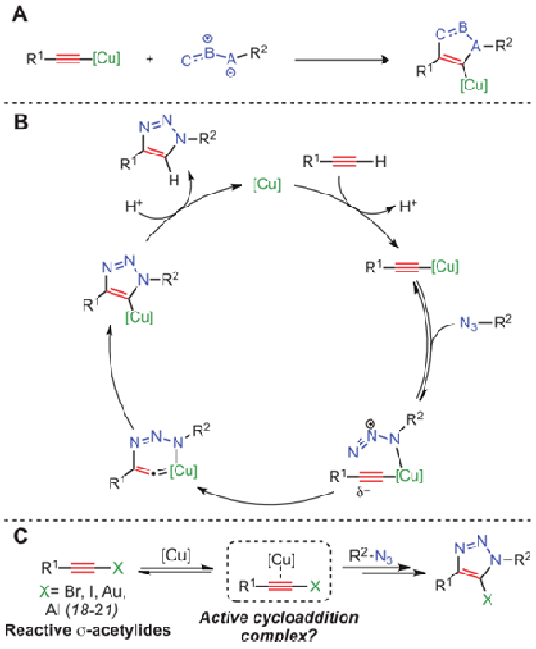

Fig. 16: Copper (I)-catalyzed azide-alkyne cycloaddition reaction mechanism. From: Direct evidence of a dinuclear copper intermediate in Cu (I) azide-alkyne cycloadditions*, Science,*(2013),457.

Click-chemistry in material science represents a big advantage for surface modification after the successful grafting of an organic layer. [52] Jean- François Lutz published a minireview showing the exponential growth publications using click-chemistry over the last few years.[53]

Most of the reactions which satisfy click chemistry to occur are now well-studied and the preparation of a specific set of conditions is simple[54–56]. The ability of modifying a surface through a click-chemistry reaction offers the possibility of designing nanomaterials with targeted response to the environment. An example of construction of bio-conjugated materials using click-chemistry was reported by J-F. Lutz and Z. Zarafshani.[57] This approach can be used for surface modification of CNTs, fullerenes, or graphene.

The experimental demonstration for changes on the electronic and optical properties of the non-covalently surface modified SWCNTs was reported by S. Campidelli, M. Prato and coworkers in 2006.[58] SWCNTs were efficiently non-covalently functionalized with porphyrin dendrons via click chemistry reaction.[40] In 2011, G. Clavé and S. Campidelli reviewed advances using click-chemistry for the preparation of CNT-functional materials.[39]

An example combining surface modification with diazonium chemistry followed by click-chemistry was reported by C. Mangeney and coworkers (see figure 17).[59]

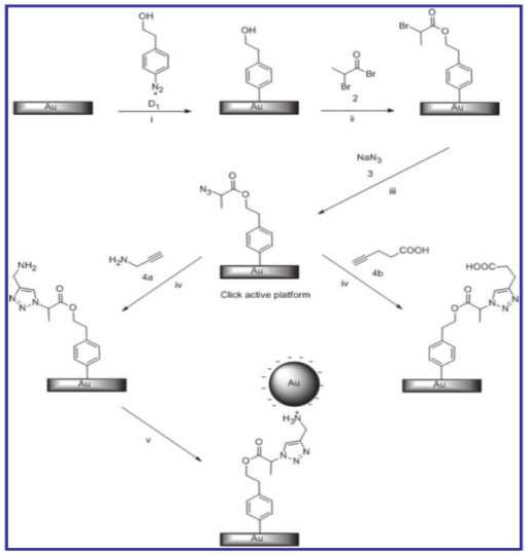

Fig. 17: Scheme for the preparation of gold modified surfaces as platforms for the immobilization of nanoparticles by click-chemistry.[59,60]

In order to modify materials by click-chemistry reactions, complementary groups for the reaction must be present on the surface (see figure 18).[61]

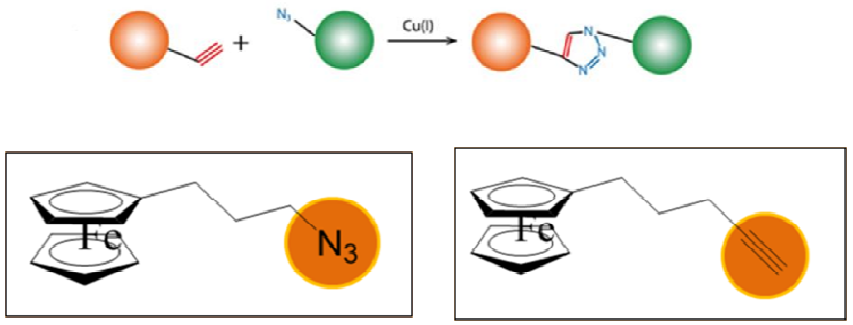

Fig. 18: Schematic representation of click-chemistry reaction from: *Prog. Pol. Sci., (2012), 27, 985-1003* (above) and Ferrocenes containing probes used during the present study (below).

In this work, for setting up the immobilization procedure, ferrocene moieties were used as redox probes during click chemistry reactions. After reaction, probes are detectable by cyclic voltammetry. The Organic chemistry group at Bologna University has synthesized two different ferrocenes containing molecules as presented in figure 20.

1.3.3. ELECTROPHYLIC ADDITIONS: 1, 3-BENZODITHIOLILYUM TETRAFLUOROBORATE

A novel approach in SWCNT-based electrodes surface modification was inspired by a theoretical work by Y. Jaeyong ET. al.[62] describing an adsorption model of 1, 3-BDYT (BDYT) on SWCNT surface. Later on it was found that the reactivity of BDYT is selective for metallic rather than for semiconducting SWCNTs: Jeong-O Lee and Hyunju Chang,[63] proved the adsorption of BDYT derivatives on SWCNT surfaces leading to a highly enhanced D-band in Raman spectra (see figure 19).

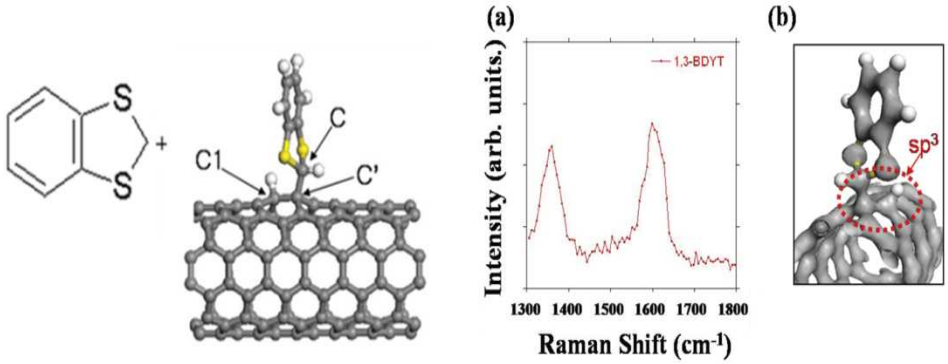

Fig. 19: Theoretical simulation for the covalent adsorption on carbon nanotubes. From: ***Journal of the Korean Physical Society, (2010) 57, 1.***

Our approach is schematically described in figure 20: reduced BDYT undergoes addition onto electron rich surfaces forming, in the case of carbon material, a covalent bond. Substitution of the highlighted hydrogen atom would allow the introduction of the desired functional moieties (R). Finally, the subsequent chemical treatment with Ni/Raney would remove benzodithiol moieties leaving the final bridged structure (see figure 22).[64]

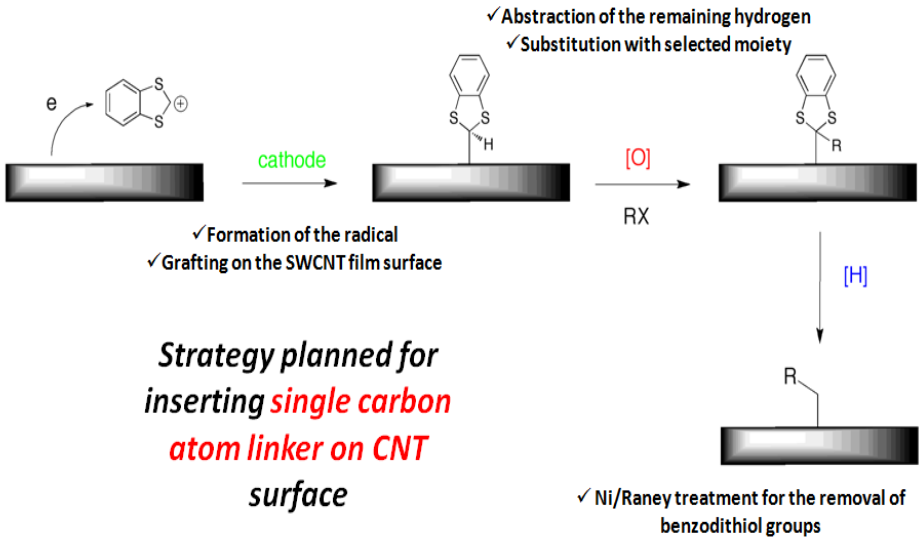

Fig. 20: Selected strategy for SWCNT surface modification with BDYT.

Notice than BDYT is a precursor of tetrathiafulvalenes (TTF). TTF and its derivatives have been widely studied over the years. Some examples of its applications are Langmuir-Blodgett films, molecular switches or building blocks, as many other contributions in the field.[65,66,67,68]

The strategy followed is based on the electrochemical surface modification of SWCNT and graphene-based electrodes upon formation of benzodithiolilyum

radicals directly on the electrode surface. This modification will have an effect on the relative intensities of the D-band (before and after the reaction) that is related with symmetry disruption on SWCNTs upon changes in the carbon hybridation **($sp^2 \rightarrow sp^3$)** due to surface modification.

CHAPTER 2: CHARACTERIZATION TECHNIQUES

During this thesis study a significant number of techniques have been used for characterization. We will introduce the **Atomic force microscopy** and the **Scanning electron microscopy** useful to reveal a topography image of the nanocarbon films. It was possible to extract information about roughness of films and to observe differences between films produced with HiPCO and CoMoCat carbon nanotubes. It was possible to determine the thickness of the films, contamination of the samples in terms of remaining catalyst, determine aggregates and measure its diameters.

Four-points-conductivity measurements will determine the surface conductivity of the films depending on the amount of nanotubes used for film preparation (Ω/□).

Contact-angle measurements were useful to determine the wettability of the surface of films. For instance, it was used to characterize SWCNT-based electrodes before and after electrochemical surface modification.

To quantify (and qualify) such modification **X-Ray photoelectron spectroscopy (XPS)** was used. Elements present on the film surface were determined; for

instance, in the C1s spectrum of a SWCNT film there is an intense band at ~284 eV related to sp^2 carbon atoms while at higher binding energies bands related to oxygenated carbon atoms are observed (-COOH,-C=O,-COH).

Raman Spectroscopy was used to observe the characteristic bands of carbon related materials. During the present study the **I_G/I_D** ratio (intensity of the Graphite band (G band) over the intensity of the defect band (D band)) before and after surface modification will be studied as a degree of functionalization. Other features in the spectra will be explained when needed.

Electrochemical techniques, as Cyclic Voltammetry and Impedance spectroscopy, are described over this chapter. Modified SWCNT-based electrodes have been prepared while monitoring the reaction by **Cyclic Voltammetry**. Differences in the electrode's charge transfer resistance have been characterized by **Impedance spectroscopy.**

2.1. ATOMIC FORCE MICROSCOPY (AFM)

Nanoscience and nanotechnologies have been explored with lots of efforts since the past twenty years and the result of such ongoing quest for miniaturization are tools as the Atomic Force microscope, here on, the AFM (see figure 1). It was invented by Binning ET. Al in 1986 and up to now has undergone much development. Here, the standard laws of physics are replaced by quantum effects.

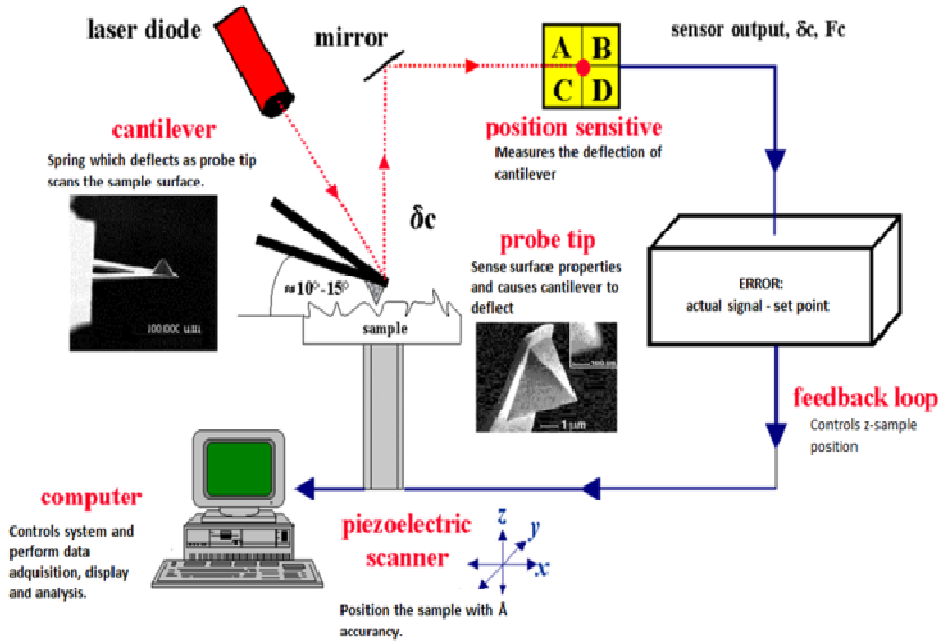

Fig.1: Schematic representation of different components present in the AFM instrument.[b]

Any material reduced to the nanoscale can show properties that are different from properties observed for the same material at larger scale. The fascination with nanotechnology came along with these unique quantum and surface phenomena that matter exhibits at the nanoscale opening a broad way for novel applications.

The ancestor of AFM is the scanning tunneling microscope (STM) where images can be taken at the atomic level measuring the tunneling current between the surface and a conducting tip (voltage difference). The first AFM

[b] *Image took from Internet.*

set up was using a vibrating cantilever technique using what is known as Light-lever mechanism.

The Piezo electric scanner is made of ceramic materials which extend or contract in the presence of a voltage gradient, developing an electrical potential in response to mechanical pressure, i.e. close to the sample surface.

V-shaped cantilevers are the most used providing low mechanical resistance values to vertical deflection and high resistance values to lateral torsion. For the detection of the displacement of the cantilever, a laser is reflected on the cantilever and is collected in a photodiode.

Modes of Tip-Surface interaction

Three different modes are available for working with an AFM. First AFM operated in **contact mode** where the tip scans the surface of the sample following the Cartesian axis. In this case the deflection of the cantilever is kept constant.

Non-contact mode was introduced in 1987 for the scanning of fragile samples as biological samples. In this mode, the cantilever oscillates close to its resonant frequency at a small distance from the sample surface. Compared to contact mode, forces on the sample are lower avoiding damage during the measurements.

Tapping mode is defined as somewhere between both, contact and non-contact modes. All AFM images acquired during this study have been performed with tapping mode.

Different composition in the sample surface will show different adhesive and mechanical properties resulting in a phase contrast. That was useful when observing SWCNT and graphene films making possible the interpretation of corrugations, estimated number of layers, chemical modification of tubes, and so on.

Forces governing when the tip is brought close to the surface lead to a deflection of the cantilever according to Hooke's law of elasticity. So, if the tip is brought close enough to the sample surface and the cantilever is deflected, this deflection will be function of the tip-sample interaction being measured at many points of the 2D surface and can be mapped spatially resulting in three dimensional images.

While the topographic image is registered the phase image is collected being possible to observe at once the topographic and material properties.

Lateral resolution depends on tip sharpness

The tip and the cantilever determine the lateral resolution of the system and the magnitude of force applied to the sample surface being critical components of the AFM.

If the tip sharp is not selected properly common artifacts are observed. That is known as the fat-tip effect and is showed in figure 2.

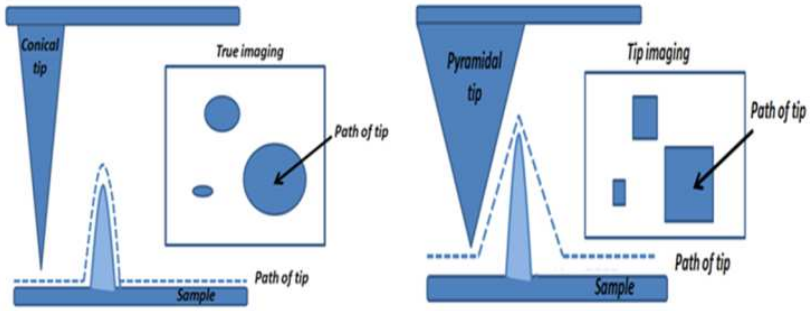

Fig. 2: Fat-tip effect upon collecting images with unapropiate tip.

A Nanoscope IIIa multimode was used for all the images shown. All the data was obtained operating in tapping mode. Two different Piezo were used for better resolution imaging; Piezo scanning from 1 µm up to 10 µm and a second Piezo scanning from 10 µm up to 100 µm images. Commercially available silicon tips.

2.2. SCANNING ELECTRON MICROSCOPY (SEM)

Electromagnetic lens were firstly developed in 1926 by **Hans Busch**. These lenses were used for focusing or deflecting charge particles in movement as electrons or ions under electro and magnetic fields by using the Lorentz force. H. Busch has laid the theoretical basis for the electron microscope, but it was the German physicist E. Ruska and the electrical engineer M. Knoll who constructed the prototype of the electron microscope in 1931.

In a scanning electron microscope an electron beam is focused into the sample and is rastered across the surface of the sample. The beam-sample interaction results in emitted electrons or photons collected with an appropriate detector

yielding valuable information about the material. The resolution of an SEM image depends on the beam diameter. The principle follows the same idea than for optical microscopes with the difference that in this case electron beams are used instead of light and the lens are magnets instead of optical materials (see figure 3).

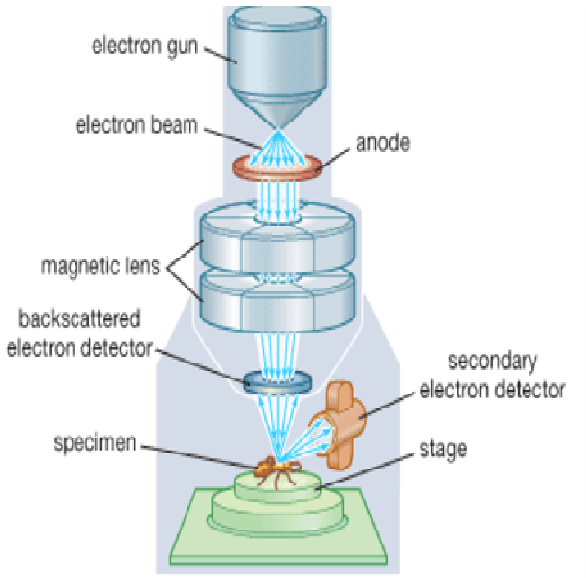

Fig. 3: Scanning Electron Microscope cartoon representation showing its principle.

The optics of scanning electron microscopes include condenser lens to focus the electron beam on the sample surface determining the size of the interaction, and electromagnetic coils which drive the raster scanning upon deflection on the electron beam.

Sample and sample holder sizes are in orders of centimeters, and can be rotated at the three different directions axis (x, y, and z).

The conductivity of the sample is required to obtain an image, so for non-conductive samples a metallic coating is needed.

Detectors can be made of a semiconductor transducer or by a scintillation device. In both cases there is a response (increase of conductivity or cascade of visible photons) when is bombarded by electrons.

The signal produced upon electron beam-sample surface interaction contains information about topography, composition, and other properties such as electrical conductivity. Signals registered by an SEM include among other characteristic X-rays, secondary electrons and back-scattered electrons (BSE).

Upon a strong relation between the intensity of the signal and the atomic number of a species, BSE images can provide an elementary analysis of elements present in the surface of the sample.

In conclusion, SEM is adapted for scanning any kind of sample surface. In case of non-conducting samples previous coating is needed in order to ensure a clear image. As it is based on surface interactions, it is not a pre-requisite to work with electron transparent samples as for example, in transmission electron microscopes (TEM).

In the present study a high resolution SEM was used from CREMEM laboratory, Pessac.

2.3. SURFACE RESISTIVITY MEASUREMENTS

The surface resistivity of a material can be described as the surface resistance to a flow of current. It does not depend on the physical dimensions of the material. According to Ohm's law, the resistance (R, ohms) of a specific material is determine by the applied voltage (V, volts) divided by the current flow (I, amperes) across the material as is showed as follows

$$\mathbf{R} = {}^{\mathbf{V}}/_{\mathbf{I}} = {}^{\boldsymbol{\rho}\mathbf{L}}/_{\mathbf{S}}$$

The electrical resistance is proportional to the length of the sample (L), and inversely proportional to the sample's cross section area (S).

Surface resistivity is expressed in Ohms (Ω), and usually is given in terms of Ω/□ (ohms/square). The surface resistivity of a tested sample with thickness equal to the unit is expected to show equal resistance in square dimensions independently of its in-plane dimensional resistance value. The expression surface resistivity (Ω/□) is the value of these calculations. Here we described methods for determination of surface resistivity values using techniques as the Van der Pauw method and the four point's method.

VAN DER PAUW AND FOUR-POINT METHODS

Van der Pauw method is widely used in semiconductors industry to determine the resistivity values of uniform samples. The original device is showed below where a thin plate sample contains small ohmic contacts placed on the periphery, in this case, on the corners. Measuring the resistivity will determine the sheet resistance $\mathbf{R}_S$. Van der Pauw demonstrates that two characteristic

resistances are associated with the corresponding terminals as is expressed in figure 4.

$$R_A = V_{4,3}/I_{1,2}$$

$$R_B = V_{1,4}/I_{2,3}$$

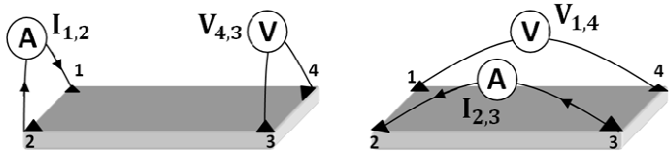

Fig. 4: Schematic representation of a Van der Pauw configuration used in the determination of the two characteristic resistances R_A and R_B.

The method used to measure SWCNT and graphene films was the four-point measurement. This method uses electrodes aligned linearly or in a square pattern to the sample surface (see figure 5).

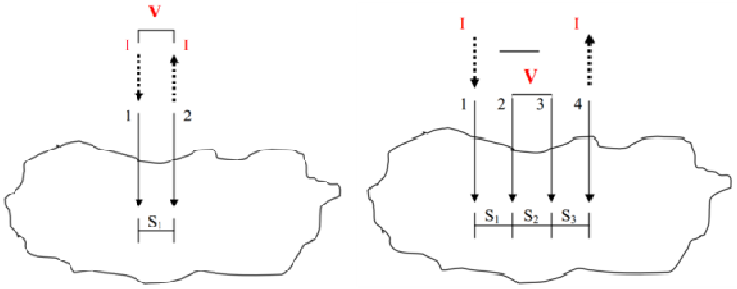

Fig. 5: Two- and four-point set up techniques. Arrows show direction of current flow.

In the case of two-point method, the voltage between the two electrodes is measured upon the passage of a flow of electrons. The expresion that results for the calculation of the surface resisitivity on this method contains a parasitic contact resisitance due to electrode-surface contact.

In contrast to this method, the addition of two more electrodes as it is showed for the four-point method eliminates the parasitic resistance due to contact and spread.

Since the measurements are done under finite sizes areas, corrections factors are needed. These factors are sample thickness dependent, among others.

2.4. CONTACT ANGLE

Contact angle measurement characterizes the wettability of a surface upon measuring the surface tension of a drop of water (or other liquid) at the interface with a homogeneous surface. It is one of the most sensitive and cheap surface analysis techniques capable of measuring from 3 up to 20 amstrong (Å) deep in the surface. When the drop comes in contact with the sample surface it can happen a complete spread of the drop over the sample surface, or that the drop will establish a define angle with the surface, named the contact angle. Thomas Young is credited with the development of the theory of capillary phenomenon while Laplace is credited to put numbers of such effect.

Many methods for measuring the contact angle are explained in literature. One of the most studied techniques is the static or sensile drop method, where the contact angle is measured for the advancing and receding contact angle as shown below in figure 6.

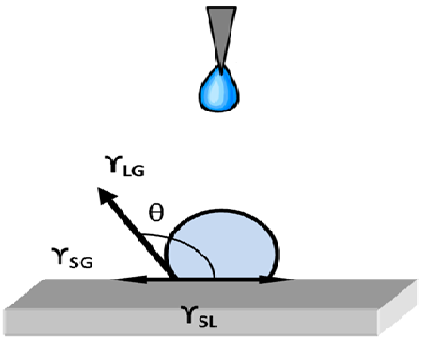

Fig. 6: Contact angle cartoon representation showing different phase contacts (solid-liquid, solid-gas, and liquid-gas).

When there is no interaction with the surface the contact angle tends to 180°, while for high interaction contact angle values go close to zero as shown in figure 7.

CONTACT ANGLE	WETTING	SOLID/LIQUID	LIQUID/LIQUID
0°	Complete	Strong	Weak
60°	High	Strong	Strong
90°	Moderate	Weak	Weak
120°	Low	Weak	Strong
180°	None	Weak	Strong

Fig. 7: Different wetabilities form different contact angles.

A sequence of the contact angle characterization of SWCNT-based electrodes is showed below (see figure 8).

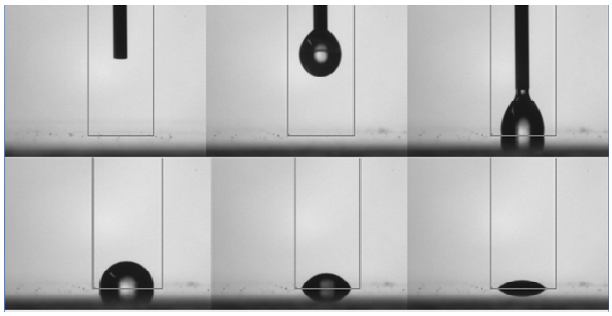

Fig. 8: Contact angle measurement of a SWCNT film deposited on glass.

During the present study a contact angle equipment from CRPP-CNRS, Pessac, was used. The static drop method with water was used to measure the contact angle of SWCNT devices before and after chemical treatment of the surface.

2.5. X- RAY PHOTOELECTRON SPECTROSCOPY (XPS)

This spectroscopic technique was developed in the fifties by K. Siegbahn, which received the novel prize for this work in 1981.

XPS analysis allows the measurement of binding energies variation resulting from the chemical environment present on the sample surface. The advantages of XPS lead to chemical nature and electronic state of elements information for most elements except hydrogen.

Matter is made of atoms, and these are made of nuclei and electrons moving around them with defined orbits. Each electron carries unique information regarding its nucleus. The goal on XPS is to collect them in order to identify from which atom they proceed. For that purpose, it is nessesary to separate

them from the attractive nucleus force upon excitation with an X-ray source. The energy will be sufficient to free them from the nucleus and they will travel through the matter reaching the surface and furthermore, leaving the solid matter to the surrounding vacuum. Once there, they will be collected by the analyzer and classified according to their unique informations.

The binding energy expressed in the spectra is the binding energy of collected electrons before leaving the atom. Each energy is related to a specific atom, as for example carbon: 286 eV, Oxygen: 532.5 eV, and so on. The peak area is proportional to the number of atoms present on the surface and a chemical composition analysis can be calculated in therms of atomic percentage (%).

Sample needs to be prepared before data aquisition ranging from few milimeters up to few centimeters depending on the equipment used.

After its preparation, the sample is introduced in a preparation chamber where the vacuum values reached are below 10^{-7} mbar and usually is left overnight to reach such values. After successful vacuum is achieved, the sample is transferred to a second chamber called the analysis chamber, where vacuum reaches limits ~ 10^{-11} mbar.

While the electron leaves the matter it can suffer interactions (shocks) which change its energy. This effect contributes to the background noise to grow up. On the other hand, the electrons who leave the matter without suffering an inelastic interaction form the collection of peaks. This effect of background noise is related to the thickness of matter crossed by the electron.

Scan aquisitions allow to identify different chemical components and bonding nature on the sample surface. To obtain this last information about chemical

bonds, it is necessary to define different aquisition windows for each indivual component. As it is showed in figure 9 for an XPS analysis of a modified SWCNT-film surface, the adquisiton done in *0.1 eV* steps allows a modelling study for each element in particular and its chemical contributions.

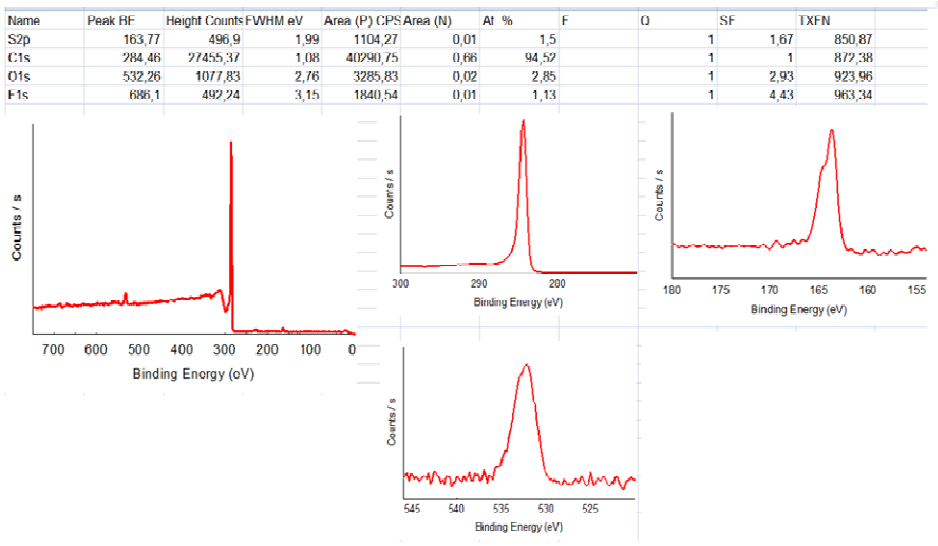

Fig. 9: XPS analysis of a surface modified SWCNT-based electrode showing the main aquisition spectra (left), and the aquisition windows for carbon 1s, oxygen 1s, and sulfur 2p (right). Peak values are shown in the table above.

Here it is shown an aquisition window for C, O, S, and F obtaining quantitavite and qualitative information of sample surface.

XPS analysis of SWCNT and graphene-based electrodes were performed in the Institut de Chimie de la matière condensée de Bordeaux (ICMCB), Pessac. As we worked with conducting samples no coating was needed. Sample size was ~ 1 cm^2 and was usually left overnight in the first chamber before being introduce in the analyzer chamber were the data was collected.

2.6. RAMAN SPECTROSCOPY

Photons can be absorbed and emitted by molecules, but besides they may also be **scattered**. The molecular effect responsible of such phenomenon is explained as follows. Scattering means the deviation of light from its original (straight) trajectory. Most of this scattered light is being scattered elastically, also named Rayleigh scattering, and a tiny amount is inelastically scattered. This inelastic scattering is defined as the event where the energy of the incident radiation is transferred between the scattered phonon and a state of the molecule (rotational, vibrational, or a phonon in the crystal lattice). The dipole scattering was calculated by Lord Rayleigh to be inferior to the λ scatter by the relation $1/\lambda^4$.

In Raman scattering the energy of the incident photon and the energy of the resulting one are different.

The difference can be higher in energy upon electron gain of energy from the molecule, or lower upon electron loss of energy from the molecule. These are described as Stokes and Anti-Stokes lines in the Raman spectra situated at higher and lower energy respectively in respect to Rayleigh scatter (see figure 10).

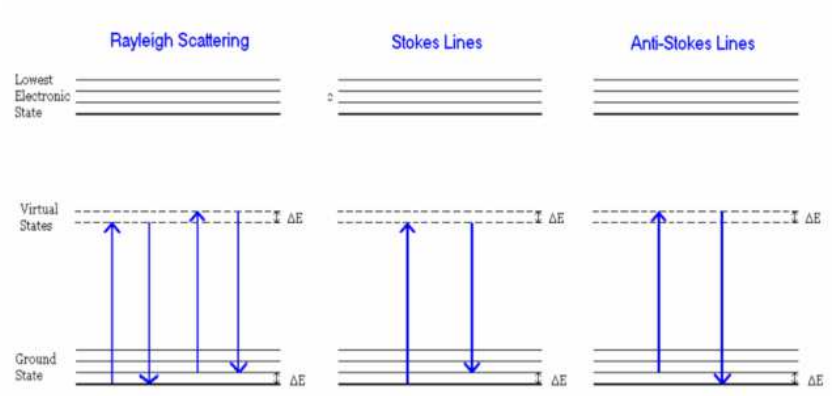

Fig. 10: Scattering of light representation and different stokes and anti-stokes lines.

The elastic scattering of light has been observed since the nineteenth century. The inelastic scattering instead, was not observed until 1930 by C. Raman and his fellow, receiving the Nobel Prize in physics for such discovery named since then, the Raman Effect.[69] But Raman spectroscopy took off with the introduction of the first lasers.

The scattering of light is not a dipole phenomenon as observed in infrared spectroscopy. Instead of that, it requires the presence of an electric field which induces polarization in atoms or molecules. The polarizability in atoms is described to be isotropic resulting in an elastic scattering of light or Rayleigh scattering. In molecules, the polarizability must be anisotropic and is dependent on the rotational and vibrational coordinates to be Raman active. By this selection rule, symmetric molecules can be studied by Raman spectroscopy. In fact, both techniques, IR and Raman, are complementary.

SWCNT Raman spectroscopy is a resonant process, where nanotube signals are enhanced by two main reasons: the incoming energy or the scattered radiation matches (or allows) electronic transitions in the sample. This intensity enhancement depends on the density of states (DOS) available for optical transitions in SWCNTs. As each individual SWCNT possess an inherent electron and phonon structure depending on the chiral vector ((n, m) indices, it is possible to determine electronic and phonon structures for specific (n, m) nanotube. Raman modes of metallic-SWCNT were published by M.S. Dresselhaus, Smalley, Pimenta and coworkers in 1998.[70] In 2003, M.S. Dresselhaus, et al.[71] reviewed Raman spectroscopy as an important tool for carbon material characterization.

In 2005, M. Burghard reviewed electronic and vibrational properties of covalent and non-covalent modified SWCNTs.[72] R. Graupner have reviewed a year later the Raman spectroscopy of covalently modified SWCNTs.[73] C. Fantini, M.A. Pimenta, and M.S. Strano published in 2008 the Raman spectra of covalently functionalized SWCNTs where they showed an electron-phonon coupling responsible of the intensity enhancement observed in some features of the spectra.[74]

A recent review on Raman spectroscopy of graphene and nanotubes was published in 2011 by Saito, Hofmann, Dresselhaus and coworkers summing up recent advances and some basics regarding the use of Raman spectra for the study of graphene and nanotubes materials.[75]

CHARACTERISTIC FEATURES OF SWCNTS RAMAN SPECTROSCOPY AND VARIATION OF THE INTENSITIES UPON FUNCTIONALIZATION

SWCNTs have characteristic features in Raman spectroscopy. Here we will describe what these features represent and which are the variations observed after surface modification of the SWCNT-based electrodes.

Radial Breathing Modes (RBMs)

They are observed at small Raman shifts and are the low energy modes observed in SWCNTs. They range from ~ 150 to ~250 cm^{-1} and are observed upon elastically scattered laser light in tubes ranging ~ 1-2 *nm* in diameter. They are called breathing modes because all carbon atoms of the tube structure vibrate radially in phase as the act of breathing. The frequency of these modes is dependent on tube diameter, and independent on the chirality of the tube (n, m). The dependence with tube diameter[76] can be described as,

$$\omega_{RBM} = \frac{A}{d} + B$$

Being A and B two constants determined experimentally. This relation is not valid for tubes diameter smaller than 1 nm or higher than 2 nm. In the case of < 1*nm* tubes, the dependence is not valid due to distortions in the tube structures resulting in a chirality dependence. For tubes with diameters > 2 *nm* the intensity of RBMs is not easily observed resulting in weak bands.

M. Strano and coworkers were pioneers in their work for the selective surface modification of SWCNTs and Raman characterization by characterizing changes on the RBMs (see figure 11).[77]

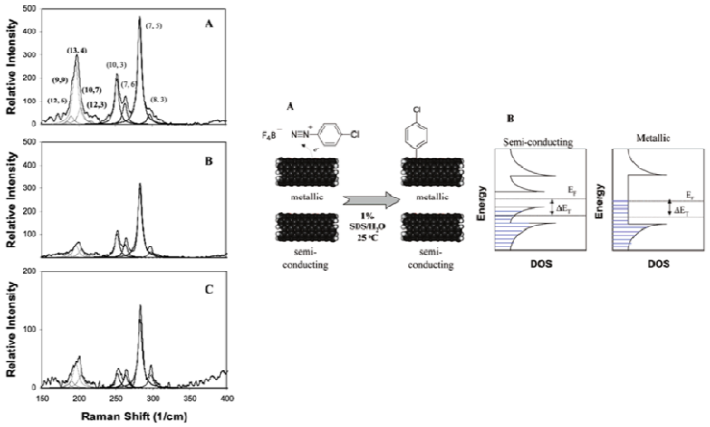

Fig. 11: RBM Raman spectra for pristine and surface modified SWCNTs showing differences in bands related to metallic nanotubes.[77]

At the same time, the grafting of aryl diazonium salts shows to be selective for metallic nanotubes rather than for semiconducting.

Tangential modes-G band

Tangential modes of SWCNT include the G-band. It results a widely studied feature (see figure 12). G comes from **G**raphite, typically observed at ~ 1600 cm^{-1}.

For graphite, a high-intense Raman-active tangential mode is observed at 1582 cm^{-1}; in a SWCNT, this mode results in a multi-peak feature depending on metallicity or semiconducting behavior of tubes. An analysis can be done

considering the two main peaks originated upon symmetry break of original G-band (graphene original sheet before wrapping up to form the nanotube).[75]

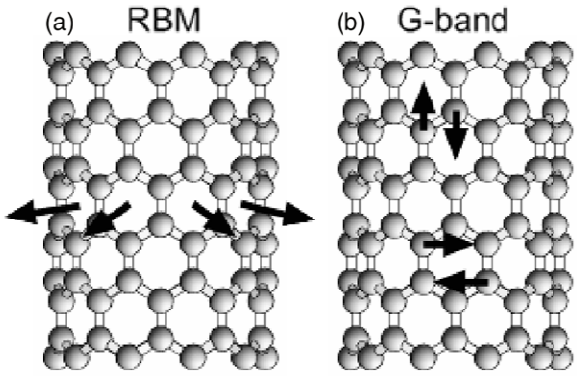

Fig. 12: RBMs and tangential modes of SWCNTs. Arrows indicate direction of vibrations. From: New J. Phys., 2003, 5, 139.1-139.17.

Disorder-induced D band

D-band has its origins in a double resonance process involving an inelastic scattering by a phonon, and an elastic scattering by a defect (observed at ~1300 cm^{-1}). The intensity of this feature increases with increasing structural disorder. It is usual to observe D-band over G-band integrated areas expresions, as a representation of the amount of defects (sp^3 hybridation carbon atoms) on the surface of the tubes.[74] In 2010, M.S. Strano and coworkers probed electrochemically modified graphene with aryl diazonium salts upon Raman spectroscopy.[78] It was explained that graphene, opposite than for SWCNTs, is not an enhancing resonant process, but instead could be used as a measure of the functionalization degree.

For the case of non-modified graphene samples, the D-band at the edges of the sheet showed a strong dependence on the polarization of the incident light, which was irreversively lost after surface modification. This phenomenon indicated that defects created upon attachment of functional groups are the main contribution to the D-band in the spectra.

D-band second-order overtone: 2D-band or G' band

This feature appears in the range of 2500-2900 cm^{-1} and shows a strong dispersive behavior depending on the excitation energy, opposite to what is observed for RBMs or G-band. Opposite to what is observed for D-band features, the 2D-band do not requires an static defect scattering process to be observed. Experimental results have shown that, semiconducting and metallic CNTs in resonance with the incident photon exhibits a D- and 2D-band features in addition to RBMs and tangential modes.

During the present study an Xplora confocal Raman microscope from HORIBA scientific has been used for all samples characterization (see figure 13). All the measurements were done using an excitation laser of *532 nm*, otherwise it will be specified along with the text.

Fig. 13: Xplora confocal Raman microscope. From HORIBA scientific.

All measurements showed were performed at CRPP-CNRS, Pessac. Three different excitation laser were available*: 532, 638* and *785 nm* wavelength with *2.33 eV*, *1.95 eV*, and *1.6 eV* respectively.

2.7. ELECTROCHEMICAL TECHNIQUES

Electrochemistry has its historical derivation from the studies of Alessandro Volta (1745-1827), a brilliant physicist of the University of Pavia, which in 1800 invented the electric battery. The inspiration of his studies probably came from the famous frog leg experiments of Luigi Galvani (1737-1798), physician and anatomist of the University of Bologna (see figure 14).

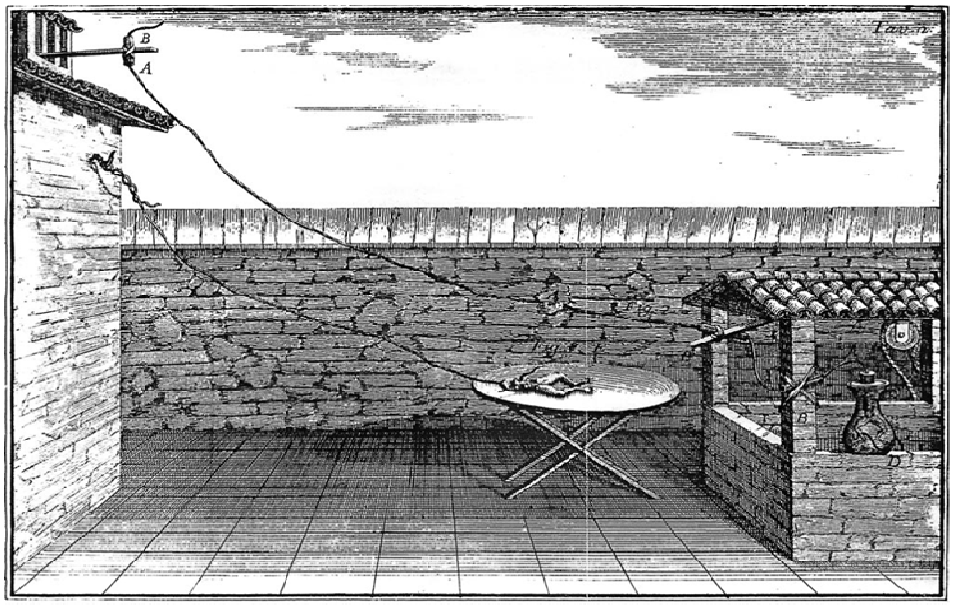

Fig. 14: Plate II of the Commentarius (1791): The experiment with the stormy atmospheric electricity.

From his studies on the effects of electricity on frogs, the scientist of Bologna L. Galvani derived his hypothesis that animal tissues are endowed with intrinsic electricity that is involved in fundamental physiological processes such as nerve conduction and muscle contraction in his main work, Viribus electricitatis in motu musculari (1791)[79] summarizing and discussing more than 10 years of research on the effect of the electricity on frogs mostly.

Volta's experiments led to the invention of the electrical battery as well as the famous voltaic pile opening a pathway to tremendous development of the physical investigations of electricity, electrochemistry, electromagnetism and related phenomena. Galvani, in the other hand, established the foundations of Electrophysiology. Alessandro Volta is immortalized in the unit *volt*, a nomenclature that dates back to 1881.

In 1820, Hans Christian Ørsted observed the magnetic effect of electric current, and following this contribution, A. M. Ampère contributed formulating his findings mathematically. The German physicist Georg Ohm introduced a law connecting voltage, current, and resistance in 1827, the Ohm's law which later on, was considered as fundamental importance in electrical circuit analysis.

Rudolph Marcus (b. 1923) won the Nobel Prize in Chemistry for his theory of electron transfer in chemical systems in 1992.[80–85]

Today electrochemistry is a rigorous science concerned with the quantitative relations among the chemical, surface, and electrical properties of systems that greatly profited from the huge advances in material science and technology.

In electrochemical systems, processes and factors that affect the transport of charge across the interface between an electrode and an electrolyte are studied. This electrode/electrolyte interface and the events that occur when an electric potential is applied and a current flows, will be explained in the following. Later on, the electrochemical techniques used for the characterization of samples during this study will be explained.

ELECTRODE PROCESSES

Charge (q) is expressed in units of Coulombs (C), where 1 *C* is equivalent to 6,24 X 10^{18} electrons. It is transported through the electrode upon electrons movement and holes. Typical electrodes include solid and liquid metals, semiconductors, and carbon. In the case of electrolytic phase, the charge is

carried by the movement of ions being the most used, liquid solutions containing ion species, either in water or in a non aqueous solvent.

Solvent-Electrolyte system should be sufficiently low in resistance in order to be useful during the measurements. Instead of approaching the idea of events at a single interface which is not easy to deal with experimentally, one must study the properties of collections of interfaces called *electrochemical cells*, defined by two electrodes separated by at least one electrolytic phase.

The overall chemical reaction in a cell is made up of two independent half-reactions describing the real chemical changes at the two electrodes surface, each of them, responding to the interfacial potential difference at the corresponding electrode. For the study of the reaction occurring at the **working - or indicator - electrode**, a three electrode configuration is usually adopted, where the **secondary –or counter-electrode** closes the circuit while the **reference electrode**, having constant composition, allows to decouple the potential difference across the electrochemical cell, and controls the working electrode potential.

Driving the electrode to high enough negative potentials the energy of electrons is raised to the point of being able to transfer into vacant electronic states on electrolyte species resulting in a flow of electrons to the solution: a reduction current. Following the same principle, the energy of electrons can be low down imposing a positive potential which will present a more favorable energy state for electrons on the electrode and they will flow right there: an oxidation current. The critical potentials at which these processes occur are related to the standard potentials (E^0) for the specific chemical substances in the system.

The number of electrons that cross an interface is related stoichiometrically to the extent of chemical reaction as the amount of product consumed and the product generated. The number of electrons is measured in terms of total charge, *Q*, which had passed in the circuit.

The relationship between charge and amount of product formed is given by **Faraday's law** where the passage of 96,485.4 *C* causes one equivalent of reaction as consumption/production of 1 *mole* of reactant/product in a 1-electron reaction. The current, i, is the rate of flow of electrons (coulombs) being a current of 1 ampere (A) equivalent to 1 *C/s*. When plotting the current as a function of the potential, a current-potential curve is obtained. It can be quite informative about the nature of the solution and the electrodes as well as about reactions that occur at the interfaces. Since these reactions are governed by Faraday's law they are called **faradaic processes**.

Besides Faradaic processes the electrochemical interface is also characterized by a capacitive behavior.

At a given potential, there will exist a charge on the metallic electrode q^M, and a charge in the solution q^S, respecting that at any time $q^M = - q^S$. This entire array of charged species and oriented dipoles existing at the metal-solution interface is named the **<<electrical double layer>>** (see figure 15).

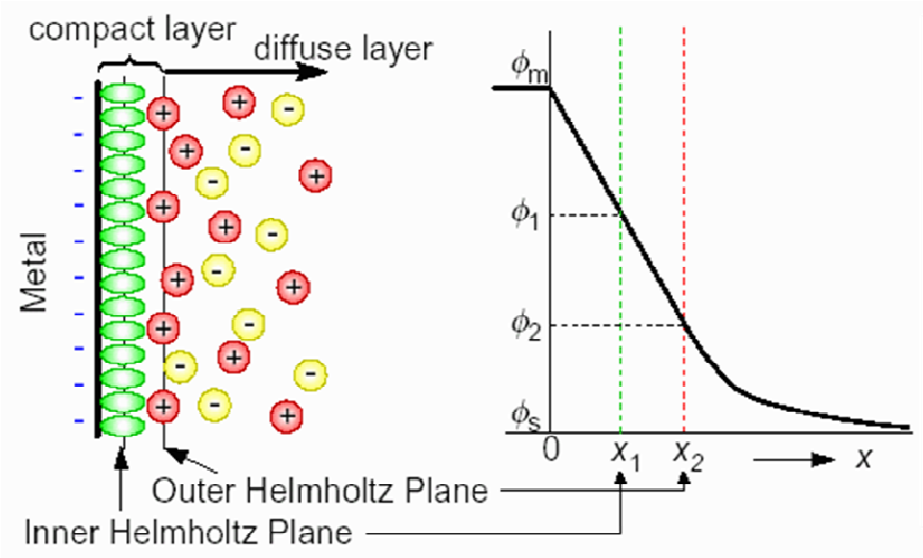

Fig. 15: Representation of the electrical double layer at the interface metal-solution.

An electrode process is a heterogeneous reaction occurring only at the electrode-electrolyte interface. The corresponding rate depends on the mass transfer to the electrode and various surface effects in addition to kinetic variables, and it is usually described in units of mol/s per unit area, where j is the current density expressed in (A/cm^2).

$$\boldsymbol{Rate(mols^{-1}cm^{-2}) = \frac{i}{nFA} = \frac{j}{nF}}$$

The electrode reaction rate considering an overall electrode reaction $\boldsymbol{O + ne \leftrightarrows R}$ composed of several steps that causes the conversion of oxidized O dissolved species to a reduced form R, will be governed by the rates

of the following processes. Some of these rates constants depend upon the potential.

- ✓ The mass transfer from the bulk solution to the electrode surface of O species.
- ✓ The electron transfer at the electrode surface.
- ✓ The chemical reactions previous or after the electron transfer.
- ✓ Surface reactions like adsorption, desorption, or electro-deposition (crystallization).

If an electrode process involves only fast heterogeneous charge-transfer kinetics and mobile, reversible homogeneous reactions, the last can be regarded as being at equilibrium and the surface concentration of species involved in the faradaic process are related to the electrode potential by a Nernstian equation, where the net rate of the electrode reaction, v_r, is totally governed by the rate of electroactive species moving to the surface by mass transport.

$$\boldsymbol{v_r = v_{mt} = \frac{i}{nFA}}$$

Mass transfer is the movement of material from one location in solution to another upon differences in chemical or electrical potential at the two locations or upon movement of a volume element in solution. The modes of mass transfer are shown and explained as follows.

- ✓ Migration. The movement of a charge body under the influence of an electric field: a gradient of electrical potential.
- ✓ Diffusion. The movement of species under the influence of a gradient of chemical potential: a concentration gradient.
- ✓ Convection. Stirring or hydrodynamic transport: natural convection of fluids caused by density gradients and forced convection.

Electrochemical systems are usually designed being possible to rend negligible one or more of the contributions to mass transfer. For example, by addition of a supporting electrolite at a concentration much larger (80 to 100 times larger) that that of electroactive species, the migrational component, can be reduced to negligible. At the same time, by preventing stirring and vibrations in the cell during the measurements, the convection component can be avoided.

CYCLIC VOLTAMMETRY

The potential of a stationary working electrode changes lineary with time. Starting from a potential where no electrode reaction occurs, it will be driven to potentials where reduction or oxidation of a solute occurs (see figure 16).

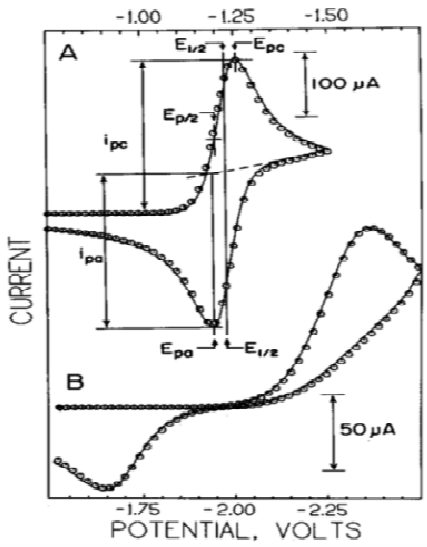

Fig. 16: Cyclic voltammograms showing main important parameters: the cathodic and anodic peak potentials (E_{pc} and E_{pa}), the cathodic and anodic peak currents (i_{pc} and i_{pa}), the cathodic half-peak potential ($E_{p/2}$) and the half-wave potential ($E_{1/2}$).[86]

After traversing the potential region in which desired reactions take place, the direction of the linear sweep is reversed and the electrode reactions of intermediates or products (formed during the forward scan) can be detected. The time scale of the experiment is controlled by the scan rate and the total potential traversed can be varied over the range of 10-10^{-3} s. A supporting electrolyte maintains the migration of charged reactants and products.

The anodic and cathodic peak currents are expressed by the relations

$$i_{pa} = 2.6910^5 n^{3/2} C_O^* \sqrt{D_O v}$$

$$i_{pc} = 2.6910^5 n^{3/2} C_R^* \sqrt{D_R v}$$

v is the scan rate of the reaction. Anodic and cathodic peak potentials are dependent on the half-wave potential $E_{1/2}$ as follows

$$\left|E_p - E_{1/2}\right| = 1.15\frac{RT}{nF}$$

the half-wave potential is expressed as,

$$E_{1/2} = \frac{E_{pc} + E_{pa}}{2}$$

The peak current is directly proportional to the square root of the scan rate, $i_p \propto \sqrt{v}$, and varies linearly with the value of concentration of the species in solution. The peak potential, do not depend on the concentration of electroactive species.

Conventional cyclic voltammetry is especially informative about *qualitative* aspects of an electrode process.

During the present study, chemically modified electrodes were prepared using cyclic voltammetry. The strong adsorption of species to the electrode surface will often change the electrochemical behavior of an electrode. Thick films can be formed on the electrode surface by irreversible adsorption, covalent attachment or as organized assemblies. The electrochemical surface modification with aryl diazonium salts and 1, 3- BDYT moieties will be discussed later on.

IMPEDANCE SPECTROSCOPY

To perturb the electrochemical cell with an alternating signal of small magnitude and observe the way in which the system follows the perturbation at steady state is another approach for studying electrode reactions. Some advantages of Impedance techniques are

- ✓ Experimental ability to perform precise measurements upon steady response which can be averaged to long term
- ✓ Treat the response theoretically by linearization of current-potential characteristics, and
- ✓ The measurements can be done over a wide range of frequencies: (10^4 to 10^{-6} s or 10^{-4} to 10^6 *Hz*, as 1 *Hz* = 1 s^{-1}).

Electrochemical Impedance Spectroscopy (EIS) is a technique where the cell or electrode impedance is plotted versus the frequency. It is a technique frequently used for evaluation of heterogeneous charge-transfer parameters and for the study of the double layer.

During the present thesis work, electrochemical measurements have been set in an electrochemical cell of three electrodes (see figure 17).

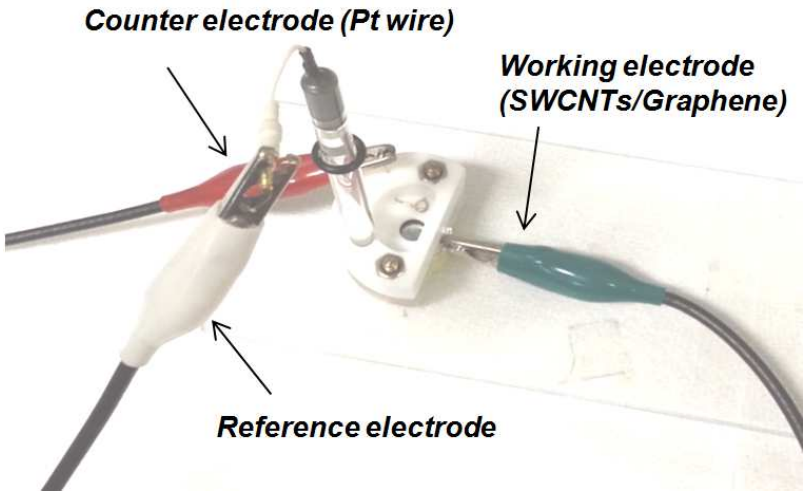

Fig. 17: Electrochemical cell used during the present study.

White was the reference electrode, red was the counter electrode, and green the working electrode made of SWCNTs or Graphene.

A CHI-potentiostat Instrument has been used during this study, being able to collect cyclic voltammograms and impedance spectra in both laboratories when needed.

Connection of the potentiostat to inert atmosphere was already set at CRPP-CNRS, Pessac, allowing measurements of air-sensitive species with no need of degas.

CHAPTER 3: SWCNT TRANSPARENT CONDUCTIVE FILMS

SWCNTs are carbon-based nanomaterials used in many field applications, for example composites, energy conversion and storage, sensors, and so on, but process them and/or prepare CNT solutions/dispersions is still a challenge for some of these applications.[87] As raw materials SWCNTs are agglomerated forming bundles upon high van der Waals forces. Those forces are difficult to counteract for separating them into individual tubes. Bundles can alter important properties in composites or SWCNT-based films so, a complete exfoliation before their use in material preparation is necessary.[88]

In 2004, at the CRPP-CNRS, Pessac, a spontaneous dissolution of a SWCN-salt in DMSO was prepared.[26] Thermodynamically stable solutions of unmodified and uncut SWCNT soluble without any sonication, surfactants or functionalization was reported.

Such polyelectrolyte salt can be filtered and deposited on alumina membranes obtaining what is defined as a film of SWCNTs; transparency will depends on the quantity of material deposited. After controlled re-oxidation, the film is handled under ambient conditions. The dissolution of the alumina in a strong

NaOH medium results in a free-standing SWCNT film that floats on the bath surface upon hydrophobic interactions.

At this moment, the deposition can be on any selected substrate, taking into account adhesion forces between the nanotubes and the substrate (higher the hydrophobicity of the substrate, higher will be the adhesion with carbon nanotubes). The result returns ready-to-use SWCNT-conductive films that will be tested as SWCNT-based electrodes.

3.1. INTRODUCTION OF THE STUDY

Previously to this study, transparent conductive films were produced and studied at CRPP-CNRS with the purpose of producing novel conducting devices which could replace actual ones like Indium Tin Oxide (ITO). Transparency was an important factor to respect as well as conductivity values.

What if we combine mechanical and electrical properties of SWCNTs with specific properties of anchored groups to create a multifunctional device? (See figure 1).

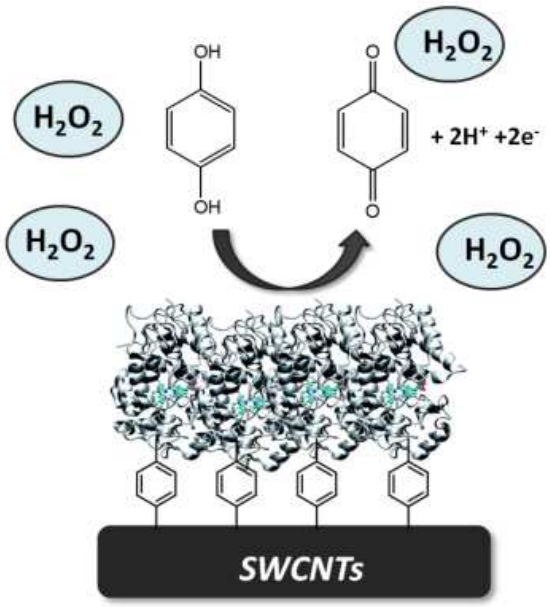

Fig. 1: Cartoon representation of modified SWCNT-based electrode.

We could produce thick films (black films; hardly transparent) made of SWCNTs with conductivity values good enough to use them as electrodes; SWCNT-based electrodes, plus the presented devices made exclusively of SWCNTs present the advantage of not presenting reactions for denaturizing proteins as it happens with metals. The study to set up a protocol for constructing a bio-sensing device by electrochemical surface modification of SWCNT films is presented.

3.1.1. SOLUTIONS OF SWCNTS

The preparation of solutions of CNTs is an air-sensitive process. During the study an Innovative Technologies Glove box was used.

SWCNT-salt preparation requires the preparation of a naphthalene salt in THF upon intercalation with metallic sodium. Naphthalene shows high reduction potential to reduce SWCNTs. After obtaining the naphthalene salt, nanotubes can be add stoichiometrically, replaced by naphthalene and resulting in a polyelectrolyte salt of nanotubes.[26,89] The stoichiometry chosen was **NaC_{10}** and naphthalene was added with 5% excess.

$$\boldsymbol{Naphthalene + Na \xrightarrow{THF} [\![Naphth^{-}Na^{+}]\!] (THF)_x}$$

Sodium was cut in small pieces after removal of the oxidized layer, added to a bottom flask and covered with some *mL* of THF. Then, naphthalene was added and dissolved in ~250 *mL* THF. A stirring magnet was added and the solution was left under reflux. After 2 hours the solution turns dark green in color due to naphthalene charges. Sodium was still visible so it was left react overnight.

The day after sodium was not reacted completely (still some traces floating on the bath) and we decided to replace it by potassium.

KC_{10}

Metallic potassium was cut in small pieces and made it react with naphthalene in ~250 *mL* of THF. A black cloud formation around potassium pieces upon reaction of the metal surface with naphthalene moieties was observed after 30 minutes of reaction. The reaction is showed below:

$$\boldsymbol{Naphthalene + K \xrightarrow{THF} [\![Naphth^{-}K^{+}]\!] (THF)_x}$$

The solution becomes dark-green after two hours under reflux as expected for the successful reaction between potassium and naphthalene moieties but, in any case, was left overnight to be sure all the potassium reacted. The obtained grams of solution (KC_{10}) contain one positive charge per potassium atom, hence one negative charge per 10 carbon atoms (KC_{10}).

$$\frac{\boldsymbol{N_{K^+}}}{\boldsymbol{g\ of\ solution}} = \boldsymbol{mol}(\boldsymbol{K^+})\ \boldsymbol{g^{-1}} = \frac{\boldsymbol{N_C}}{\boldsymbol{10}}$$

Single-walled carbon nanotube (SWCNT) sources

During the present study three sources of SWCNTs have been tested in order to compare properties of the resulting films. Early with the study, CoMoCAT (labeled CG200) and HipCo SWCNT (lot 0556), announced to be richer in metallic nanotubes, were used. HiPCO SWCNT commercially available from Unidym-carbon for electronics was introduced during last step of the study.

50 *mg* of single-walled carbon nanotubes were chosen to prepare the corresponding nanotube salt. Calculating number of mol of carbon (N_C) and the grams of naphthalene solution need for the salt preparation, carbon nanotubes were added to the naphthalene solution and covered with Aluminum foil to avoid light contact. Photochemical processes could be in competition during the reaction time.

$$[\boldsymbol{Naphth^-K^+}]\ (\boldsymbol{THF})_{\boldsymbol{x}} + \boldsymbol{CNTs} \rightarrow\ [\boldsymbol{K^+CNTs^-}](\boldsymbol{THF})_{\boldsymbol{X}} +\ \boldsymbol{Naphthalene}$$

The solution was filtered in a polyvinylidene difluoride membrane (PVDF) of 0.45 μm in pore size and the remaining powder was rinsed with distilled THF until filtration remains colorless. The product obtained is the SWCNT-salt. Normally the salt is placed in the antichamber overnight for the elimination of

the remaining THF. The resulting salt contains THF molecules, probably coordinated to the alkali metal as described in literature.[26]

$$(\boldsymbol{THF})_{\boldsymbol{x}}[\boldsymbol{K^{+}CNTs^{-}}]$$

Upon stirring overnight in dry DMSO a homogeneous SWCNT-salt solution is obtained. The relation used was 2 mg of SWCNT salt per mL of DMSO.

3.2. SWCNT FILMS

On Alumina membranes

For the preparation of SWCNT films, the SWCNT-salt solution in DMSO (stable in the glove box) was centrifugated in order to eliminate the insoluble part (4000 rpm/1 hour; rtc~2800). The SWCNT solution remains on the top.

The centrifuge tubes were sealed accurately to avoid oxidation of the solution when carrying them outside the glovebox. After centrifugation time, the tubes were placed back in the box and the insoluble part was eliminated. There was a partial lost into the aggregates during centrifugation for CoMoCAT SWCNTs. H-SWCNT showed higher concentration values compared with C-SWCNT films. It can be possible due to higher dissolution of HiPCO tubes vs CoMoCAT.

The concentration of the SWCNT solution was calculated by dry extract where 2.5 mL were left overnight for solvent evaporation. C-SWCNT or H-SWCNT solution concentration (*mol*/*mL*) was calculated by the relation

$$\boldsymbol{n(KC_{10}) = mg\ KC_{10}/Mw(KC_{10})}$$

Whatman Anodisc Filter Membranes (0.02 *μm* pore size; diameter=47 *mm*) from Fisher Scientific were used to prepare films of carbon nanotubes. The equipment used is shown below (see figure 2).

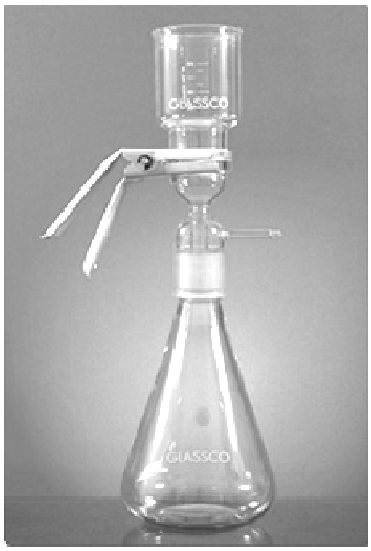

Fig. 2: Glass equipment used for the preparation of SWCNT-based electrodes.

Dilutions were prepared in clean dry DMSO per each film prepared. The resulting films were, as expected, quite transparent when using low quantities of the solution and dark (black) when larger quantities of nanotubes were used. SWCNT films on alumina membrane are kept in special labeled boxes inside the glove box until their use.

Controlled re-oxidation of SWCNT films

During re-oxidation (neutralization) of the films, they are transferred outside the glovebox and placed under a control flow of dry air. The equipment used allows to dry 4 films each time consisting in a hermetically sealed box with a

transparent wall on the top and 4 screws which connect upper and bottom part of the box. The box is connected to a dry air column that has been previously prepared. The preparation of the colum takes 2 days and consist on preparing the drying agent (in the oven under vacuum) until there is no presence of humidity.

After that, the box containing SWCNT films is opened (two valves: one left and one right) and connected slowly to the dry air column. The control in the flow of air will control films not to be damaged. Films are left to dry for at least 2 hours until complete drying.

Transfer of SWCNT films on selected substrates

The dissolution of the alumina membrane results in films made exclusively of SWCNTs. Here we used a bath of sodium hydroxide (1.5 *M*). The alumina takes 8-9 minutes to get dissolved. Time should not exceed 12 minutes otherwise SWCNTs could be damaged. After complete dissolution, the bath should be neutralized by rinsing with deionized water until pH~7. After that, the substrate must be placed at the bottom of the bath and by removing it SWCNTs will be deposited on any selected substrate. They will dry overnight in the oven at 40-50 *°C* protected from dust with a glass cover.

Substrates: problems of the study

Following precedent studies on SWCNTs film deposition, the substrates selected were Glass slides and thin film of polyethylene terephthalate (PET). Due to problems detected in Bologna when trying to characterize SWCNT surface modification by Raman spectroscopy, we were constricted to look for a new substrate that does not interact with the instrument. The flexibility was

also an important factor to consider; rigid substrates when placed in the electrochemical cell can present problems in terms of lost of conductivity due to o-ring contact and possibility of micro-break formation. Many materials were tested with solvents, Raman spectrum at different wavelengths, transparency, flexibility, etc., and polystyrene was highlighted as the best candidate for the present study.

- **Glass slides.** The adhesion of the nanotube film onto glass leads to detachment and loss. Silanization of the glass substrate results in the improvement on the adhesion forces but resulted in a significantly longer procedure, deciding to keep going with PET samples.

- **PET.** It was the perfect substrate in terms of adhesion, thickness and manipulation as well as for its resistivity to organic and non organic solvents. Polyethylene terephthalate displays Raman bands in the same region of SWNTs under specific excitation laser. At this moment of the study performed in Bologna a less-interacting substrate was need for continuing with the study of the SWCNT surface modification.

- **Polystyrene.** After collecting some candidates, Raman spectra for each material was measured at different wavelength. Polystyrene bands at 532 and 638 *nm* lasers showed not to overlap with the bands under study. The polystyrene used for this study was Polystyrene foil (0.25 *mm* thick) from Goodfellow Inc (see figure 3).

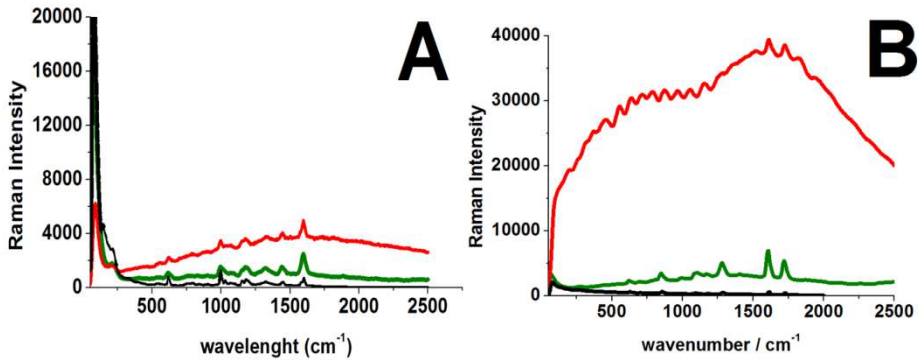

Fig. 3: Raman spectra at 532, 638 and 785 *nm* excitation laser (green, red and black lines respectively) of: (A) Polystyrene (PS) and (B) Polyethylene terephthalate (PET).

Observations

1. During HiPCO-SWCNT film preparation nanotubes passed across the alumina membrane (0.02 μm pore size). The study of the filtrated solution by Dynamic Light Scattering analysis (DLS) did not reveal the hypothesis of short tubes crossing the pore membrane. The pore size used for the SWCNT films preparation is 0.02 μm.

In order to compare original solution of SWCNTs with the filtered solution, samples were sealed with liquid parafilm (to avoid self oxidation) and left for sedimentation for three weeks. Angles from 40° to 70° were measured. It was not possible to measure bigger angles than 70° because the solution was too diluted to obtain enough results for statistics. Other method was to dropcast the filtered solution on a clean mica surface. The resulting deposition was observed by AFM but no presence of tubes was observed.

2. During the dissolution of the alumina there is a partial dissolution of SWCNT aggregates. The fact is in accordance with the idea of tubes trapped on the membrane pores during film preparation. Besides, the aspect of the film changes apparently upon formation of micro channels in the internal structure. The partial lost of nanotubes during alumina dissolution allows water to reach the surface of the SWCNT film (figure 4).

Fig. 4: HiPCO-SWCNT film (left) during dissolution of the alumina membrane and (right) after deposition in PS and dried in the oven overnight.

After drying the resulting films in the oven (overnight at <50 °C) their aspect became homogeneous. Further characterization with AFM confirmed it. Apparently, during the drying process there is a reorganization of the material. CoMoCAT SWCNT films did not show any of these particularities. The aspect of the films did not change at any moment along the process.

3.3. SWCNT FILMS CHARACTERIZATION

CoMoCAT-SWCNT (C-SWCNT) and HiPCO-SWCNT (H-SWCNT) films were studied in parallel. Dilutions of 400, 600 and 1000 *μL* of the original SWCNT solution were prepared in 50 *mL* of DMSO respectively and the resulting films containing different quantities of tubes are shown. The techniques used and the information obtained is explained as follows.

Near-Infrared absorption spectra of both films on PET were measured for the study of the characteristic spectral signatures corresponding to the respective electronic transitions of HiPCO tubes after dissolution and film preparation (see figure 5).

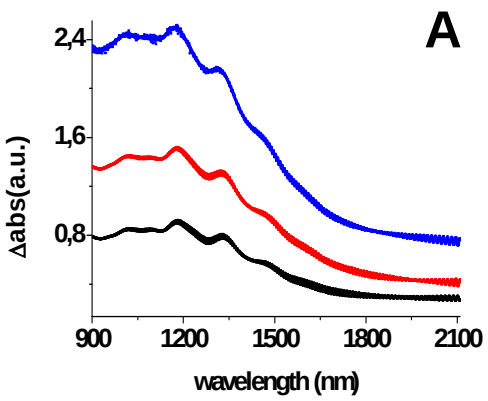

Fig.5: Near infrared absorption spectra of (from black to blue line): 400, 600 and 1000 *μL* HiPCO-SWCNT films.

In 2008, the corresponding study of individual nanotubes in DMSO solution showed S_{11} transitions of n-doped and p-dope **K [h-NT]**.[90,73] **Scanning electron microscopy** revealed the first images of the film surface. HiPCO-SWCNT surface

results to be clean and homogeneous while CoMoCAT-SWCNT surface contains catalyst residues and aggregates (see figure 6).

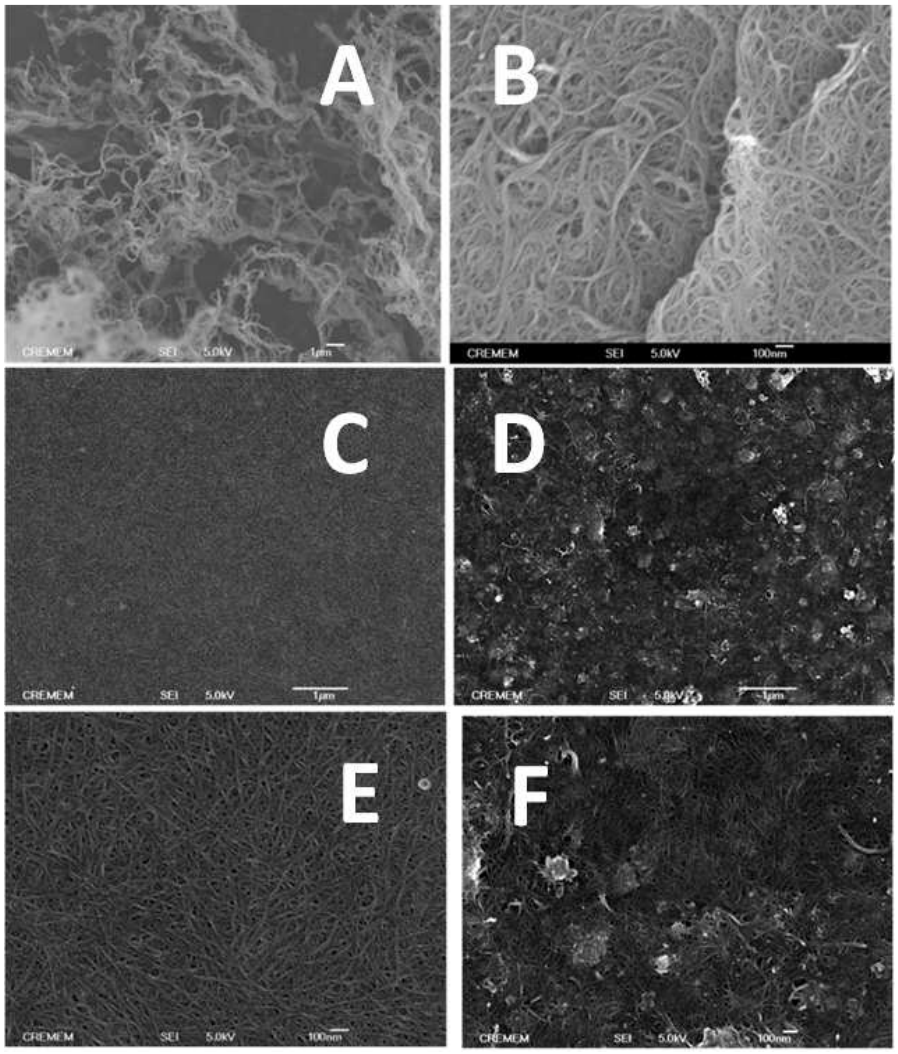

Fig. 6: Scanning electron microscopy of (a) HipCo-SWCNTs powder, (b-c) H-SWCNT film 1 *μm* and 100 *nm* scale, (d) CoMoCAT-SWCNTs powder, (e-f) C-SWCNT film 1 *μm* and 100 *nm* scale. Films were prepared with 1000 *μL* of the respective SWCNT solution.

This characterization will be important for the subsequent surface modification. Cleaner will be the surface easier would be to detect modifications. The roughness and thickness of the films was revealed by **Atomic force microscopy** (see figure 7).

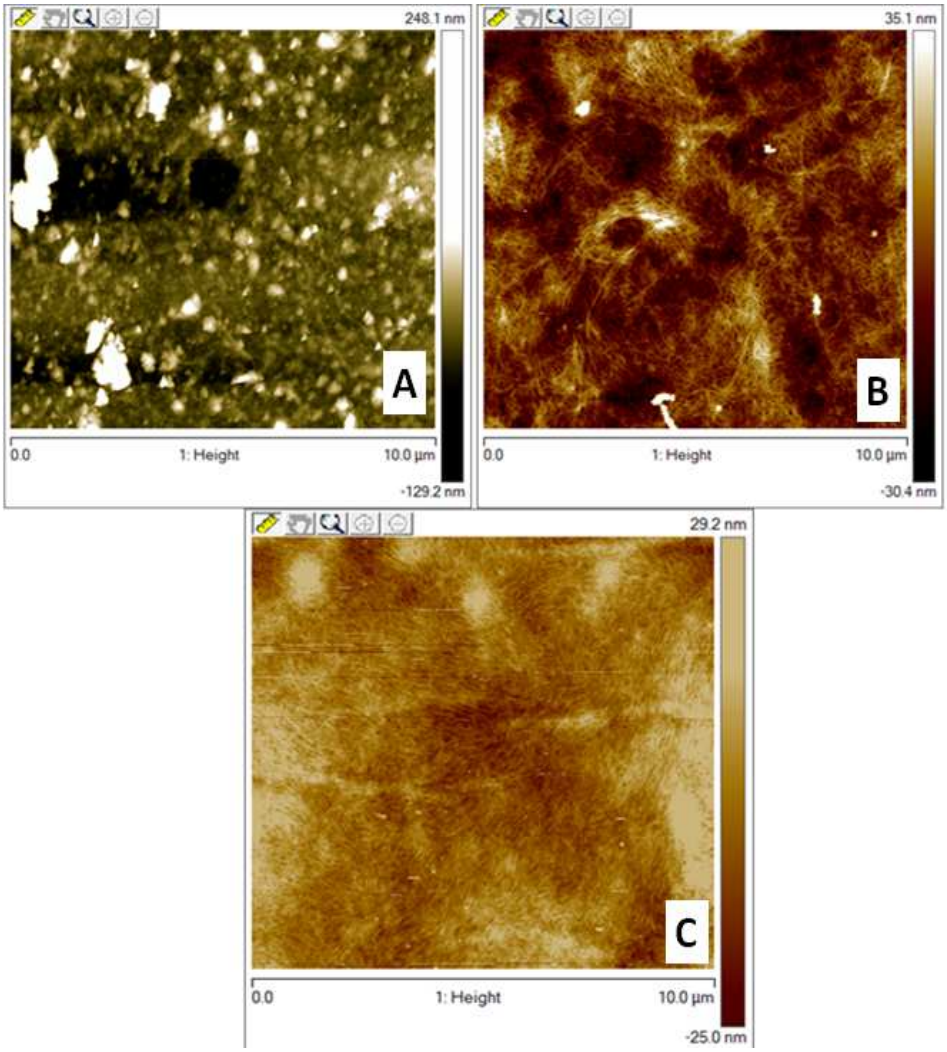

Fig. 7: Atomic force microscopy images of (A) C-SWCNTs (1000 μL) on PET; (B) H-SWCNTs (1000 μL) on PET; (C) H-SWCNTs (400 μL) on PS.

It was confirmed that SWCNT films are cleaner when they are prepared from HiPCO-SWCNT solutions. In that case, the films are homogeneous and they can be described like a mat of nanotubes. The deeper zones could be formed during dissolution of the alumina membrane where tubes are partially lost. The thickness of H-SWCNT films was measured ~60-70 *nm* for films prepared with 0.58 *mg* of tubes.

Contact angle measurements will show changes in the wettability of SWCNT film surface before and after surface modification. In figure 8, it is shown a SWCNT film on glass where it is possible to observe the advancing and receding angle measured for the pristine material. Higher contact angles were found with CoMoCAT-SWCNT films.

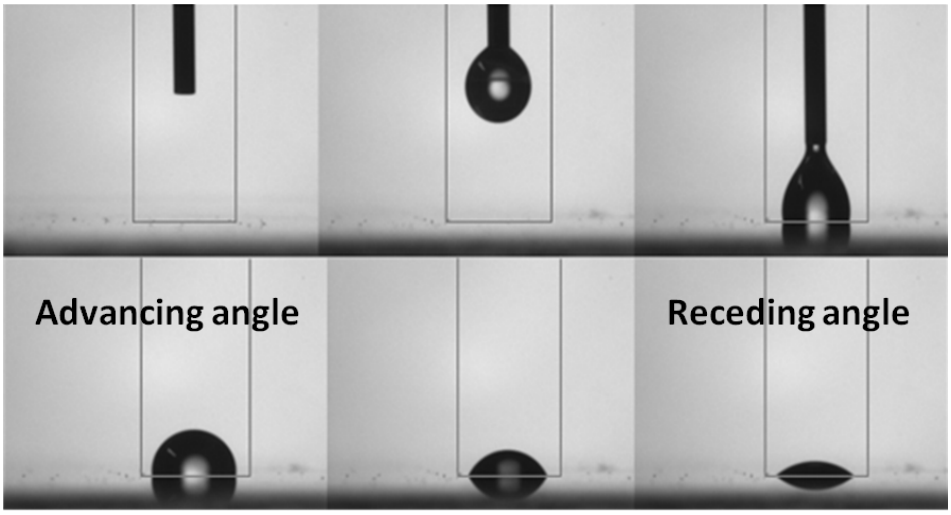

Fig. 8: Advancing and receding angles measured for HiPCO-SWCNT film on glass.

Four-point conductivity shows surface resistance values for the six films prepared (see table 1).

SWNTs	Quantity of CNTs (mg)	Resistance (Ω/□)
HipCO_solution [ ]= 1,45 mg/ml	**0,58**	**307**
	0,87	167
	1,45	84
CoMoCat_solution [ ]= 0,6 mg/ml * Much less soluble than other CNTs	**0,24**	**2300**
	0,36	939
	0,6	647

Table. 1: Different SWCNT solution concentrations and corresponding surface resistivity values (*Ω/*□) measured for the respective 400, 600, and 1000 *µL* dilutions express in quantities of tubes (*mg*).

The presented values result from an average value of several R_s values of each film prepared. The corrective factor provided for these measurements was 4.53 (numerical value of $\pi/ln2$) accepted when measuring thin (< 1*µm*) compared to large surfaces (~1 cm^2).

$$R_s = C\,\frac{V}{I} \quad ; \; C = 4.53$$

An **X-ray photoelectron spectroscopy** analysis of the film surface can give us an atomic percentage (%) of different elements present in the sample surface (see table 2). We considered the purification of raw HiPCO-SWCNTs from Unidym because the presence of catalyst was higher than for previous sources (HiPCO-0556).

Source of SWCNTs	XPS sample	Atomic (%)				
		C	O	Fe	S	Cl
HiPCO-0556	SWCNTs film	(96.33)	(2.7)	(0.82)	(0.15)	----
HiPCO-Unidym non purified	Powder	(91.35)	(6.63)	(2.02)	-----	-----
	SWCNTs film	(94.83)	(3.69)	(1.22)	(0.26)	-----
HiPCO-Unidym purified	Powder	(87.64)	(9.2)	(0.9)	-----	(1.65)
	SWCNTs film	(94.01)	(4.98)	(0.33)	(0.3)	(0.38)

Table. 2: XPS analysis of HiPCO powder and HiPCO-SWCNT films resulting from purified and non purified sources.

For HiPCO-0556 SWCNT films the amount of iron catalyst was 0.82%. The atomic % of iron on the film surface was 1.22% for films prepared with non-purified SWCNTs versus the 0.33% when the film was prepared with purified tubes. We consider that, compared to the time consumed for purifying the tubes using procedures that implies manipulation of large quantities of strong acids, was better to prepare SWCNT solutions starting from the non purified SWCNTs.

It is a fact that the preparation of the solution itself cleans the nanotubes resulting in lower atomic quantities of oxygen and iron after film preparation. The presence of sulfur could be due to reaction with DMSO during disolution of nanotubes. At this point, we considered that non-purified HiPCO-SWCNT films were the best candidates to continue with the study of the electrochemical surface modification of SWCNT-based electrodes.

Raman spectroscopy reveals information about SWCNT modes before and after their electrochemical surface modification. At low wavenumber, the main features of the Raman spectra of SWCNTs are the shifts situated between 150 and 350 cm^{-1} named the radial breathing modes (RBMs). The band situated at ~1300-1400 cm^{-1} (D-band) is responsible of the disorder induced mode of nanotubes (sp^3 carbons) and the band situated at ~1500-1600 cm^{-1} (G-band) is a tangential mode related to the degree of orden in the sp^2 system (C-C streching). More details about this technique can be found in chapter 2.

The Raman spectrum of an HiPCO-SWCNT film prepared on polystyrene substrate is shown in figure 9.

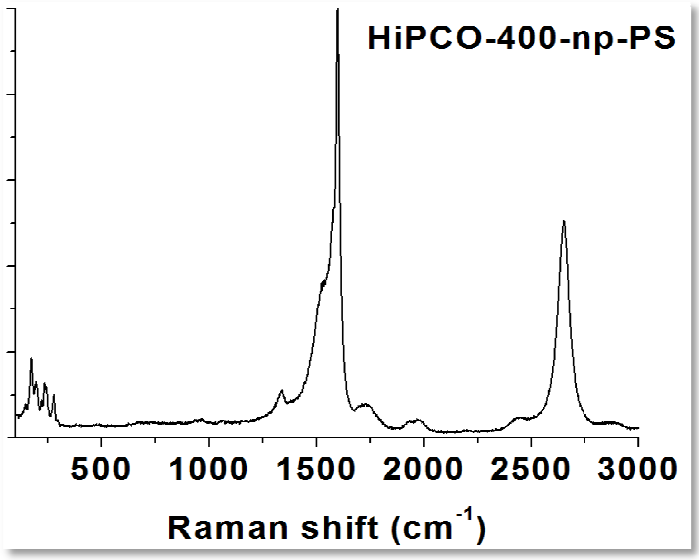

Fig. 9: Raman spectra of HiPCO-SWCNT film on polystyrene. Excitation laser used for the measurement was 532 *nm*.

SWCNT solutions and films from Rice University tubes available at CRPP-CNRS were prepared (Figure 10). Here is reported the Raman spectra of these films

showing differences on the RBMs depending on the excitation energy laser used.

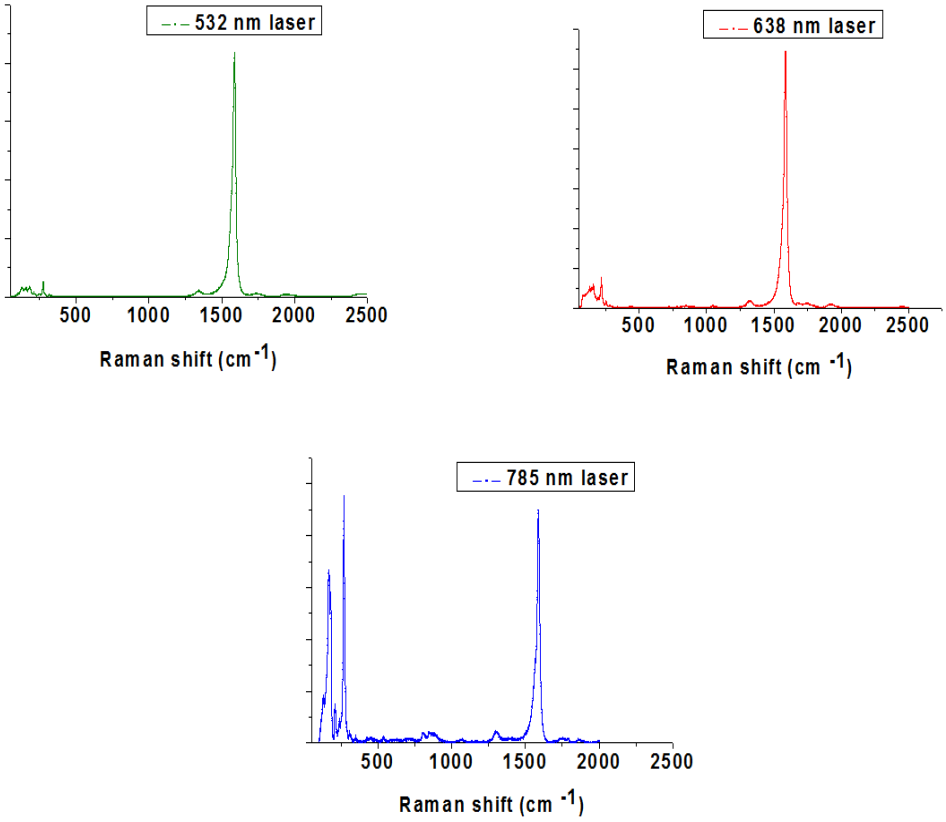

Fig. 10: Raman spectra of Rice-SWCNT film on silanize glass measured at three different excitation lasers.

They were defined to be richer in conductivity. Films were prepared on silanized glass for further Electrochemiluminescense experiments (ECL) running in Bologna at that time.

3.4. CONCLUSIONS

HiPCO and CoMoCAT SWCNT films were prepared at the CRPP-CNRS, Pessac, following described methodologies for preparing spontaneous dissolutions of SWCNTs upon intercalation chemistry performed in the same laboratory. H-SWCNT and C-SWCNT filtered solutions were deposited in thin and transparent polystyrene substrate resulting in transparent conductive hybrid films.

The characterization reveals 400 *μL* HiPCO SWCNT film to be the best candidate for further studies. This film has ~40% transparency and surface resistance values around 307 (*Ω/□*). The thickness of the film ranged between 60-70 *nm*. The surface is mainly composed by carbon atoms with a small presence of oxygen and iron species. The Raman spectra showed define RBMs as well as D- and G-band that will be considered for comparing the results after electrochemical SWCNT film surface modification.

All solutions during this time were proposed with the aim of the optimization of the SWCNT film for performing further electrochemistry on the surface in terms of homogeneity, neatness, amount of residues, substrate adhesiveness, transparency, compatibility with organic solvents, and so on. The resulting optimized SWCNT-based electrode will be modified upon selected electrochemical reactions at the surface and we will study such chemically induced disorder by several techniques.

CHAPTER 4: ELECTROCHEMICAL SURFACE MODIFICATION OF SWCNT-BASED ELECTRODES

Over this chapter we will explain the preparation and characterization of chemically modified SWCNT-based electrodes. Following the idea of setting up a sensing surface made of SWCNTs upon electrochemical modification, three precursors were chosen: EDA, PhDA, and TMS. Those molecules were selected in accordance with literature because they have been used with similar purpose of direct surface modification of carbonaceous materials through aryl diazonium chemistry. The three precursors have in common an amine group which is necessary for the formation of diazonium salts that will react with the surface of the carbon nanotubes creating new covalent bonds on the electrode surface. Moreover, the covalently linked organic moieties have a second reactive group (depending on the precursor selected) where

further chemistries can be performed. As SWCNT-based electrodes were chosen for setting up a bioconjugation protocol with the objective of preparing biosensing surfaces based on carbon nanotubes, Cu(I)-catalyzed azide-alkyne cycloaddition or "click"chemistry was selected for anchoring selected probes on the electrode surface. As a first try, HRP enzyme was immobilized on the SWCNT electrode surface.

Ongoing with the study, the surface modification of SWCNT devices with 1, 3-BDYT moieties was proposed. Getting inspiration from literature (see chapter 1) the present moiety shows to covalently link to the tubes. The possibility of performing a second substitution on the remaining carbocation and the removal of benzodithiol moiety with Nickel-Raney treatment would lead to a novel carbon-carbon bond formation on the surface of the carbon nanotube. Unexpected results were obtained and analyzed. We will try to explain them and present all data obtained ongoing with the experiments.

Before introducing the results obtained, it is important to explain that the electrochemical surface modification of SWCNT electrodes is not resulting in the formation of mono-to-few layers of organic molecules on the surface of the electrode material, but in more complicated polymeric structures with ramifications already introduced in chapter 1. In this case, more complicated structures can be observed. These can often show different electrochemical properties and may be useful, as in this study, in applications as sensors. Processes that can occur at modified electrodes are shown in figure 1,

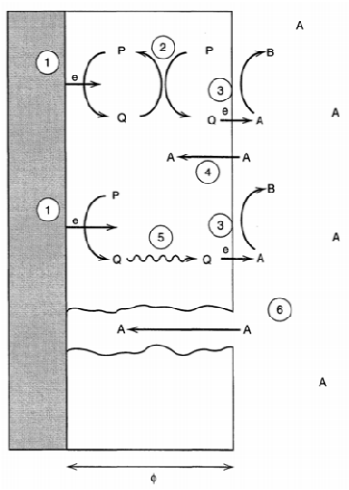

Fig. 1: Schematic diagram of processes that can occur at a modified electrode.[c]

where

1. Heterogeneous electron transfer of P to be reduced to Q.
2. Electron transfer from Q to another P in the film (electron

diffusion or hopping in the film)

3. Electron transfer from Q to A at the film/solution interface
4. Penetration of A into the film, where it can react with Q

or at the substrate film interface.

5. Mass transfer of Q within the film

[c] *Electrochemical methods: Fundamentals and applications, A. J. Bard and L. R. Faulkner, Willey, second edition.*

6. Movement of A through a pinhole or chanel in the film to

the substrate, where it can be reduced

can occur. P and Q represent reducible and oxidative species in a film electrode surface and A, species in solution.

4.1. Electrochemical surface modification with diazonium chemistry

4.1.1. Reduction of aryl diazonium salts

The experimental conditions for performing the electrochemical reduction of amino-phenyl diazonium salts on SWCNT electrodes were reproduced from literature (D. Bélanger in 2006).[38] The three precursors (see figure 2) were selected as previously explained.[37,41]

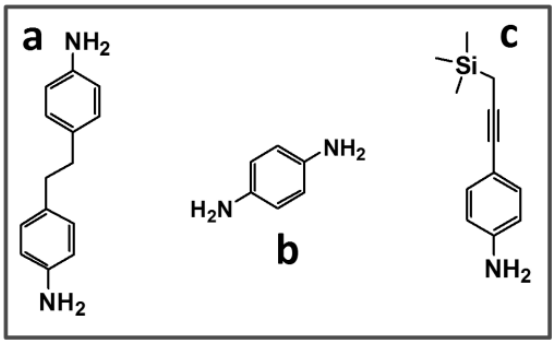

Fig.2: Aryl-amines selected for the electrochemical surface modification of SWCNT based electrodes. (a) 4, 4'- Ethylene dianiline (EDA), (b) p-Phenylenediamine (p-PhDA)., and (c) 4-[(Trimethylsilyl) ethynyl] aniline (TMS).

Due to free rotation of ethylene bonds on EDA molecules, there exists the possibility that the same grafted molecule will react with the SWCNT substrate

and thus would determine, at the end of reaction, the available quantity of amine groups on the SWCNT-based electrode surface. PhDA molecule was introduced as an alternative precursor for EDA.

The electrochemical reduction of the respective diazonium salts from EDA, PhDA, and TMS in acidic medium results in successfully modified SWCNT films monitored by cyclic voltammetry. The experimental details are explained as follows.

5 *mM* solutions of EDA, PhDA, and TMS, were prepared in acidic medium HCl, $5 \times 10^{-2} M$ (10 *mL*). At the same time, 0.1 *M* sodium nitrite aqueous solution ($NaNO_2$, needed for the diazotation reaction) was prepared. The mono diazonium salts were formed in situ upon addition of $NaNO_2$ solution to the amino phenyl solution resulting in the described compounds:

EDA: $\boldsymbol{2Cl^-_3^+HN - C_6H_4 - CH_2 - CH_2 - C_6H_4 - N_2^+}$

PhDA: $\boldsymbol{2Cl^-_3^+HN - C_6H_4 - N_2^+}$

TMS: $\boldsymbol{(CH_3)Si - C \equiv C - C_6H_4 - N_2^+}$

EDA, PhDA, and **TMS** solutions were placed in the electrochemical cell and the sodium nitrite was added obtaining an intense yellow solution. The electrografting of the three different diazonium salts was monitored by cyclic voltammetry from the open circuit potential (E_{ocp}) to -0.2 *V* versus an Ag/AgCl reference eletrode with 20 cycles at 50 $mV\ s^{-1}$. After that, samples were generously washed with distilled water in order to eliminate any adsorbed species. The respective cyclic voltammetries (see figure 3) showed different dynamics of reaction during the process. A passivated electrode behavior was obtained after ~ 6 potential cycles.

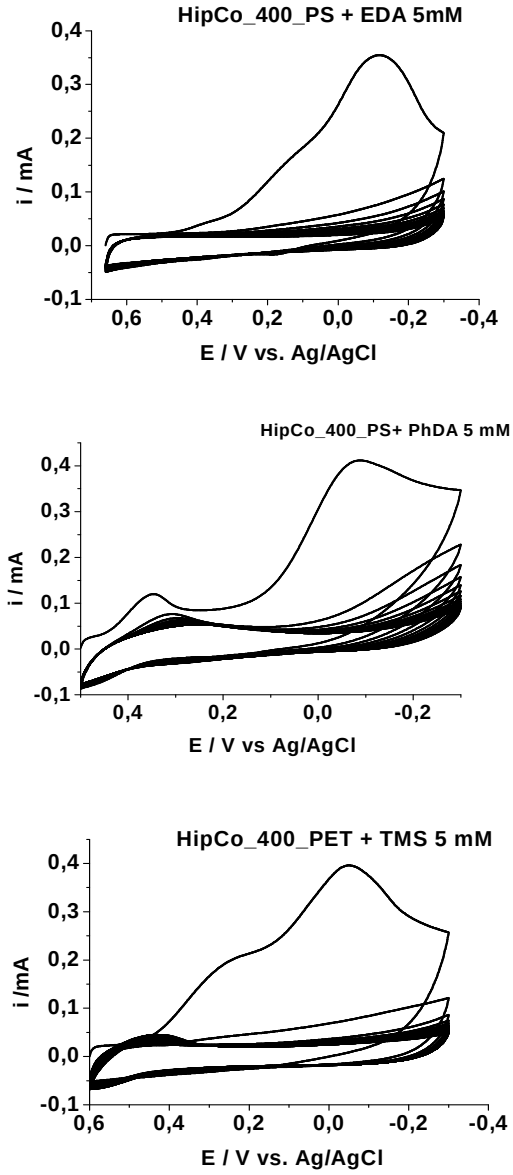

Fig. 3: Cyclic voltammetries for the electrochemical surface modification of SWCNT-based electrode with aryl diazonium salts (5 mM in HCl). Cyclic voltammetry was run at 50 mV s^{-1} until surface passivation (~6 cycles).

SWCNT-based electrodes were characterized before and after surface modification upon monitoring the electrochemical redox process of the mixture potassium ferricyanide/ferrocyanide ($3^-/4^-$) at the electrode surface. Cyclic voltammetry and impedance spectroscopy of EDA modified surface are shown in figure 4a and 4b.

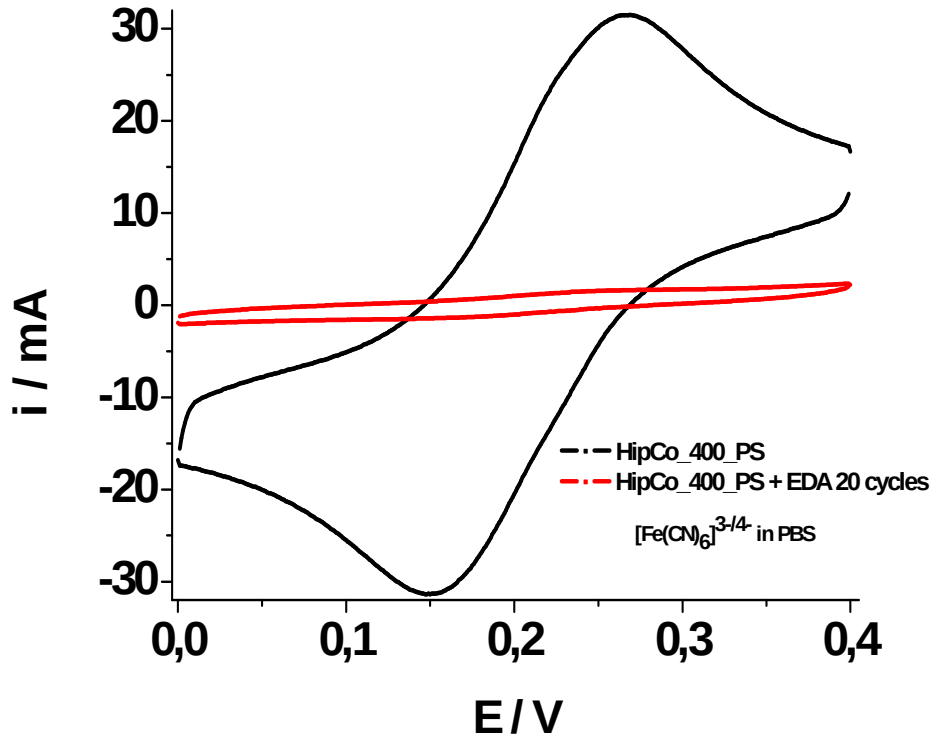

Fig. 4a: Cyclic voltammetry of $K_x[Fe(CN)_6]^{3-/4-}$ at the electrode surface before (black line) and after (red line) electrochemical modification with 5 *mM* EDA in PBS; scan rate 100 *mV* s^{-1}

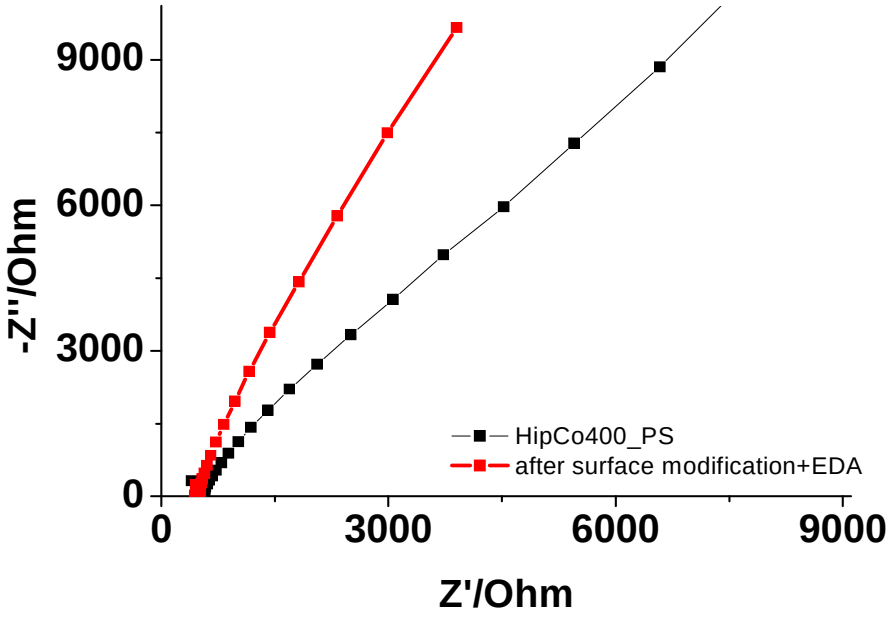

Fig. 4b: Impedance spectra of $K_x[Fe(CN)_6]^{3-/4-}$ at the electrode surface before (black line) and after (red line) electrochemical modification with 5 *mM* EDA in PBS; scan rate 100 *mV* s^{-1}.

Shortly, the black line shows the response for the redox process of $K_x[Fe(CN)_6]^{3-/4-}$ at the electrode surface before any treatment. A reversible wave is observed, defining a half-wave potential $E_{1/2}$ = 0.2 *V*; the scan rate was 100 *mV* s^{-1}. After surface modification (red line) processes are still visible but current values have diminished significantly upon formation of a thin layer on the electrode surface which makes the electron transfer slower to occur. In accordance to that, impedance spectra results show higher charge transfer resistance values for the modified surface of SWCNT electrodes compared with the pristine material.

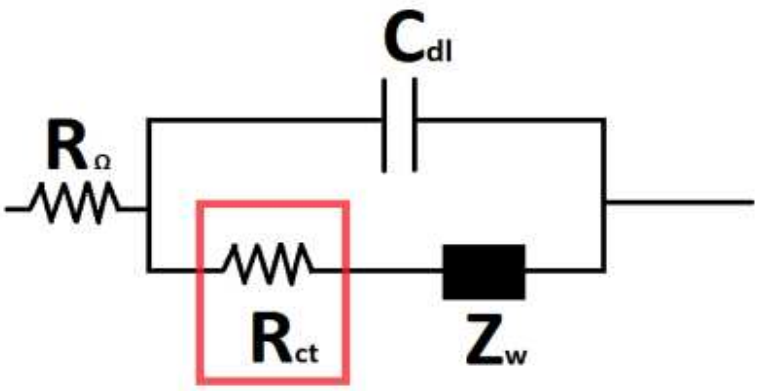

Scheme 1: Representation of the electrochemical circuit system under study where R_Ω is the SWCNT film resistance, R_{ct} is the resistance to charge transfer, C_{dl} is the double layer capacitance, and Z_w is the semi-infinite Warburg element.

The contact angle measured for the electrode surface after modification with EDA (and PhDA) moieties was smaller compared to the unmodified material in both cases (see figure 5). This was expected after introducing hydrofilic moieties on the film surface. Opposite to that, TMS modified film shows higher contact angle due to the contribution of hydrophobic moieties (-$Si(CH_3)_3$).

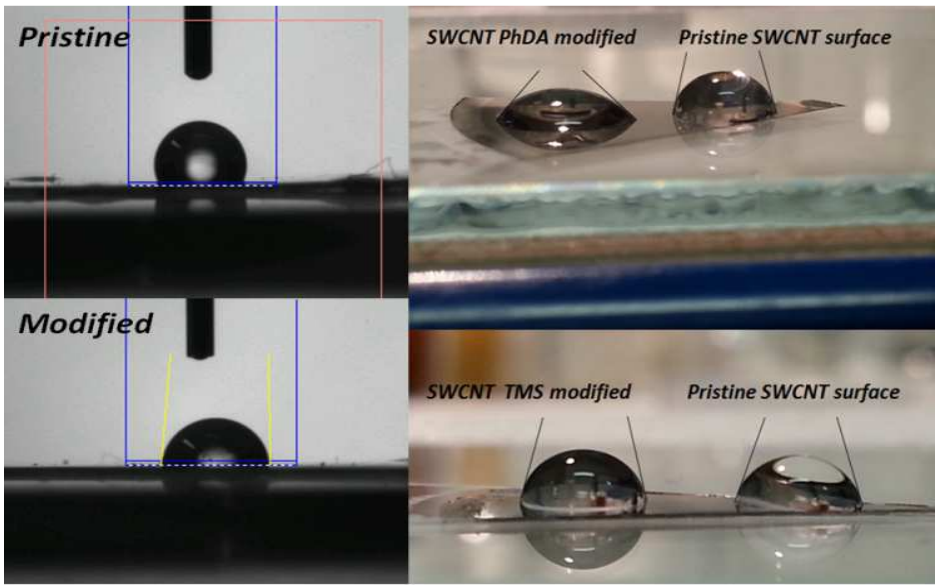

Fig. 5: Left: Contact angle measured before and after the electrochemical surface modification of SWCNT-based electrodes (on glass) with EDA moieties. Right: Pictures took after SWCNT-based electrodes (on polystyrene) surface modification with PhDA (above) and TMS (below).

The modified films with different precursors were characterized by Raman spectroscopy in order to identify changes on main features of the SWCNT electrode surface. In particular the band situated at ~1300 cm^{-1} (D-band) would demonstrate the creation of covalent bonds at the nanotube surface upon changes on the relative intensities in respect to the G-band situated at ~1600 cm^{-1}. The results obtained are shown in figure 6. Notice that the set up of the experiments allows the characterization of pristine and modified material of the same sample.

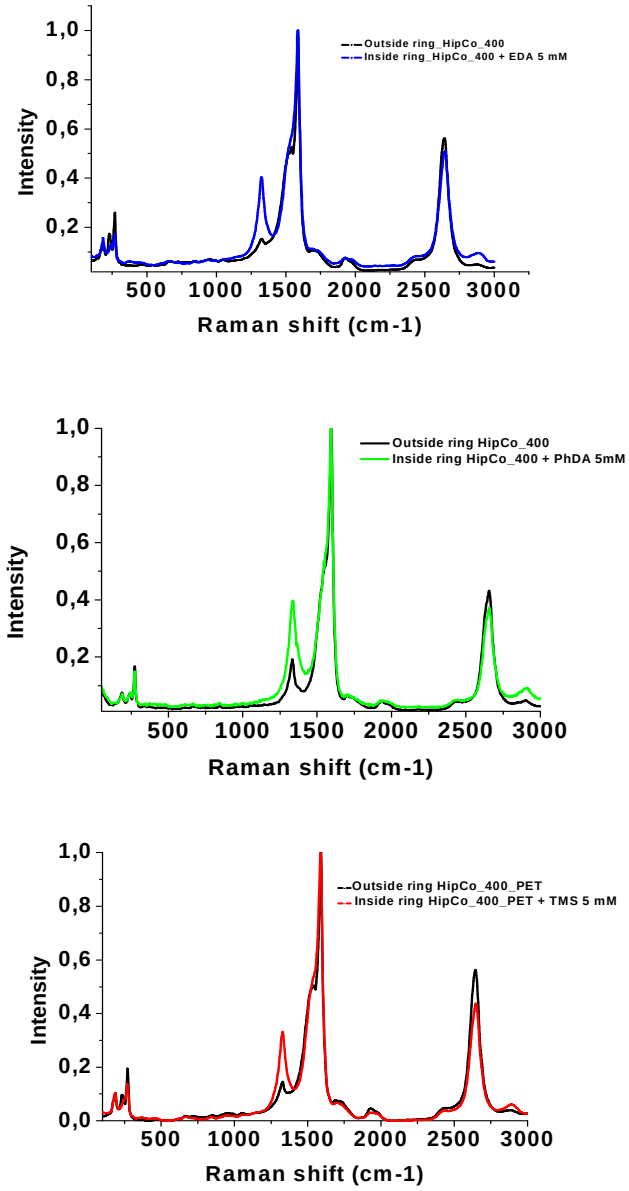

Fig. 6: Raman spectra for the three different surface modifications of SWCNT-based electrodes. All the measurements were done with a 532 *nm* excitation laser.

A large increase in the intensity of the D-band with respect to the G-band is evident for all three cases, indicative of breaking the symmetry of the tube surface (sp^2 hybridation) upon formation of covalent bonds between the tubes and the molecules (sp^3 hybridation). The second phonon of the D-band, the 2D-band, situated at ~ 2600 cm^{-1} shows a decrease in the intensity along with changes of the D-band (see figure 6). It is known that this band shows changes upon changes on the D-band (see Raman spectroscopy in chapter 2).

X-ray photoelectron spectroscopy (XPS) surface analysis of modified films shows the presence of Nitrogen groups as well as the presence of Trimethylsilyl moieties as expected. Observing the C1s spectra for EDA and TMS samples (see figure 7), there is an increase of the intensity on the signal at 286 *eV* related to sp^3 carbons in accordance with the formation of covalent bonds on the surface. Besides, there is a decrease in the intensity of bands related to oxygenated carbon on the surface (~288 eV).

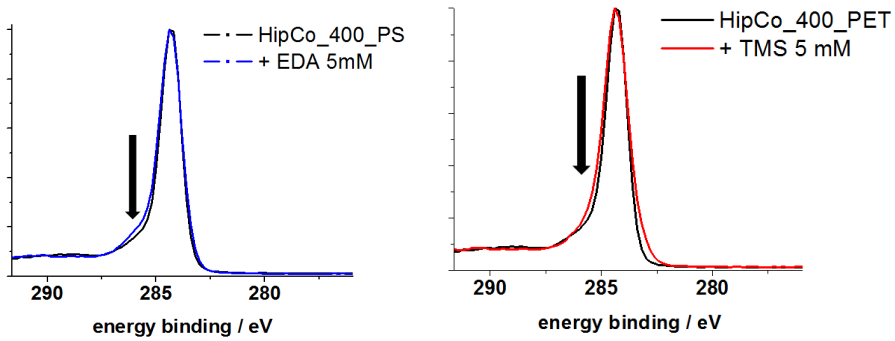

Fig. 7: XPS C1s spectra of SWCNT-based electrodes with EDA (left) and TMS (right). The black arrows indicate changes observed. Blue and red lines are the signals obtained after surface modification with EDA and TMS respectively. Black line represents the pristine electrode surface of SWCNTs.

This is in accordance with Raman spectroscopy where an increased D-band related to sp^3 carbon atoms is observed after surface modification in comparison with the spectrum of the pristine material (see figure 6).

4.1.2. TRANSFORMATION OF THE REMAINING ACTIVE MOIETIES

SWCNT modified films were treated chemically in order to prepare the reactive functional groups for the subsequent cycloaddition reaction. In the case of EDA and PhDA moieties, the remaining amine groups need to be transformed in azide groups while TMS molecules need to be unprotected to obtain a final alkyne.

Such transformations will allow the cycloaddition reaction to occur between those groups and ferrocene complementary moieties synthesized for this purpose. The amine to azide transformation was obtained upon formation of a second diazonium salt with 0.1 *M* $NaNO_2$ and reaction with 0.2 *M* solution of sodium azide (NaN_3). The formation of bubbles indicates production of nitrogen molecules. First experiments were performed upon dropcasting the solution on the film surface but the amount and size of nitrogen bubbles formed hindered the reaction.

As an alternative, films were softly stirred in the solution for two hours, insuring contact between film surface and solution at any moment. After the reaction, the films were washed with distillated water.

Deprotection of TMS moieties to obtain the alkyne requires the use of TBA^+F^- solution. This strong chemical dissolves polystyrene substrates. We were

obliged to work with PET substrates and most of times samples did not resist the treatment making impossible further characterizations.

The Raman spectra of the resulting modified films are shown in figure 8, where the relative intensity of the 2D-band is slightly diminished. The only differences that can be observed in the Raman spectra are the bands situated from ~2850 to ~3100 cm^{-1}. It was found in literature that aryl modified surfaces contribute with bands in this Raman shifts range.[91]

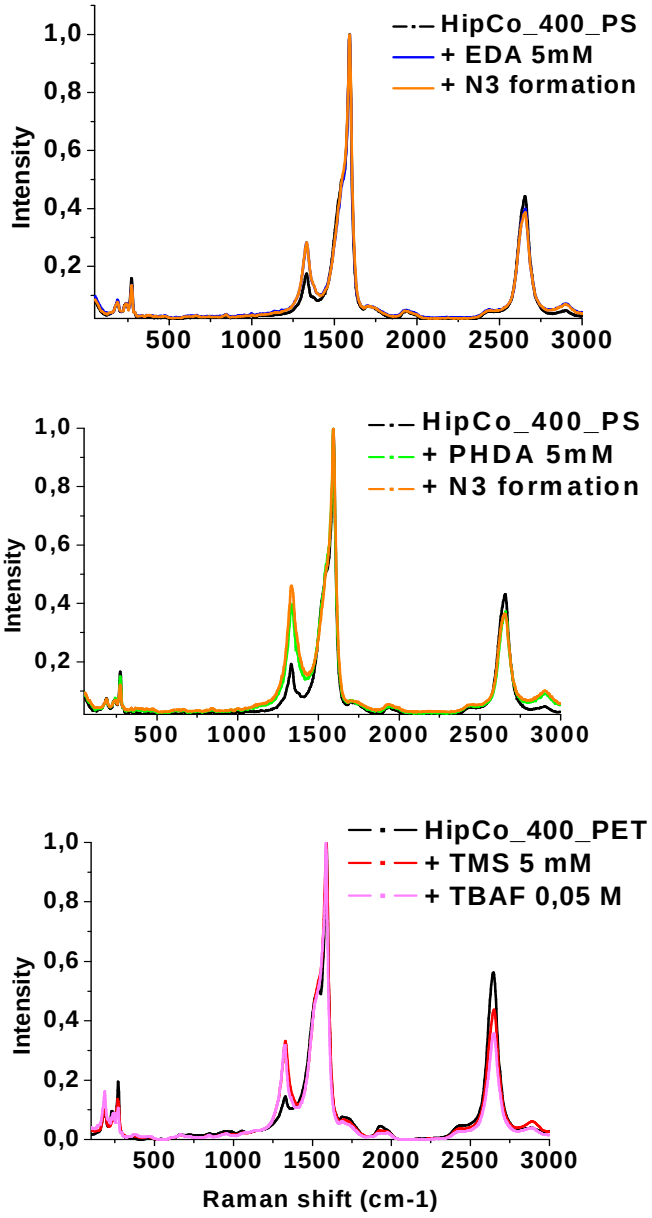

Fig. 8: Raman spectra of SWCNT films after chemical transformation of modified surfaces for the three different approaches (EDA, PhDA, and TMS molecules). Excitation laser used was 532 *nm* for the three measurements.

In parallel infrared spectra were measured for the three different modified surfaces at any single step, but unfortunately, the amount of material deposited was too small compared with SWCNT film and substrate (PS) making it difficult to observe any significant change of the best spectra obtained. Anyhow, here it is presented the best obtained (see figure 9). The small change in the orange spectra may be related to the formation of N_3 moieties that are known to display a strong band at ~ 2100 cm^{-1}.

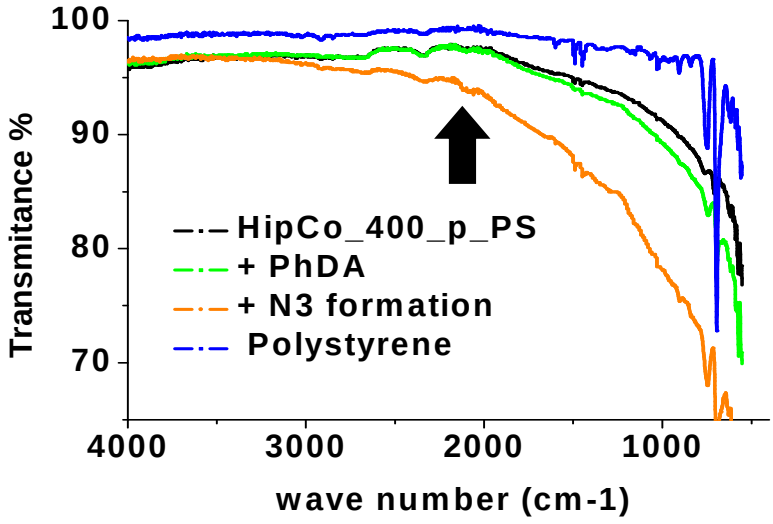

Fig. 9: FIT-IR spectra for the PhDA modified SWCNT film showing different steps of the reaction.

Attempts were made to obtain a better IR characterization of the films (at Belo Horizonte University, Brazil) using several IR modes. However in all cases the spectra were dominated by the substrate (polystyrene) signal.

4.1.3. AZIDE-ALKYNE CU (I) CYCLOADDITION REACTION: CLICK-CHEMISTRY

After the transformation of the remaining groups, modified SWCNT based electrodes were prepared for performing cycloaddition reaction between transformed groups and the complementary ferrocene-containing moieties (see figure 10).

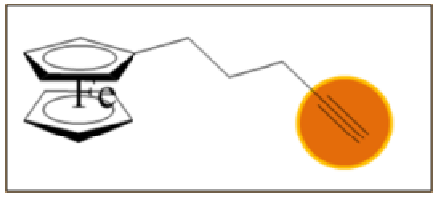

Fig. 10: Alkyl-Ferrocene probe for click chemistry reaction on the modified films.

Click-chemistry reactions were performed as follows. 1 *mg* of the corresponding alkyl ferrocene (Mw=251.84 $g\ mol^{-1}$) was dissolved in 0.4 *mL* of distillated water obtaining a 0.01 *mM* solution. Parallel to that, a solution of 0.025 *g* and 0.020 *g* of copper sulfate penta hydrate and sodium ascorbate respectively, in 100 *µL* of distilled water were prepared. Copper-ascorbate solution was added to the ferrocene solution and the resulting mixture was stirred until homogeneous solution. This homogeneous Cu (I)-Ferrocene solution was drop casted on the film surfaces. Samples were placed on an ice-bath to stabilize the catalyst, and left reacting for 2 hours.

After the reaction, samples were washed generously with distilled water and sonicated < 1 minute in order to remove any adsorbed or trapped species. The

resulting films were analyzed by Raman spectroscopy. The spectrum for PhDA-SWCNT modified electrode is shown in figure 11.

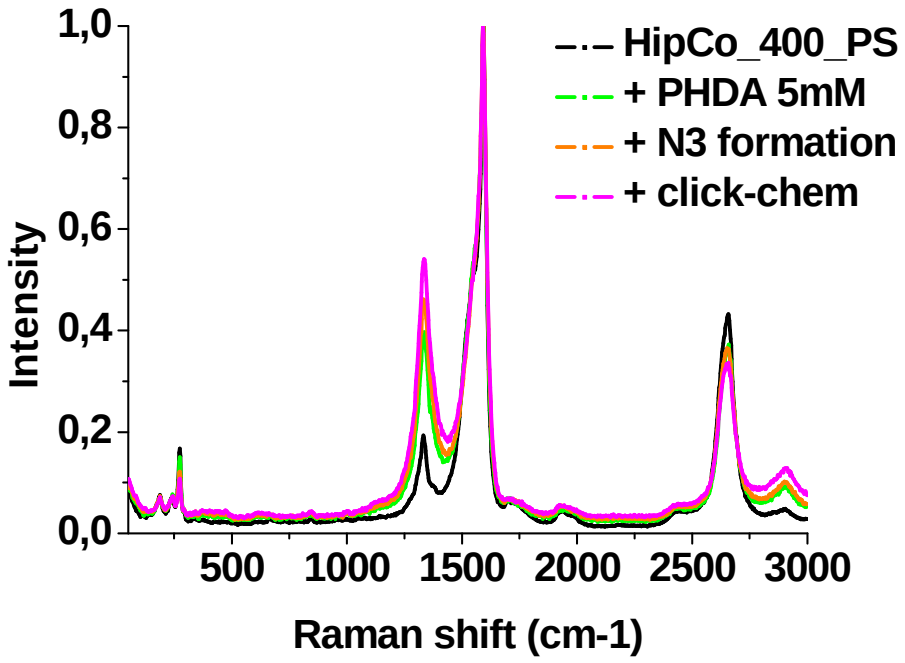

Fig. 11: Raman spectra showing different steps of reaction of PhDA surface modified SWCNT-based electrodes.

No significant change in the spectrum is observed except for the band at ~2800 cm^{-1}, related with aryl modified substrates.

The presence of aryl moieties on a modified surface was recently shown to contribute with a band between ~2800 and 3100 cm^{-1}. This is in fact observed in the spectra displayed in figure 12, and the small shoulder in the final spectrum can be attributed to the formation of the triazolic ring.[92]

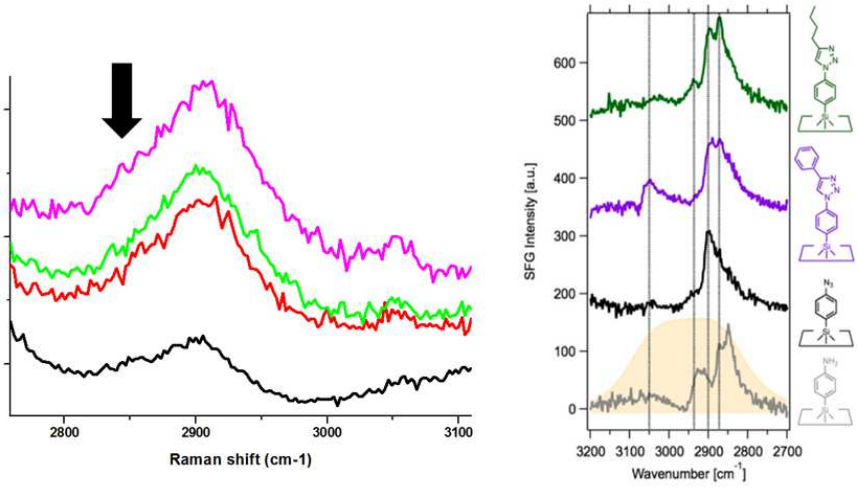

Fig.12: Zoom of Raman spectra from Figure 11, on the region of related aryl and aryl-triazolic modified surfaces (from black to pink lines: pristine film, PhDA modified surface, azide formation, and click reaction. Right image Sum Frequency generation spectra from: J. Am. Chem. Soc., 2012, 134, 20681.

Cyclic voltammetry was run for the electrochemical detection of ferrocene redox probe immobilized on the SWCNT electrode surface (see figure 13a). The PhDA-SWCNT modified electrode was placed in the electrochemical cell filled with a phosphate buffer solution (PBS) (1x) solution. Cyclic voltammograms from the OCP to 0.7 *V* were registered at different scan rates and a reversible peak is observed relative to the oxidation/reduction of ferrocene species at the electrode surface. The curves are highly asymmetric indicative of hindered electron transfer kinetics as expected for the presence of insulating polymeric layer.[93]

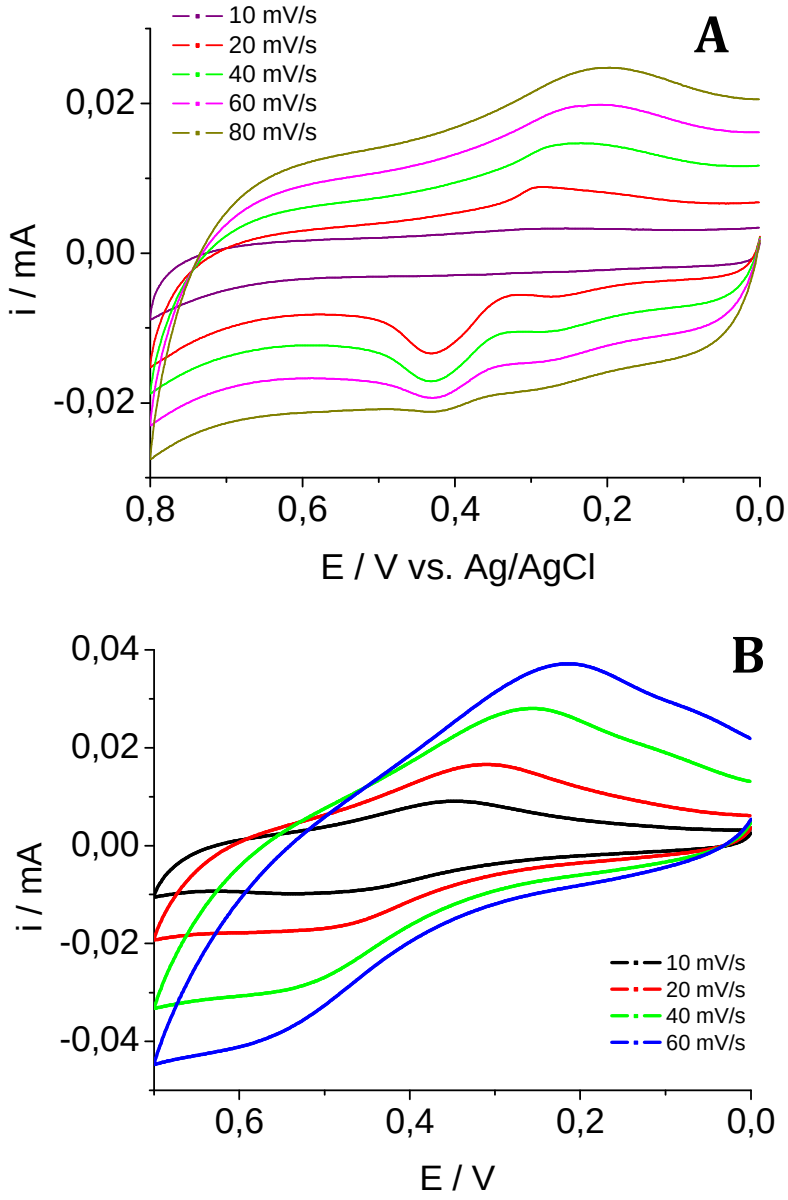

Fig. 13a: Cyclic voltammetry of SWCNT-alkyl ferrocene surface modified electrodes: (A) EDA-N_3-alkyl ferrocene B) PhDA-N_3-alkyl ferrocene. Measurements were run in PBS solution and different scan rates showing a half-wave potential $E_{1/2}$= 0.345 *V* and 0.415 *V* respectively.

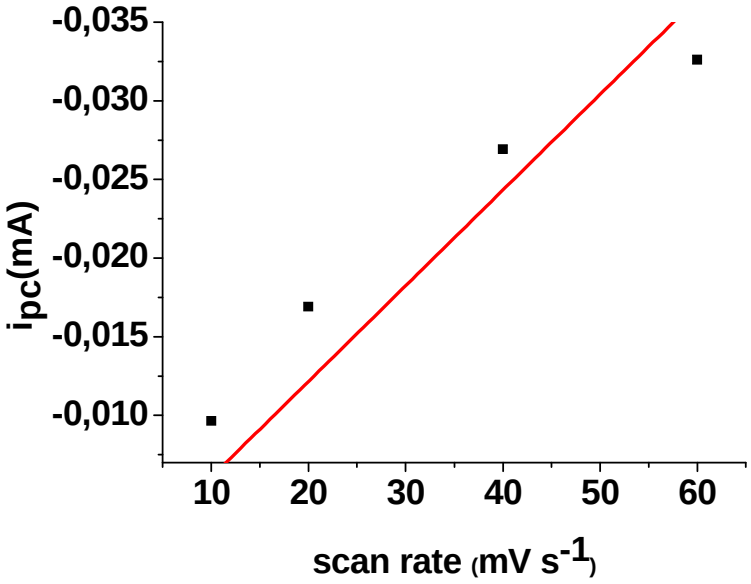

Fig. 13b: Linear dependence of the peak current with the scan rate of reaction defining immobilization of species on the electrode surface.

The analysis of the scan rate dependence of the peak current indicates that the redox species is immobilized at the electrode surface (see figure 13 b) with calculated value of $\Gamma=2x10^{15}$ *molecules* cm^{-2}. This value is significantly higher than for monolayers where $\Gamma=\sim10^{12}$ *molecules* cm^{-2}. Such value is in accordance with functionalized polymeric films. As introduced in chapter 1, the electrografting of aryl-diazonium salts leads to the formation of polymeric films. In consequence, the number of species immobilized should be significantly higher as observed.

4.1.4. IMMOBILIZATION OF A REDOX ENZYME: HORSERADISH PEROXIDASE (HRP)

A proof-of-principle experiment to show the utility of these films for the bio conjugation was realized by immobilizing HRP at the SWCNT modified electrode. The HRP enzymes, anchored to the surface of the film, will consume H_2O_2 in solution generating a flow of electrons that reaches the electrode surface through the hydroquinone/benzoquinone redox shuttle.[61,94–96]

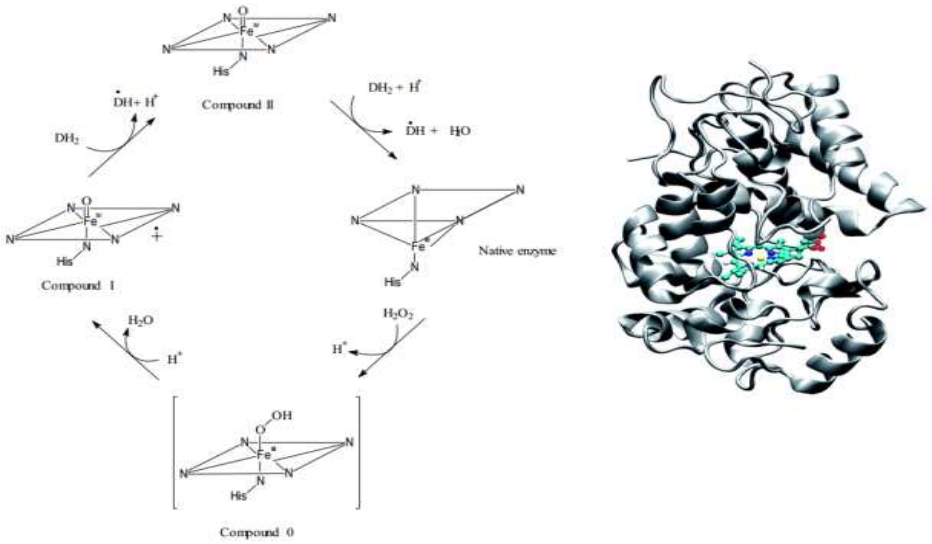

Scheme 2: Catalytic cycle of HRP (left) and cartoon representation of the enzyme (right).

SWCNT modified electrodes with EDA moieties were reacted with freshly prepared 1 mM solution of HRP enzyme in PBS with the presence of N-Hydroxysuccinimide (NHS) as activating agent. Amine groups react with the enzyme acidic terminal groups upon formation of an amidic bond upon

overnight reaction. The sample was kept at low temperature to maintain enzyme properties. Before the analysis, the sample was repeatedly and carefully rinsed removing any trace of adsorbed species.

The modified electrode surface was characterized by cyclic voltammetry studying the evolution in the current in response to an increasing concentration of hydrogen peroxide in the presence of 1 mM Hydroquinone in PBS (see figure 14a and 14b). HRP, in the presence of hydrogen peroxide, will oxidize hydroquinone which will get reduced at the electrode surface (as shown in scheme 3).

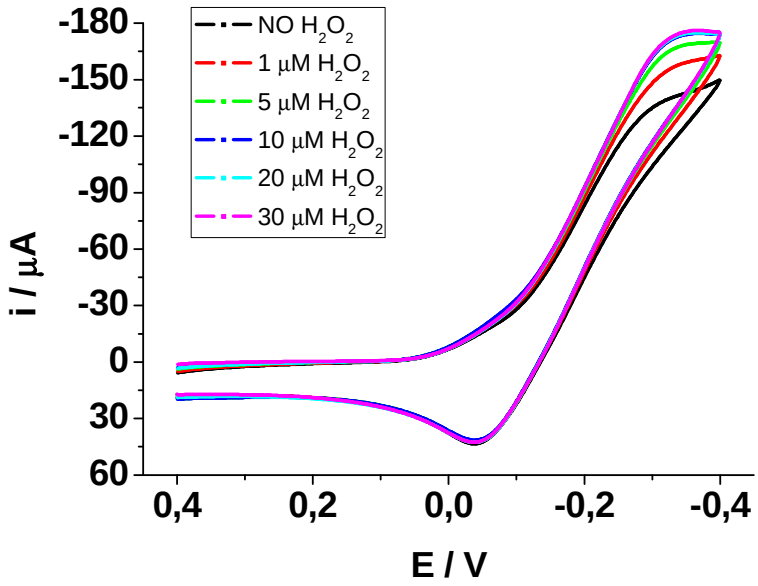

Fig. 14a: Cyclic voltammetry for the electron transfer of the redox shuttle HQ⇆BQ (1 mM Hydroquinone in PBS) at the SWCNT-modified electrode upon an increasing concentration of hydrogen peroxide. Reference electrode was Ag/AgCl.

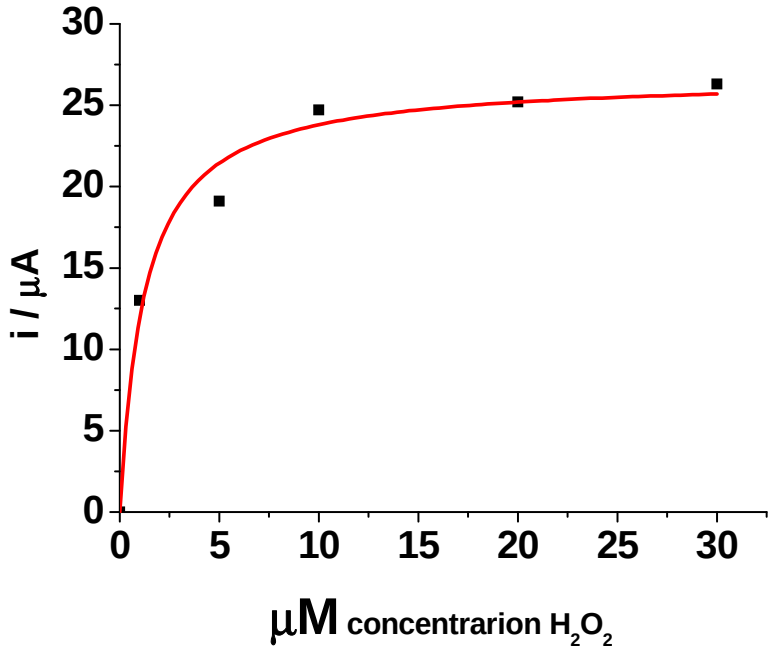

Fig. 14b: Michaelis-Menten fitting obtained from curve showed in figure 14a.

Cyclic voltammetry was run between the OCP and -0.4 *V* at a scan rate of 50 $mV\ s^{-1}$ recording current-potential curves with the increasing concentration of H_2O_2.

Figure 14a shows the cyclic voltammetry for the redox process $\boldsymbol{HQ} \rightleftarrows \boldsymbol{BQ}$ at the modified electrode surface. Upon increasing the concentration of H_2O_2 in solution there is an increase on the flow of electrons at the electrode surface monitored by the redox shuttle $\boldsymbol{HQ} \rightleftarrows \boldsymbol{BQ}$. We can observe a catalytic response of the HRP enzyme reaching the limiting current upon the progressive increment of hydrogen peroxide in solution. The current

increments (at the peak potential) were plotted as a function of hydrogen peroxide concentration and fitted by the Michaelis-Menten equation

$$\mathbf{v} = \frac{\mathbf{V_{max}[S]}}{\mathbf{K_m} + \mathbf{[S]}}$$

resulting in a K_M value of 1.238 μM and V_{max} equal to 1.38×10^{-4} $\mu mol\ cm^2\ s^{-1}$. The obtained i_{max} = 26.7 μA has been transformed into µmol/s by

$$i \propto nFv \qquad v = {}^{i(Cs^{-1})}\Big/_{nF(Cmol^{-1})}$$

where n are the number of electrons involved in a single process (as shown in scheme 3) and F is the Faraday constant.

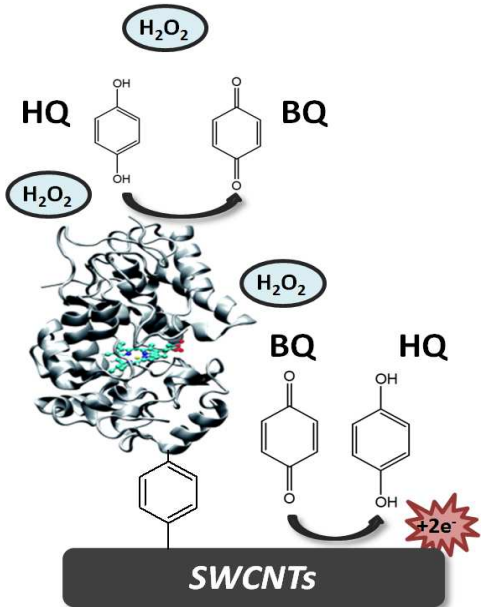

Scheme 3: HRP Immobilized on a SWCNT-based electrode modified with PhDA. Redox shuttle Hydroquinone/benzoquinone used for monitoring catalytic activity of HRP while increasing concentration of hydrogen peroxide.

The resulting detection limit is 1.2 μM. After such value the curve reach Plato. The K_M obtained is smaller than values reported.[97–99] This may be related to small values of enzyme loading on the electrode surface.

4.2. ELECTROCHEMICAL SURFACE MODIFICATION WITH 1, 3-BENZODITHIOLILYUM TETRAFLUOROBORATE

The electrochemical covalent adsorption of 1, 3-Benzodithiolilyum tetrafluoroborate molecules (here on, BDYT) on SWCNTs was an alternative approach for surface modification. The inspiration came along with two articles found in literature.[62,63] Since this molecule was shown to react with SWCNTs (with higher reactivity with metallic tubes) resulting in a covalent bond formation, we investigated the surface modification of SWCNT-based electrode through the electrochemical generation of radical species at the electrode surface. This study is preliminary to the possibility of surface functionalization according to the scheme shown in figure 15. In addition, the electrochemical surface modification would represent an advantage with respect to thermal reactions since it is a more controlled process.

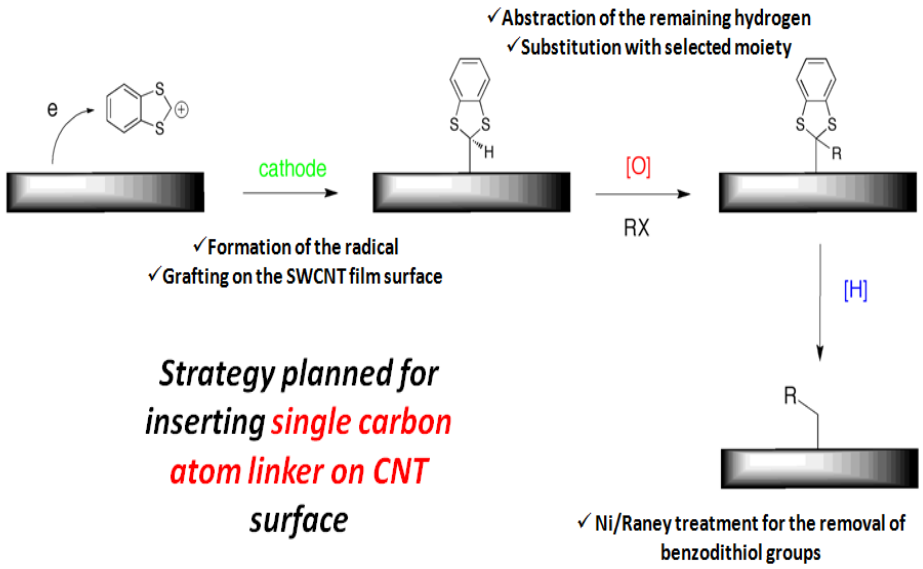

Fig. 15: Schematic representation for the surface modification of SWCNT based electrodes with BDYT moieties.

First studies on the electrochemical surface modification of SWCNTs with BDYT moieties were performed on glassy carbon (GC) and SWCNT based electrodes. The formation of the radical species at the electrode surface was observed only when running the experiment with no oxygen present in solution. For that purpose, closed electrochemical cells were designed. 10 *mM* solution of BDYT in acetonitrile and 0.1 *M* $TBA^+PF_6^-$ salt as a supporting electrolite was bubbled with Argon for at least 30 minutes under stirring in order to eliminate any traces of oxygen present in solution.

The formation of the radical was observed to occur at ~ - 0.6 *V* on glassy carbon. The cyclic voltammetry obtained (see figure 16a) shows a decrease of current when increasing the number of potential cycles (without reaching zero values) characteristic of a passivated electrode. This was also demonstrated by

monitoring Ferrocene-methanol redox mediator at the electrode surface (see figure 16b) where the black line shows the electrochemical process at the pristine electrode surface while the red line shows the process at the modified electrode surface.

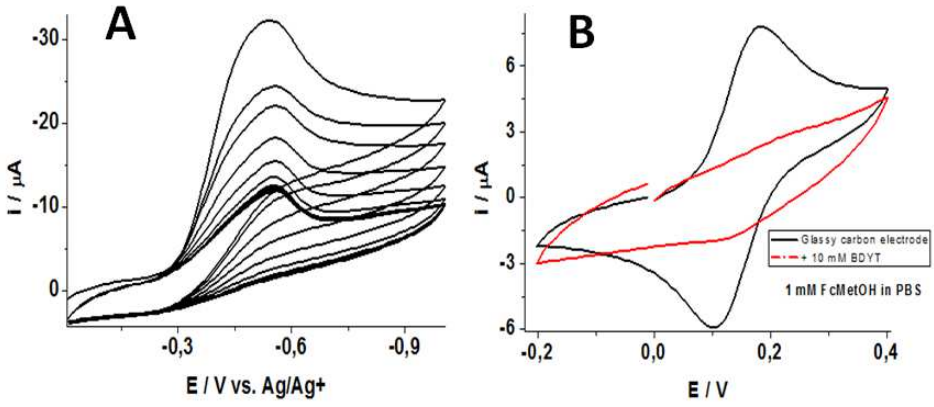

Fig. 16: A) Cyclic voltammetry for the electrochemical surface modification of a glassy carbon electrode with 10 mM BDYT in acetonitrile. Scan rate: 50 *mV* s^{-1}. B) Cyclic voltammetry for the pristine (black) and modified (red) electrode surface.

After setting up the reaction conditions the electrografting on SWCNT films was performed by cycling the potential from the OCP towards reductive potentials. HiPCO and CoMoCAT SWCNT based electrodes were tested to react with BDYT moieties in acetonitrile and $TBA^+PF_6^-$ as a supporting electrolyte. Depending on the SWCNT starting material, films with different conductivities were obtained.

Upon performing several potential cycles, formation of a white thin layer was observed on the electrode surface (see figure 17).

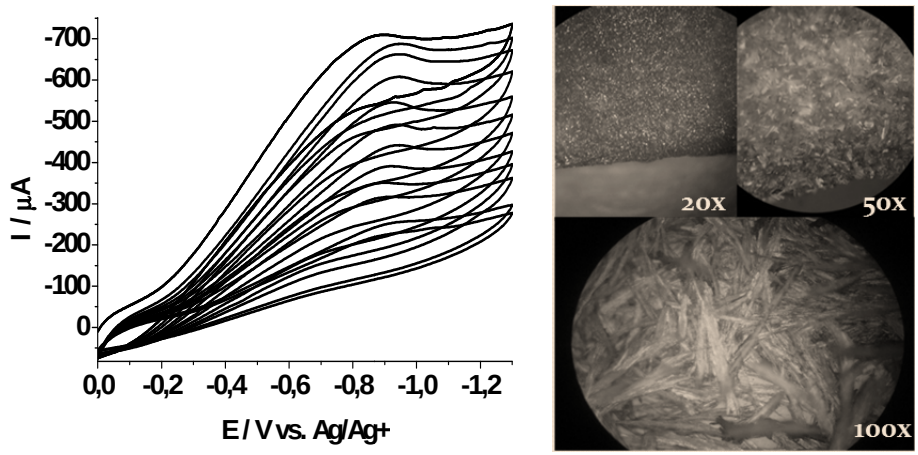

Fig. 17: Cyclic voltammetry for the electrochemical surface modification of CoMoCAT SWCNT based electrode with 10 mM solution of BDYT in acetonitrile. Scan rate: 50 *mV* s^{-1}. Optical images for the resulting crystalline film formed during the process at different magnifications.

This white material remains strongly attached on the SWCNT film after washing it repeatedly with acetonitrile. Optical images showed the presence of crystals/fibers on the electrode surface. As described for glassy carbon, the electrochemical surface modification of SWCNT-based electrodes with BDYT moieties leads to the formation of a thin layer that develops in big crystalline fibers visible by eyes (see figure 17 right).

The sample was characterized by SEM (see figure 18) showing the presence of bright spots on the surface of the SWCNT film when scanning at high resolutions. In agreement with these results atomic force microscopy also showed the formation of spots grown onto the nanotubes.

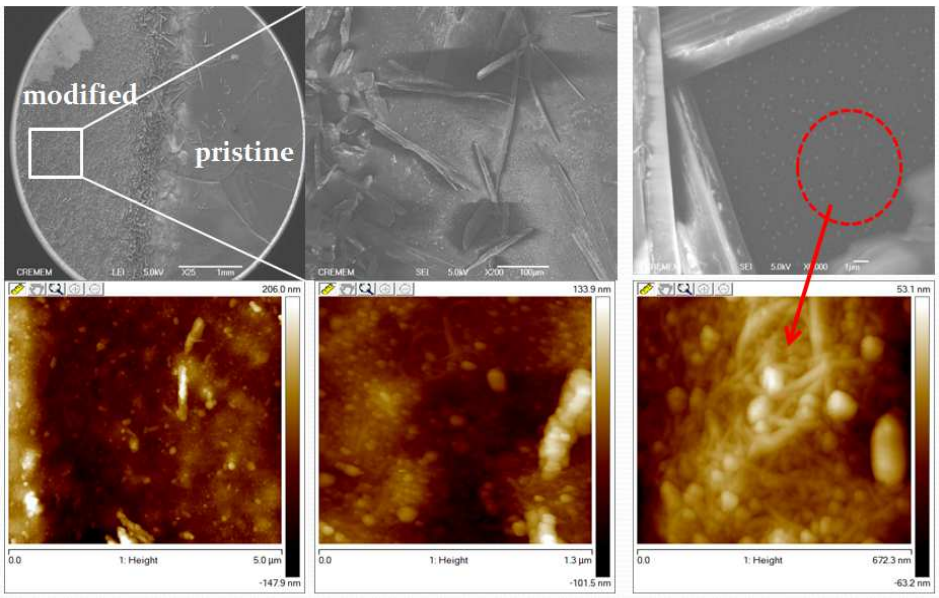

Fig. 18: SEM (above) and AFM (below) of the electrochemically modified CoMoCAT SWCNT based electrode with 10 mM of BDYT in acetonitrile.

In order to identify the composition of the layer formed on the surface of the SWCNT film the sample was characterized by XPS. The resulting modified surface shows an evolution of bands with respect to the pristine material in the C1s and S2p spectra (see figure 19).

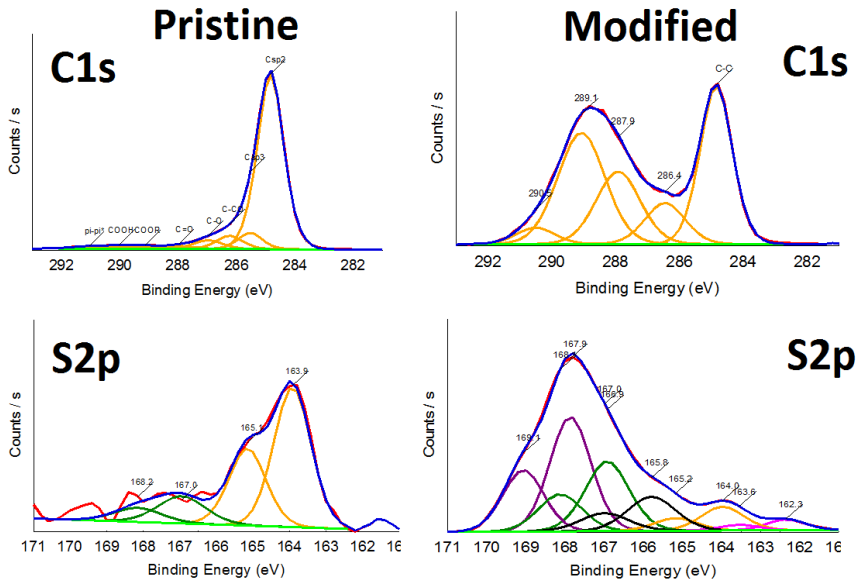

Fig. 19: C1s and S2p XPS spectra for the pristine (left) and electrochemically modified (right) SWCNT-based electrodes.

The appearance of bands at 286 *eV* visible after surface modification are related to sp^3 carbon atoms on the surface while higher binding energy bands are related to other carbon environments. For SWCNTs these bands are related to oxygen groups linked to the carbon surface of the tubes. After reaction with BDYT moieties, there is an evolution in the spectrum related to the formation of the film on the surface. The resulting spectrum shows three different environments that can be related to a) the sp^2 carbon of nanotubes at lower energy bindings ~285 *eV* b) the sp^3 carbon bands at ~286 *eV* related to the covalent attachment of BDYT moieties to the surface and c) signals at higher energy bindings ~287-290 *eV* resulting from the environment of carbon atoms in the film. The S_{2p} spectral region of the pristine material may come from solvent moieties (DMSO) as we explained in precedent sections. This sp2

region shows a band with two main peaks at ~ 163-165 *eV* characteristic of Sulfur 2p. After surface modification, the situation is quite different observing the shift of the main peaks to higher binding energies and the formation of the band at ~162 *eV* that was associated to the covalent attachment of BDYT moieties on the SWCNT surface.

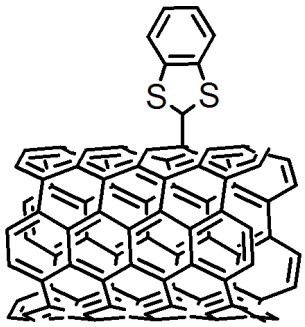

Scheme 4: Representation of BDYT covalently linked to the SWCNT surface.

In order to confirm the relation between the covalent attachment and the formation of the band at ~162 *eV* another sample was prepared by dropcasting a 10 *mM* BDYT solution in acetonitrile on the SWCNT surface. The resulting spectra showed, as expected, no presence of this band (see figure 20).

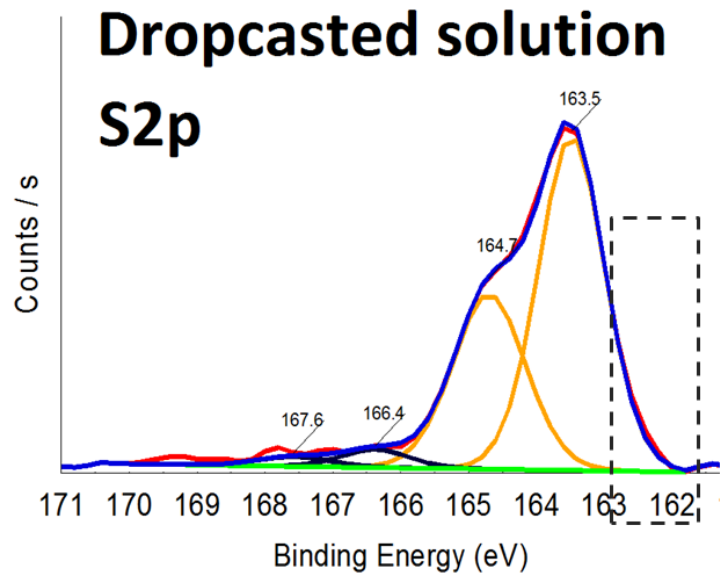

Fig. 20: S2p XPS spectra for 10 mM BDYT dropcast on SWCNT surface.

In order to clarify the film structure, the amount of material deposited on the nanotubes was diminished. The concentration of the BDYT solution was reduced from 10 *mM* to 5 *mM* and several samples were prepared using different numbers of potential cycles in order to investigate the evolution of the band situated at ~162 *eV.* The band grows with the number of cycles up to 30 cycles. For larger number of cycles the spectra is dominated by an intense band at 168 *eV* attribute to a polymeric form of BDYT, with smaller signal at ~164 *eV* in agreement with the presence of DB-TTF[100] (see figures 21a and 21b) which could be generated by the coupling of two BDYT radical species.

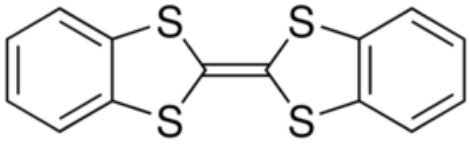

Fig. 21a: Chemical structure of DB-TTF.

Notice that the dropcast solution do not shows a peak at this position.

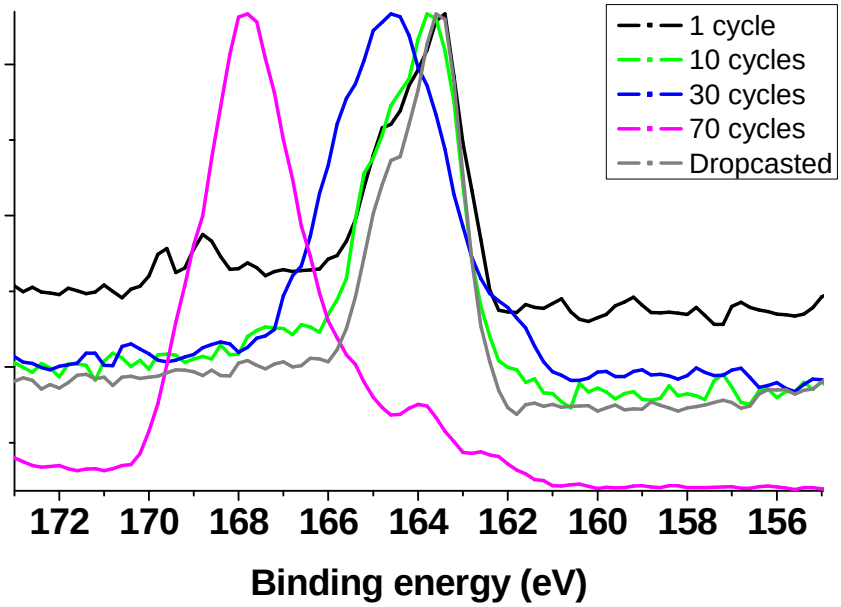

Fig. 21b: XPS spectra (S2p) of SWCNT surface modified films with BDYT solution prepared with different number of potential cycles showing the evolution of the ~162 *eV* band.

Raman spectroscopy investigation confirmed the results obtained by XPS. Crystalline BDYT Raman spectrum showed characteristic bands over a strong fluorescence signal, when exciting the sample with an excitation source of 532 *nm*. Other excitation energies were tested but fluorescence covers all the

spectra. After surface modification of SWCNT films with BDYT moieties we observed the presence of the characteristic bands related to BDYT as well as the quenching of the fluorescence that was associated to a strong interaction (covalent bond) SWCNT-BDYT. The sample was mapped in order to obtain an overall Raman spectrum of the surface. An increase of the D-band when with the number of potential cycles is also in agreement with the XPS results (see figure 22).

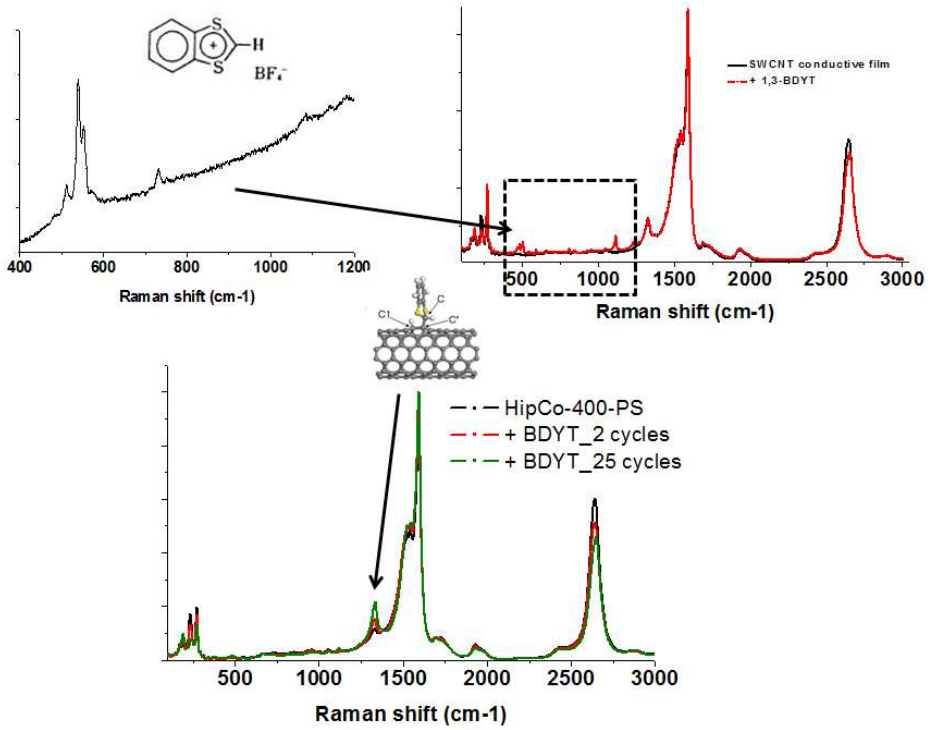

Fig. 22: Raman spectra of BDYT powder (top left) and after interaction with SWCNT film (top right) with resulting quench in the fluorescence. Evolution of the D-band with the number of potential cycles (bottom).

The topography of the films obtained with an increasing number of potential cycles was investigated by AFM. Diminishing the amount of material deposited allows to observe the nanotube film structure (see figure 23a)

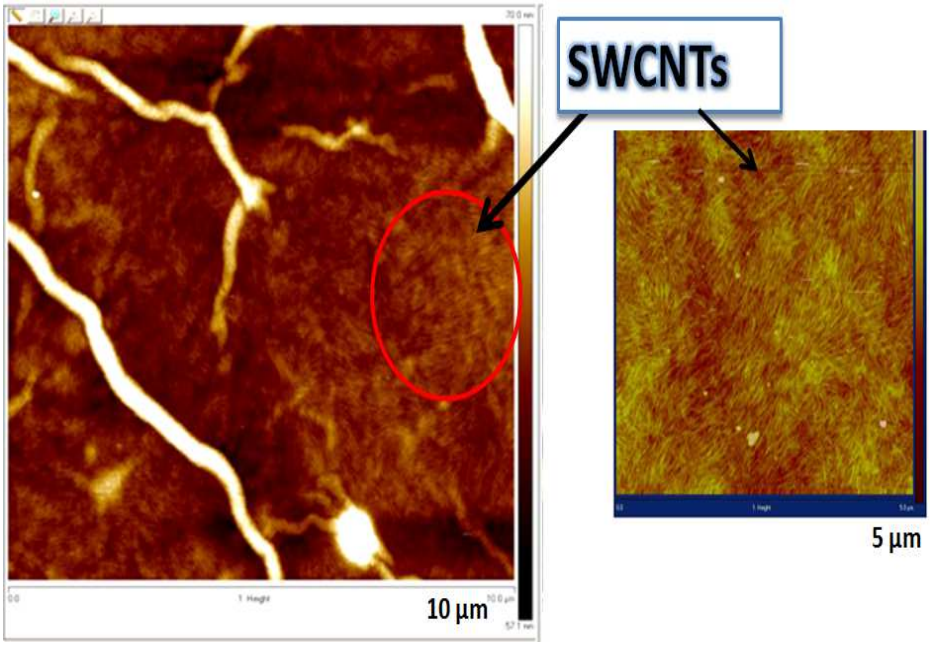

Fig. 23a: Pristine SWCNT film (right) and resulting electrochemically modified SWCNT film (left) with 5 mM BDYT and 2 potential cycles.

The images obtained gave unexpected results (see figure 23b). The resulting modified surface shows unexpected twisted ropes, and the ropes grow in number with the number of cycles.

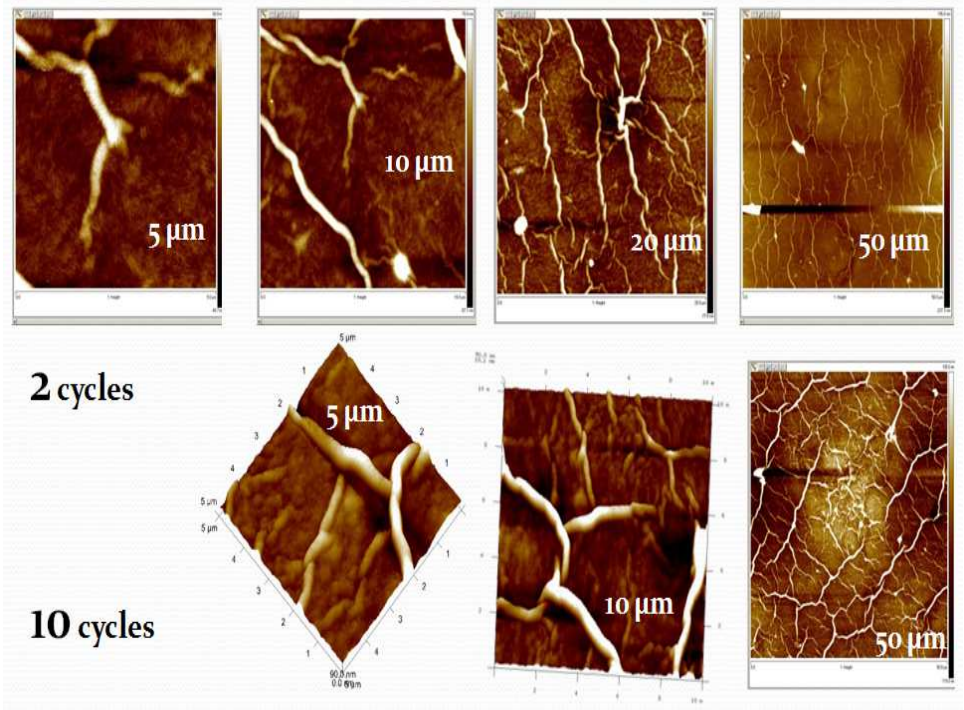

Fig. 23b: AFM of SWCNT modified surfaces with BDYT prepared with different number of potential cycles.

The AFM analysis of the ropes showed heights around 10-15 *nm* and width around 0.5 *µm* that are confirmed by SEM and optical microscopy.

The image 23c shows the cyclic voltammetries, AFM images and C1s XPS spectra when increasing the number of potential cycles.

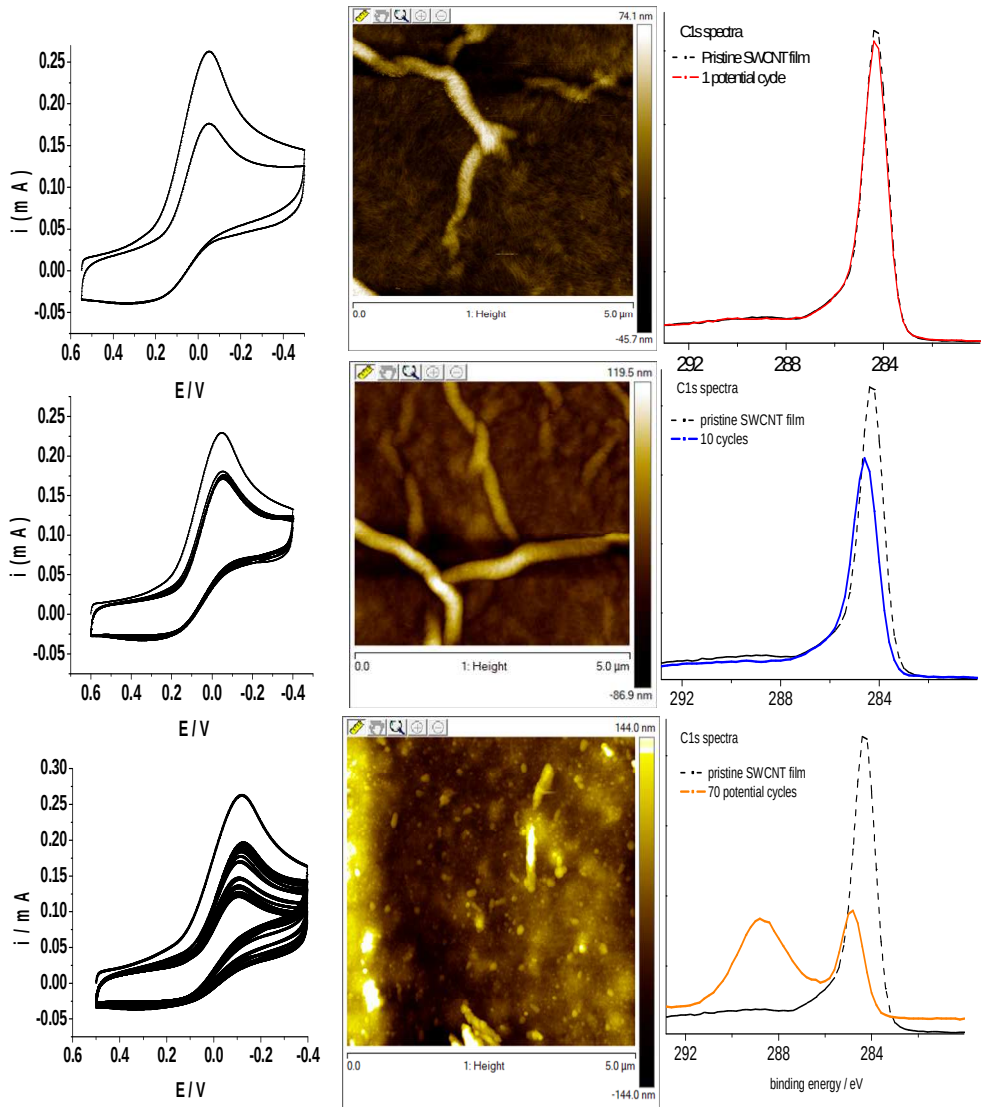

Fig. 23c: CV, AFM, and C1s XPS analysis of (5 mM) electrochemically modified electrode with: 2 (above), 10 (center), and 70 (below) potential cycles. The scan rate was 50 *mV* s^{-1}.

The SWCNT film surface shows increasing deposition of material expressed in lower current values with increasing number of potential cycles (CV). That is in

accordance with AFM resulting images where twisted ropes are formed with low number of potential cycles. When the potential is applied for higher number of cycles, a polymeric material fully covers the surface of nanotubes and twisted ropes are only visible at small scan sizes (see figure 23d).

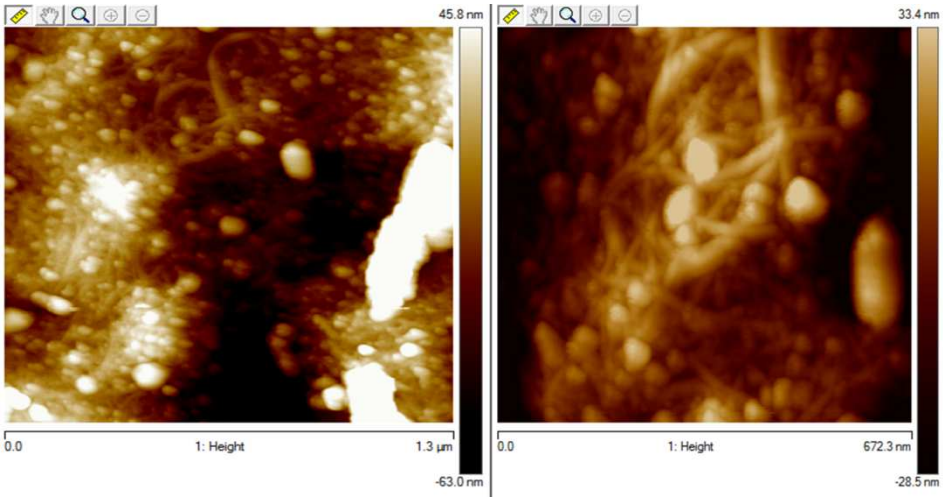

Fig. 23d: Low scan sizes AFM images of HiPCO-SWCNT-BDYT electrochemically modified electrode showed in figure 23c. Polymeric material and fibers were observed after 70 potential cycles.

The XPS analysis shows in accordance to that an evolution of the C1s band at ~284.83 *eV* (related to sp2 carbons) to higher energy bindings at ~285.53 *eV* with higher number of potential cycles (10 cycles) related to sp3 carbons. This intensity still diminishes when increasing the number of potential cycles to 70, leading to the formation of new bands at ~287-290 *eV*.

The hypothesis that such patterns would form because of capillary effects during the drying process was discarded by exposing the film to the BDYT solution without application of any potential.

After removing the solution and rinsing the film AFM analysis was performed that did not show the presence of any deposit (see figure 24).

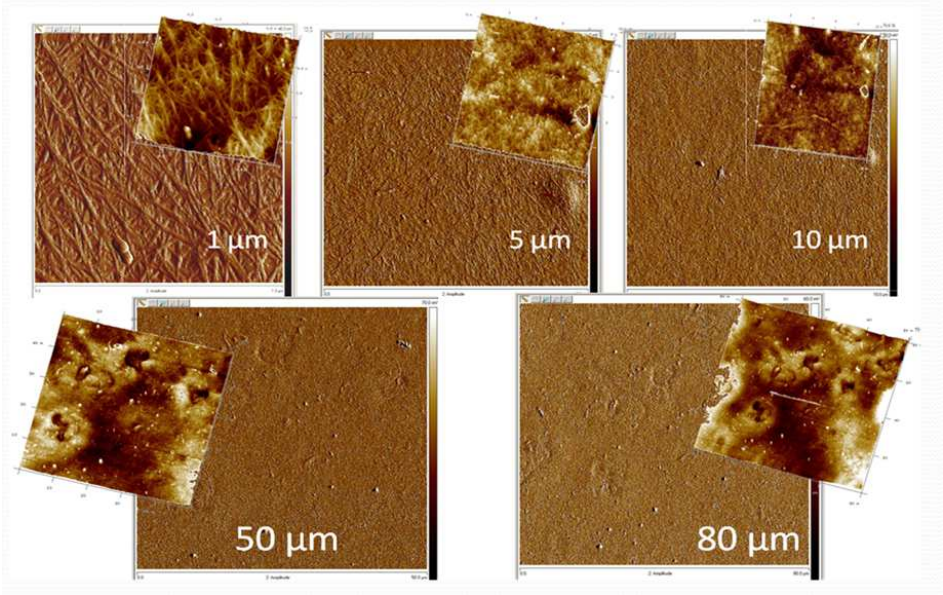

Fig. 24: SWCNT film after being in contact with BDYT moieties in acetonitrile. No potential was applied.

At this point we were able to say that those twisted ropes formed in the surface are electrochemically generated.

To get chemical and structural information about the material formed a MALDI-TOF experiment was performed (70 potential cycle sample). Experiments were run in order to identify a mass distribution of the material electrochemically generated at the electrode surface. Unfortunately (see figure 25) only features characteristic of carbon nanotubes film were observed.

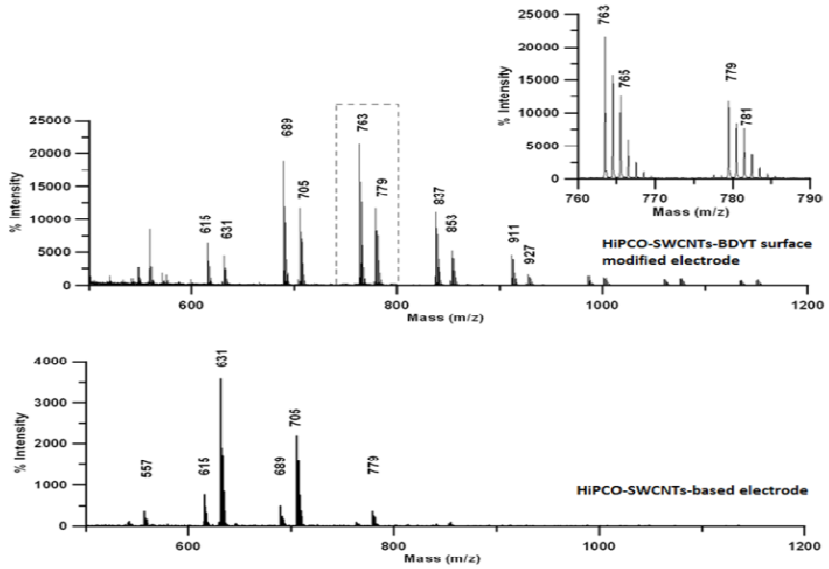

Fig. 25: MALDI-TOF spectra of pristine and modified HiPCO-SWCNT-based electrode.

Therefore in order to perform a mass spectrometry analysis of the material formed the substrate should be removed.

In order to identify possible ordered structures the modified samples were observed under polarized light in an optical microscope. Upon polarization of light generated film was described as ordered system thus an X-ray diffraction (XRD) analysis was performed.

XRD is a non-destructive analytical technique resulting in a unique fingerprint (Bragg reflections) associated with a crystal structure. A crystal structure is a construction of layers or planes acting as a semi transparent mirror. A source of x-rays with a wavelength similar to that distance between crystal planes can be reflected. The angle of such reflection is equal to the incident angle.

The diffractogram shows an amorphous behavior in the case of SWCNT film surface (red line), but after electrochemical surface modification with BDYT sharp reflections appear being related to a highly ordered deposit (see figure 26a).

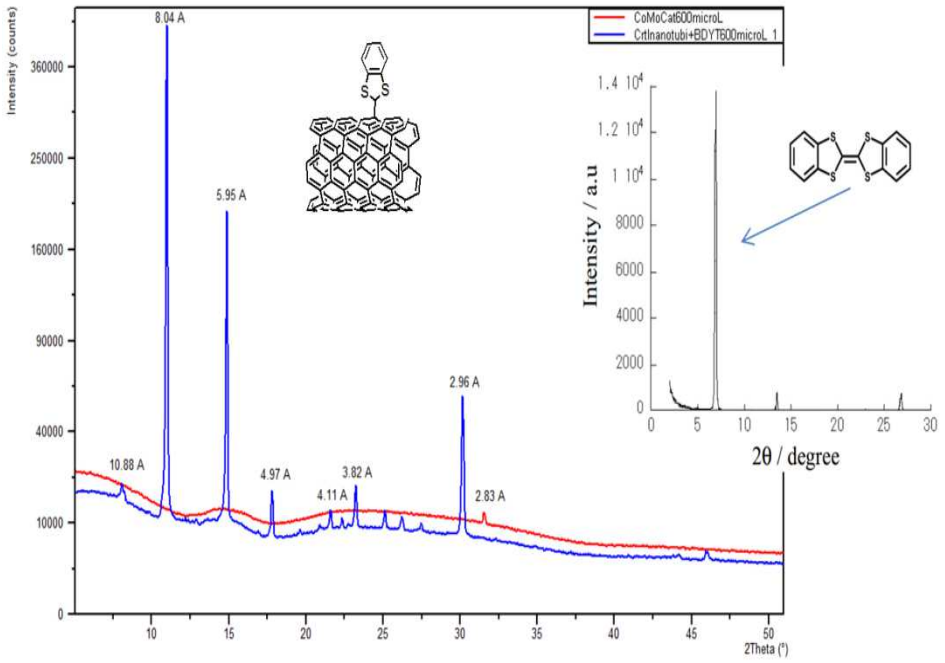

Fig. 26a: XRD spectra of CoMoCAT-SWCNT-based electrode before (red line) and after (blue line) electrochemical surface modification with BDYT moieties. Small capture: X-ray diffraction of DB-TTF film deposited at room temperature.[101]

Although the results are very encouraging, an identification of the crystalline phases has not still been possible. However, some of the reflections are in agreement with those reported in films of TTF derivatives (see figure 27a).[67,102]

The formation of tetrathiafulvalene (TTF) derivatives was already proved by XPS analysis (see above). The probability of dimerization of BDYT moieties was quite high resulting in dibenzo-TTF (here on, DB-TTF). There is no evidence of electrochemical formation of TTF molecules at the electrode surface scanning to oxidative potentials. After the formation of BDYT radical species at the electrode surface upon reductive potentials, the potential was driven to positive potentials and a oxidation peak was observed at E_{ap} = 0.6 V (related to DB-TTF moieties).[67] The formation of DB-TTF species could not occur at the electrode surface, but instead, the formation of the BDYT cationic radical species leads to formation of DB-TTF moieties in solution. DB-TTF molecules are widely studied as semiconducting materials for the performance of highly-oriented field effect transistors (OFETs)[67,102–104] and its crystals showed an XRD spectra in accordance to the spectra obtained, thus indicating that apparently we have obtained a thin film made of DB-TTF crystals (see figure 26b).

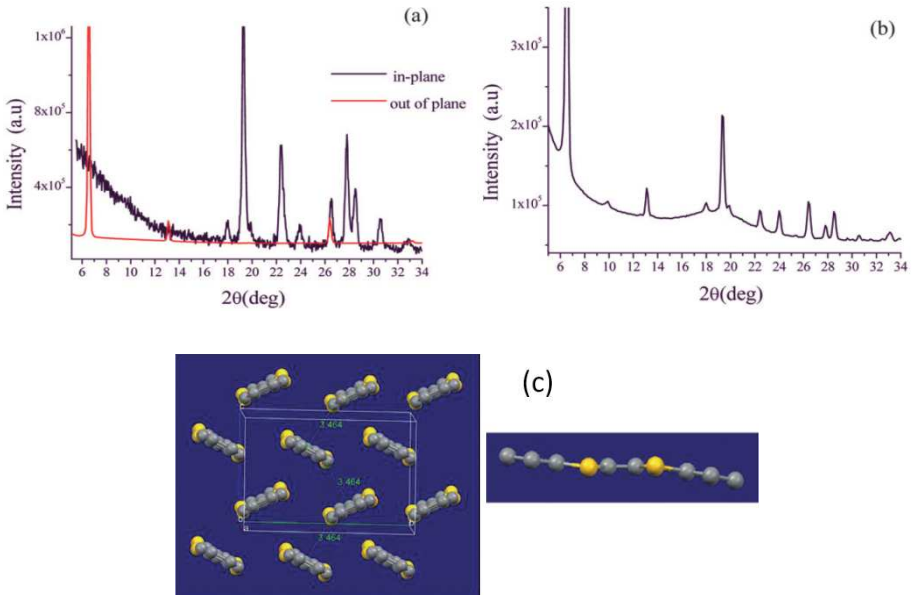

Fig. 26b: (a) Diffraction patterns of evaporated DB-TTF film, (b) Out-of-plane diffraction patterns of DB-TTF film prepared by dropcasting (the λ used was 0.154 *nm*), and (c) crystal structure of the β-phase of DB-TTF along the molecular axis. Sulfur atoms are identified in yellow.[102]

As we mentioned at the beginning of the chapter, the material electrochemically generated on the surface of a carbonaceous material (like carbon nanotubes or glassy carbon) is strongly adsorbed due to the formation of covalent attachment between BDYT and the electrode surface. Performing the reaction on a non carbonaceous material still leads to the formation of material, but in this case there is no covalent attachment with the electrode surface. The collection of the electro-generated material is therefore possible by rinsing the electrode. Two substrate materials were tested to react with 5 *mM* solution of BDYT moieties in acetonitrile: ITO and Gold. Cyclic voltammetries were recorded showing the formation of the radical species

followed by the passivation of the electrode surface after cycling the potential several times at a scan rate of 50 milivolts per second (see figure 27).

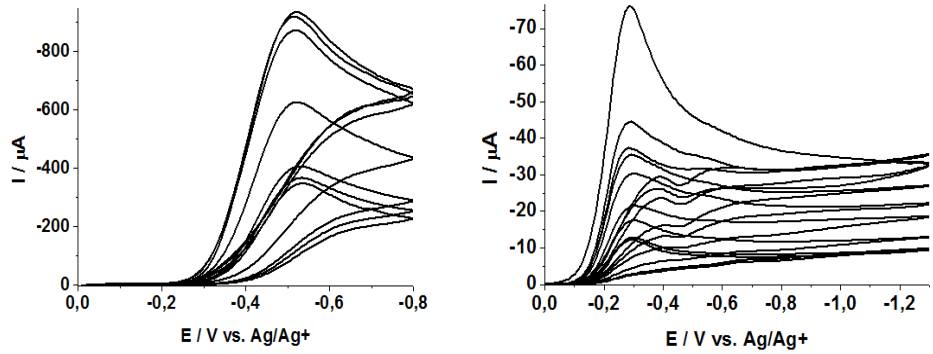

Fig. 27: Electrochemical adsorption of BDYT in ultraflat ITO electrode (left) and the electrochemical adsorption in gold electrode (right).

ITO electrode showed the same reaction behavior than glassy carbon electrode. The main difference was that the thin film created during surface modification was successfully removed while rinsing the electrode with acetonitrile.

Surface modified ultraflat ITO was analyzed by AFM and the related images are shown in figure 28. A polymeric film covers most part of the ITO surface with balls-shaped polymer.

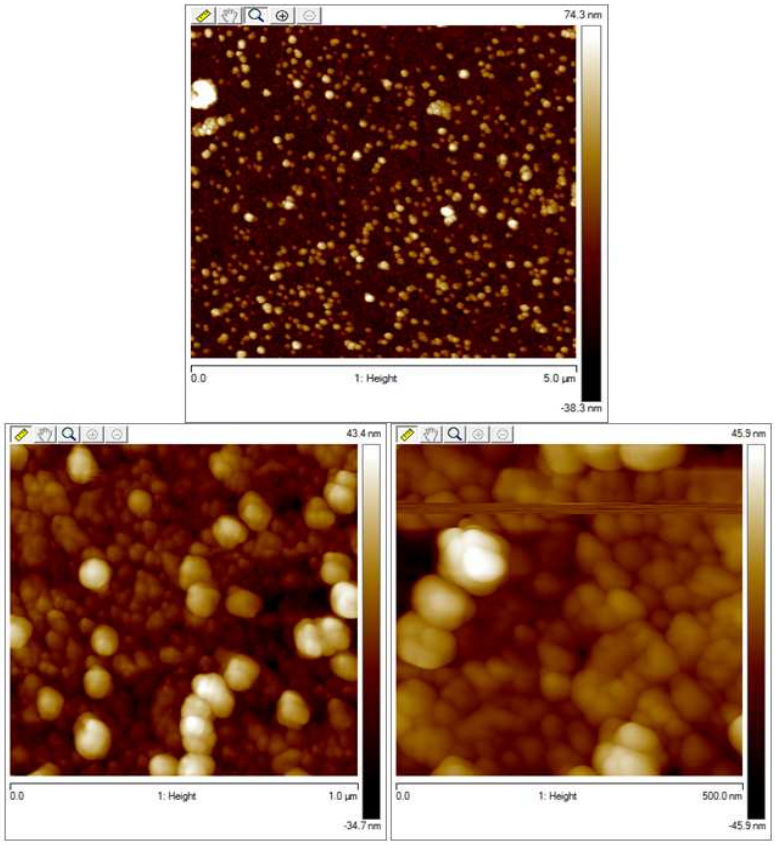

Fig. 28: AFM images of electrochemical adsorption of BDYT moieties on ultraflat ITO electrodes.

The resulting material on the surface was collected and was analyzed by mass chromatography showing an intense peak related to dibenzo tetrathiafulvalene moieties (DB-TTF) (see figure 29).

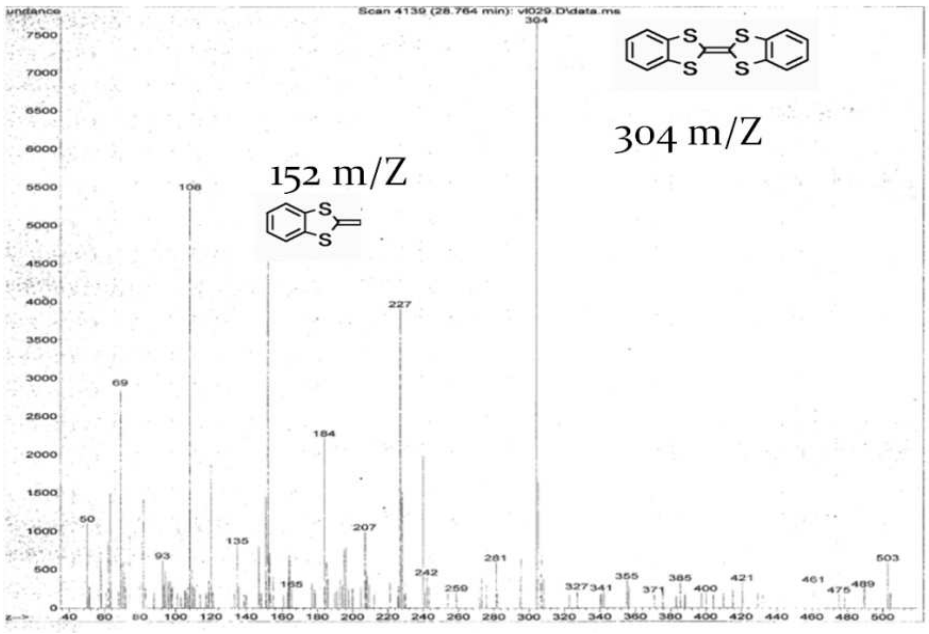

Fig. 29: Mass chromatography of the material formed on the surface of an ITO electrode.

XRD analysis supports such idea showing highly oriented material on the electrode surface possibly containing DB-TTF moieties (still under evaluation).

4.3. CONCLUSIONS

SWCNT-based electrodes have been electrochemically modified following two routes: the electrochemical modification of aryl diazonium salts and the electrochemical surface modification with 1, 3-BDYT. Both approaches lead to successful covalent modification of the electrode surface characterized by Raman and XPS spectroscopy, among other techniques.

SWCNT-modified electrodes with aryl diazonium salts undergo further transformation of the remaining active groups. A post cycloaddition reaction with complementary Ferrocene species results on the detection of those moieties on the electrode surface by cyclic voltammetry showing an electrochemical response related to species that have been immobilized in a non-uniform electrode surface explained by Marcus-Hush-Chidsey theory.[93]

The electrochemical modification with 1, 3-BDYT was successfully characterized by Raman and XPS analysis (among other techniques) showing BDYT characteristic bands after the interaction with nanotubes. At the same time, fluorescence was quenched after interaction with the SWCNT surface. The growth of the band situated at 162 *eV* on XPS spectra with the number of potential cycles is related to the covalent attachment of BDYT moieties on the electrode surface. At the same time, there is a shift towards higher energy bindings with increasing potential cycles. Now that we have introduced the idea of DB-TTF moieties in the surface, it is relevant to look again to the spectra showed in figure 22b, where dynamics of the reaction on the electrode surface lead to the formation of a visible band at 164.0 *eV* (70 cycles). It has been found in literature the XPS spectra of DB-TTF-C_{60} moieties showing an s2p band at 164.0 *eV*.[105]

The study of the reaction under inert atmosphere and a small number of potential cycles leads to the formation of patterns on the electrode surface. It has been characterized by AFM and SEM microscopy. In order to gain some information regarding the formation of these patterns further efforts should be done on an in situ AFM imaging SWCNT electrochemical surface modification experiment.

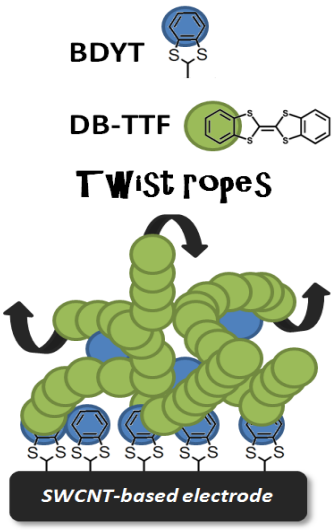

Hypothesis formulated for the mechanism involving formation of twisted ropes patterns.

At the same time, the hypothesis of producing DB-TTF molecules in solution during the electrode surface modification reaction (oxidative potential at 0.6 *V* corresponds with DB-TTF moieties as found in literature[67]) it is being possibly responsible for the formation of helical structures by π-π stacking interactions between BDYT covalently linked to the surface and DB-TTF molecules in solution. Such interactions could result in a 3D modified electrode surface.

Helical structures were found in literature to be formed through π-π stacking interactions involving naphthyl rings for several TTF compounds.[106]

CHAPTER 5: TRANSPARENT CONDUCTIVE FILMS FROM GRAPHITE INTERCALATION COMPOUNDS (GICS)

Graphite is described as a semi-metal and shows a complex electronic band structure.[29,107] Its thermoconductivity is highly anisotropic resulting in a material that is highly conductive in plane but almost insulating in perpendicular to it. Intercalated compounds may be obtained from graphite with different stage index, determined by the number of layers of graphite between the intercalate species layer. Intercalation allows the modulation of the free carrier concentration in compounds, being possible to control the electrical, thermal, and magnetic properties of the graphitic material. Intercalation with alkali metals is one of the most studied, like KC_8 compounds. These are classified as donor-type compounds, where the metal atom transfers its charge to the graphite conduction band resulting in a large increase of the

in-plane and c-axis conductivity. Many of the GICs are sensitive to air requiring encapsulation to ensure chemical stability. The sample color gives qualitative information on the stage index: for alkali compounds, yellow, gold, or red is characteristic of stage one compounds, steel blue for stage two, dark-blue for stage three and metallic black for higher stages.

As we mentioned in chapter 1, the surface modification of carbon-based materials is well studied.[108,109,110] Over the present chapter, the synthesis, solutions and depositions of GIC solutions has been investigated. Likewise, the electrochemical surface modification of graphene films (from GIC solutions) has been studied. These films are suitable to be used as electrodes for performing surface modification, as in the case of SWCNTs.

In our laboratory three different sources of graphite were used during the study: natural graphite from Sigma-Aldrich, graphite from Brazil (labeled as G4), and from Madagascar.

GICs prepared with natural graphite (Sigma-Aldrich) resulted in a mixture of different stages of KC_8; when prepared with natural graphite from Brazil (G4) the stage obtained was mostly one.

5.1. SYNTHESIS AND SOLUTIONS OF KC8 COMPOUNDS

To prepare KC_8 compounds the two-zone vapour transport method was used. In this method the intercalant (potassium) is heated up to some temperature T_i and the graphite, some distance away is heated to a higher temperature T_g. The sublimation of the metal leads to the formation of the intercalated compound.

Tubes were filled with the corresponding calculated amounts of natural graphite and metallic potassium. An excess of potassium is added to ensure a complete intercalation between graphite flakes. This preparation takes place under inert atmosphere reaching pressure ~$8.3x10^{-4}$ *mbar*. Overnight reaction gave high quality stage-one graphite intercalation compound with a nice gold color. The resulting compound was placed back to an inert environment and preserved from oxidation.

Procedures for the preparation of Graphene solutions have been set up at CRPP-CNRS, Pessac, over the last years.[27] Deposition from such solutions showed large graphene flakes under TEM (see figure 1).

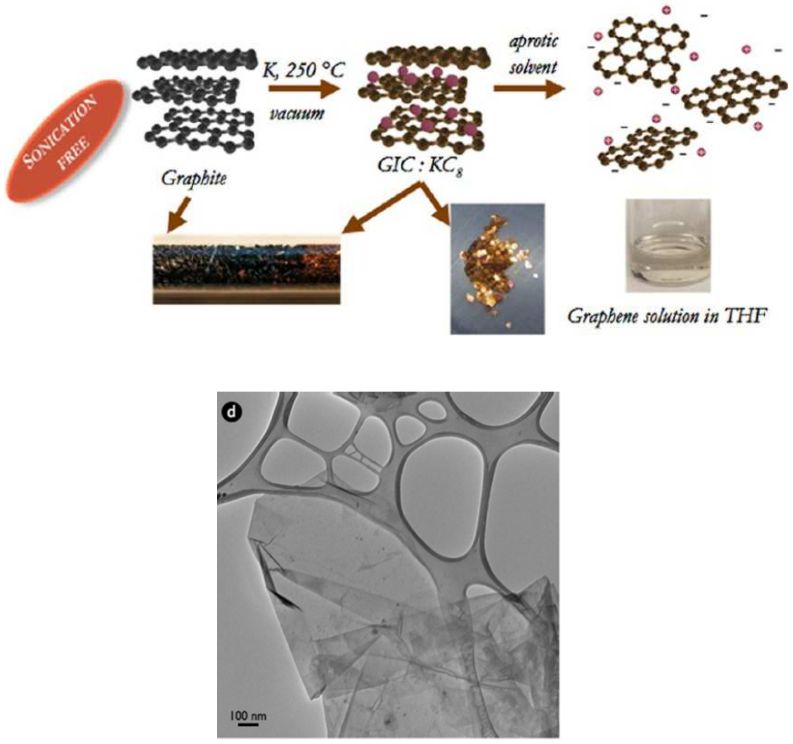

Fig. 1: Route representation to produce graphene solutions (above). Multi-folded graphene flake image by high resolution TEM (below).[28]

Solutions of graphite intercalated compounds gives “graphenide” solutions.[28] The term "graphenide" was introduced in 2012 during ChemOnTubes2012 conference in Arcachon to describe negatively graphene sheets.

The dissolutions of GICs were performed using distilled methyl-tetrahydrofuran (M-THF) and distilled cyclopentyl methyl ether (CPME) (2 *mg* of KC_8 per milliliter of solvent). They were covered with aluminum foil and mildly stirred for 48 hours. The resulting solution was centrifuged (2000 *r.p.m.* per 10 minutes at room temperature) and the supernatant was collected.

A first attempt to prepare films from the above solutions was made by dropcasting on glass substrates. Deposition was performed following two different strategies, (i) dropcasting on glass under inert conditions followed by dry air oxidation, or (ii) dropcasting on glass directly in air.

5.2. FROM SOLUTIONS TO GRAPHENE FILMS

In order to produce thin films of graphene, two different routes were followed:

a) dropcasting of the solution under inert atmosphere before oxidation of the flakes (by dry oxygen)
b) dropcasting of the solution in air from deareated solutions.

In both cases glass slides (A= 1.5 cm^2) were used as substrates.

Starting from route (a), solutions of methyl tetrahydrofuran (M-THF) and cyclopentyl methyl ether (CPME) were spincoated in the glove box. The resulting deposits were re-oxidized using dry air and labeled as **DN_2-MTHF** and **DN_2-CPME** meaning deposit under nitrogen atmosphere with the respective solvent.

For the preparation route (b), samples of the corresponding M-THF and CPME solutions were taken by air-tight syringes under inert atmosphere and spin coated in air, obtaining **DO_2-MTHF** and **DO_2-CPME** deposits that were characterized by high-resolution-SEM (see figure 2).

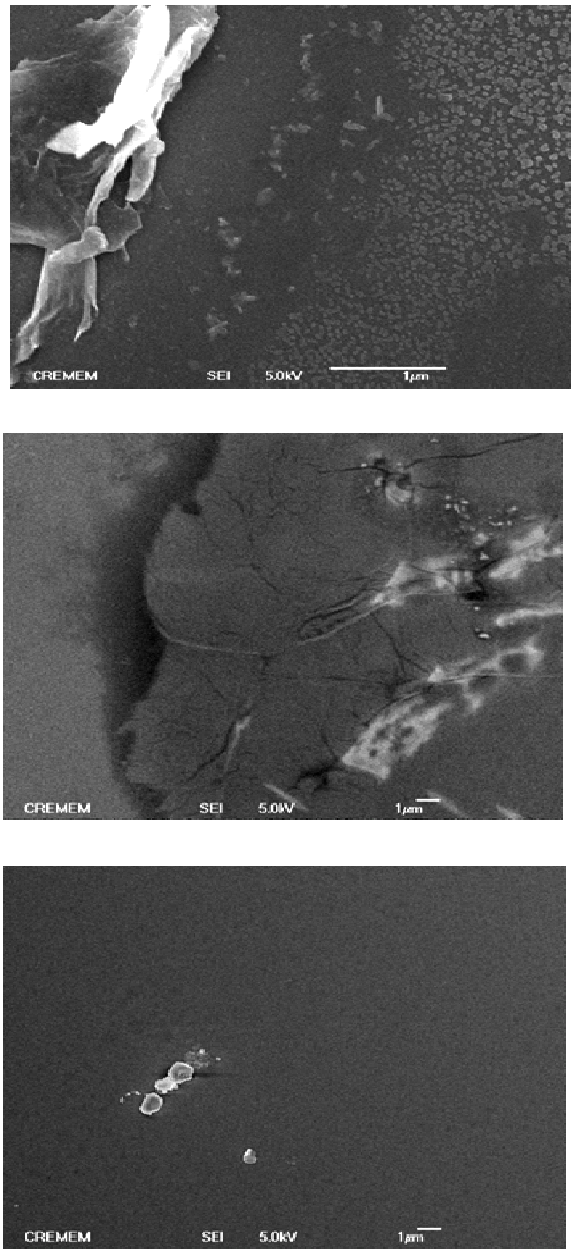

Fig. 2: SEM images of GIC depositions on glass substrates. From top to bottom: DO_2-CPME, DN_2-CPME, and DN_2-MTHF.

Samples were characterized at the CREMEM institute, Pessac, after metallization with gold.

While for DN_2-CPME and DO_2-CPME flakes are observed, for M-THF solutions there is no evidence of their presence.

Further studies would be necessary in order to optimize the film preparation procedure. However, the following study was concentrated on films prepared according to a method set up by Y. Wang, Ph.D. student at CRPP-CNRS, Pessac.

Briefly, the GIC solutions were filtrated following the same protocol used for preparing SWCNT films, obtaining graphene films supported on PS (see figure 3).

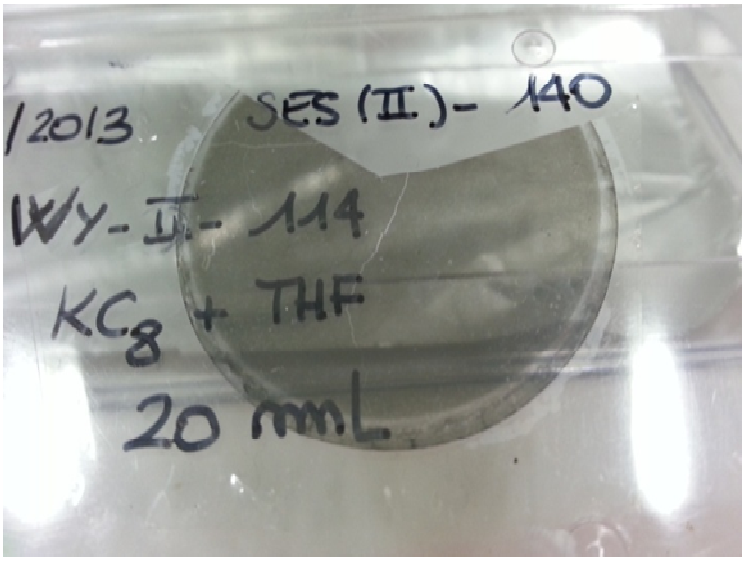

Fig. 3: Graphene film on polystyrene (PS) substrate.

These are transparent and conductive films that resulted to be composed mainly by single-to-few layers graphene[d] suitable to be used as electrodes for performing surface modification as in the case of SWCNTs.

5.3. GRAPHENE-BASED ELECTRODES

Electrochemical surface modification of graphene-based films is well known in literature and has been recently reported by P. Lu et al.,[111] as novel applications of functionalized graphene sheets. M. Prato and coworkers showed the functionalization of graphite sheets (produced by solvent extraction procedures) upon dipolar cycloaddition reaction[112] where they demonstrate successful click reaction yielding to highly functionalized material.

AFM (introduced in chapter 2) was used for the characterization of the films. Firstly, polystyrene substrate was analyzed (Figure 4).

[d] Y. Wang, private communication

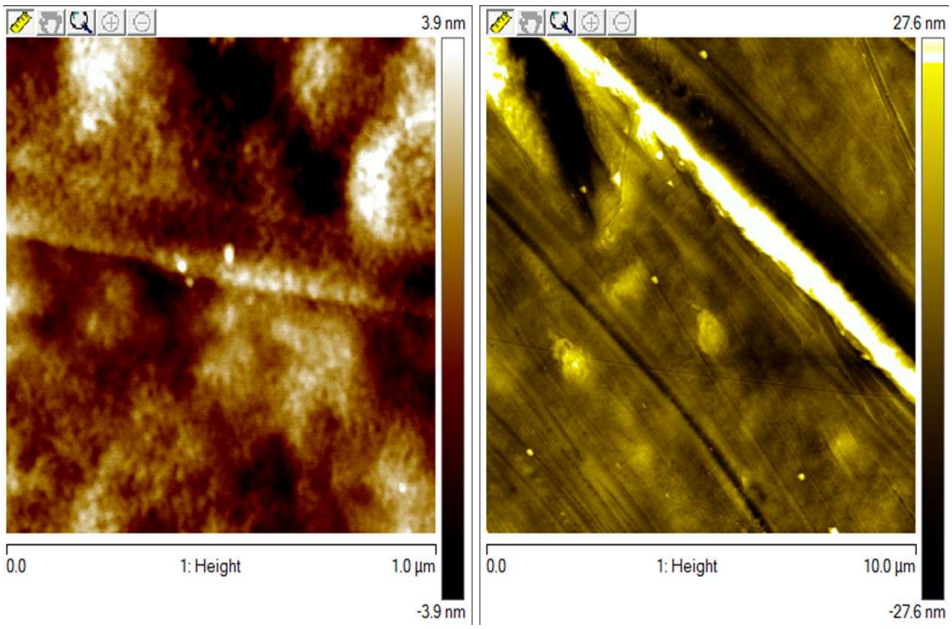

Fig. 4: AFM of polystyrene foil (height image). Polystyrene substrates are commercially available from Goodfellow.

The AFM images showed quite flat, clean, and homogeneous surface of polystyrene. The graphene film shows several flakes partly corrugated and folded (Figure 5).

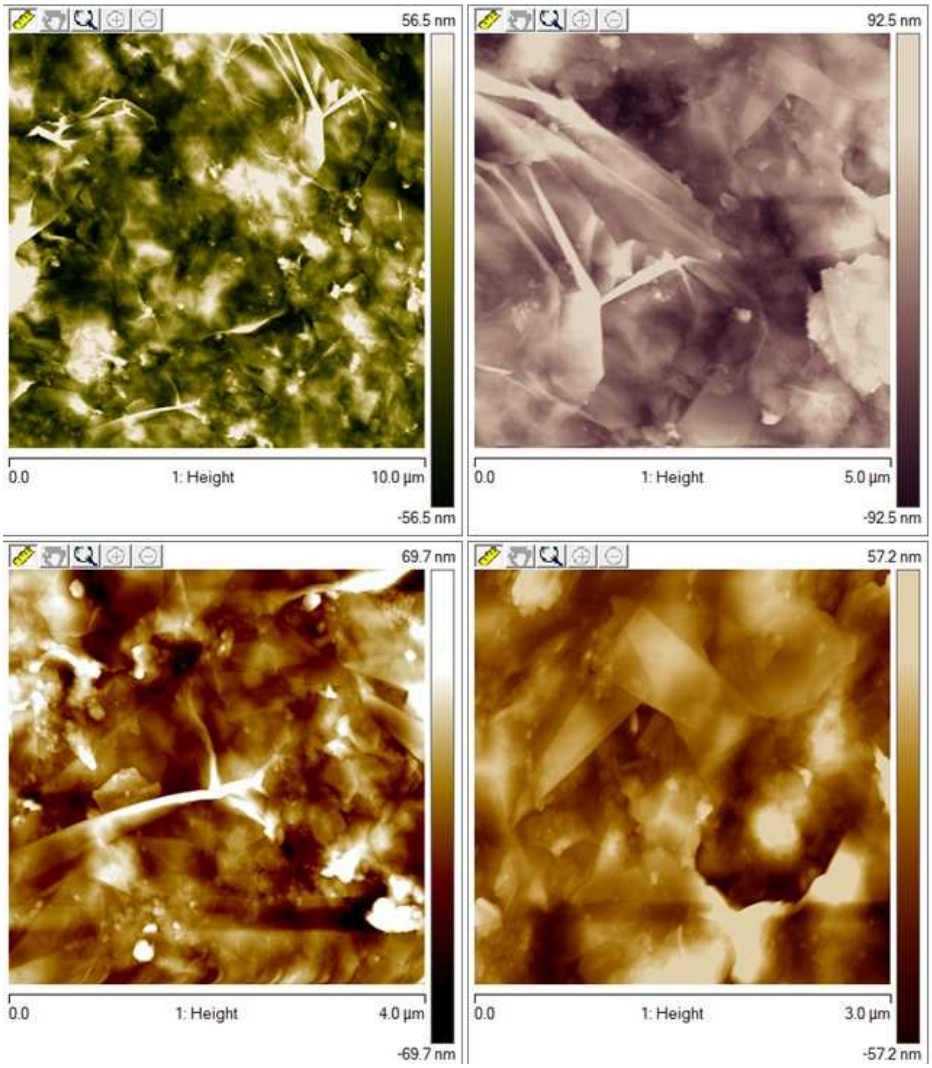

Fig. 5: AFM image collection of Graphene film on a PS substrate.

Some origami-folded graphene flakes show different contrast that may be associated to various numbers of folds and layers. In any case, the deposition of GIC solutions is not yet resulting in a very clean deposit (see figure 5a). An XPS analysis of the surface gives information regarding such an issue.

XPS shows the presence of nitrogen and silicon atoms (0.46 and 0.23 atomic % respectively) together with carbon (95.82 %) and oxygen (3.47 %) thus indicating there is no potassium residues (see figure 6 and table 1).

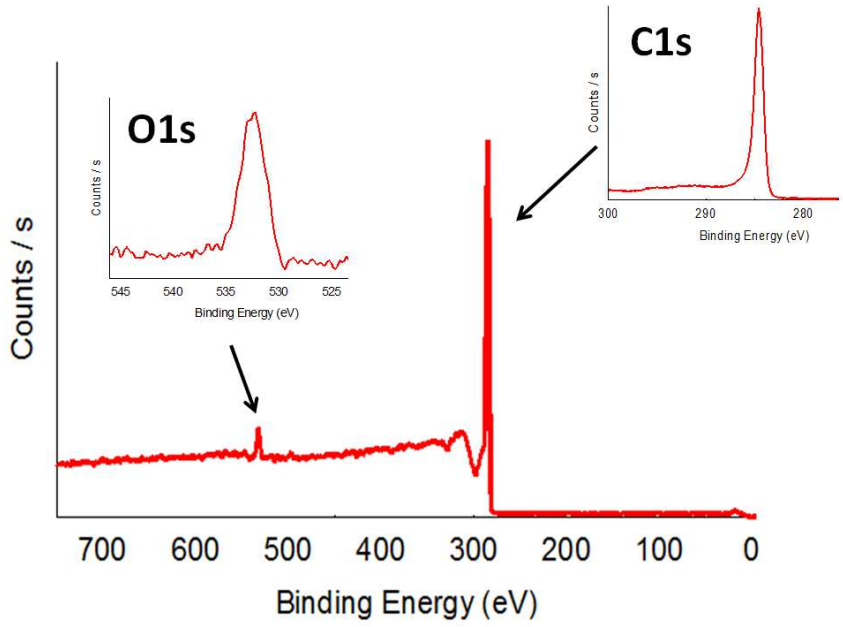

Fig. 6: XPS spectrum for graphene-based film. Carbon 1s and Oxygen 1s bands are shown as small captures. The arrows indicate the band position.

Name	Peak BE	Height Counts	FWHM eV	Area (P) CPS.eV	Area (N)	At. %
C1s	284,59	23218,71	1,1	36655,39	0,6	95,84
N1s	403,62	132,79	0,37	303,97	0	0,46
O1s	532,44	1152,81	2,98	3587,03	0,02	3,47

Table 1: XPS of graphene-based film shows the quantification of different atoms present in the surface.

Main XPS spectrum (see figure 6) shows an intense peak at ~284.5 *eV* related to sp^2 carbon and a small peak at 532.4 *eV* related to oxygen.

The Raman spectrum of a graphene film on PS is reported in figure 7.

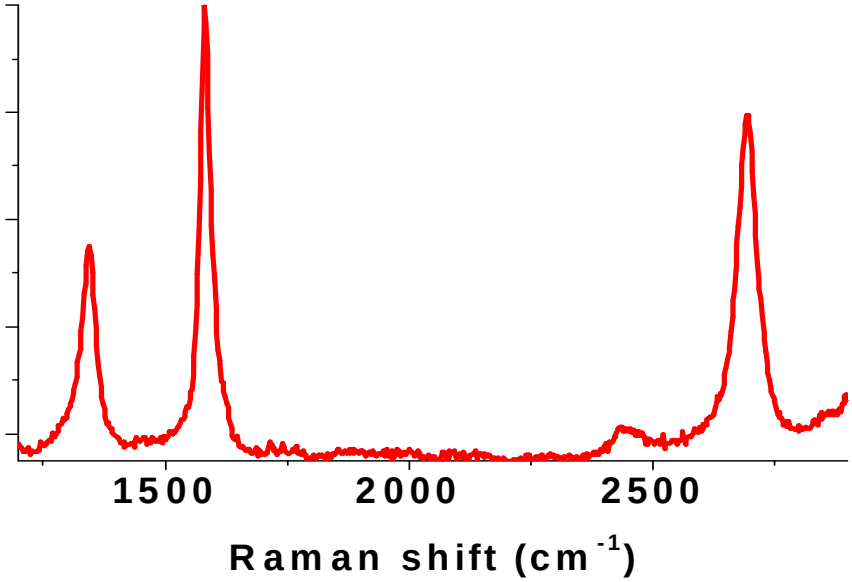

Fig. 7: Raman spectrum of graphene film on polystyrene. Excitation wavelength used 532 *nm*.

The main information that can be obtained by Raman is crystallinity /orientation of the sample (stage index of the compound) by analysis of the D-band, and the number of graphene layers by analysis of the width of the band at ~2700 cm^{-1}. An increase of the D-band intensity in Raman spectroscopy determines break in the symmetry of carbon nanomaterials. The modified material will show hybridization changes from sp^2 to sp^3 carbons resulting in a symmetry break and it will be reflected on the D-band situated ~1300 cm^{-1}.

Mapping of the surface gives an average value of these bands and their intensities. Raman spectrum of a graphene film displays (see figure 7) three characteristic bands: the D-band (ca. at 1300 cm^{-1}), the G-band (ca. at 1600 cm^{-1}), and the G'-or 2D-band (ca. at 2700 cm^{-1}). The sharpness of the G'-band indicates uncorrelated graphene layers, i.e. exfoliated material.

The electrochemical surface modification with aryl diazonium salt onto graphene films was performed. In parallel, surface modification with 1, 3 - BDYT was also investigated. For both reactions, the film was placed in the electrochemical cell (figure 8), where the surface area of the film in contact with the solution during measurements is fixed and equal to A= 0.21 cm^2.

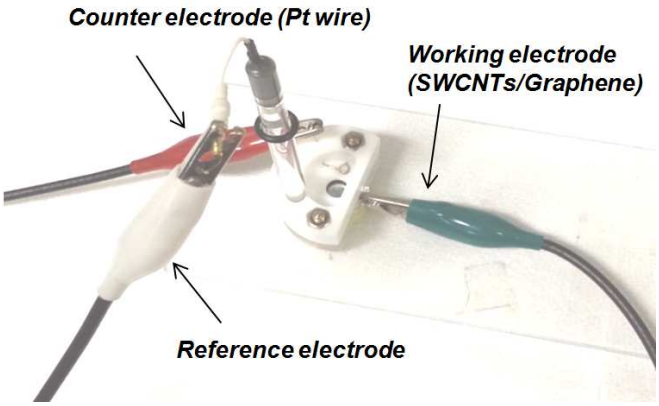

Fig. 8: Electrochemical setup of the cell. Contacts were made with crocodile electrodes.

In the first approach, the reaction takes place in aerated solutions while for the second reaction inert conditions are needed, due to high reactivity of the electrogenerated radical with oxygen in solution. In our laboratory (CRPP-Bordeaux), we had the possibility to carry out such reactions in the glove box.

5.3.1. SURFACE MODIFICATION UPON ELECTROGRAFTING WITH ARYL DIAZONIUM SALTS

The electrografting of aryl diazonium salts on graphene films was performed with PhDA moieties following the same procedure as for the surface modification of SWCNT films.

The graphene film was placed in the electrochemical cell as the working electrode. The reference electrode was Ag/AgCl in a saturated solution of KCl and the acidic solution (HCl) ensured conductivity in solution acting as a supporting electrolyte. 5 *mM* of p-PhDA was prepared in a 0.5 *M* HCl, and parallel to that another solution 0.1 *M* $NaNO_2$ was prepared. The stoichiometry was calculated for the reactivity of only one amino group and the corresponding volumes were added to the cell. P-PhDA solution turns yellow upon addition of NaNO2 equivalents indicative for the formation of diazonium salts. Besides, formation of bubbles during the reaction ($-N_2$) is indicative for nitrogen elimination with the ongoing reaction.

A starting potential of 0.55 *V* (OCP) was chosen that ensured that no current flew before starting the scan. The potential was cycled 15 times from 0.55 *V* to -0.25 *V* leading to formation of a visible layer on the surface of the film (see figure 9).

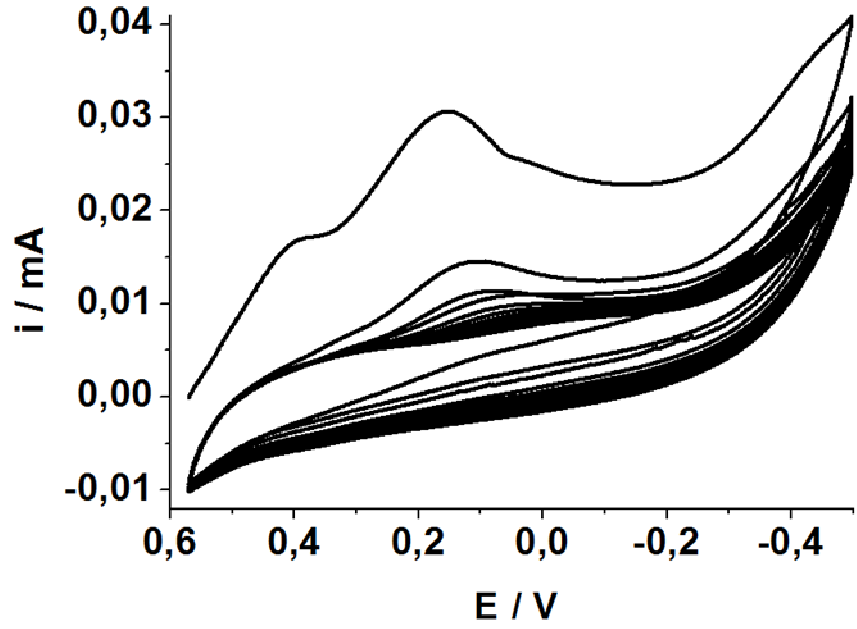

Fig. 9: Cyclic voltammetry for the electrografting of diazonium salts on graphene-based electrodes. Scan rate of 100 *mV* s^{-1}.

After reaction, the film was rinsed carefully with distilled water in order to neutralize the resulting layer for the subsequent Raman characterization. An increase of the intensity of the D-band (normalized to the G-band) is observed after surface modification indicating successful covalent surface modification of graphene flakes. The increase of fluorescence is indicative of organic material deposited on the film surface (see figure 10).

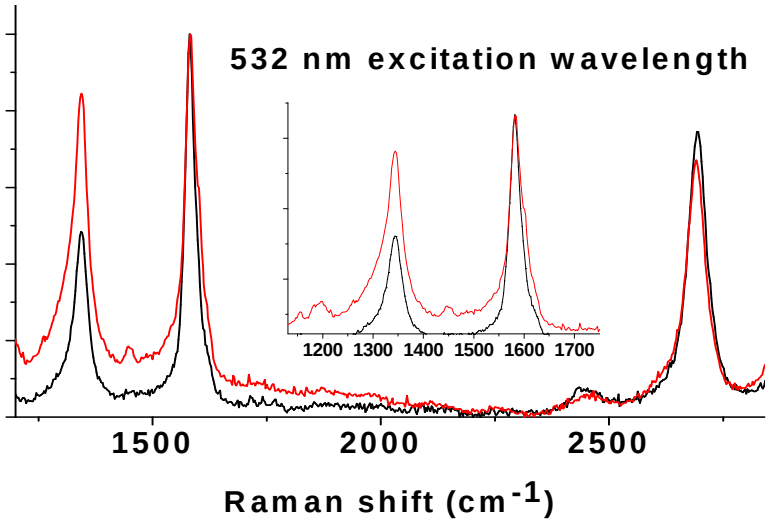

Fig. 10: Raman spectra of graphene film before (black line) and after (red line) electrochemical surface modification with PhDA.

The transformation of the immobilized amines in azide groups was performed. The resulting film was rinsed with distilled water and dried under a flow of argon.

The cycloaddition reaction with ferrocene containing probes (previously introduced in chapter 4) was investigated. 1 *mg* of alkyne-ferrocene was dissolved in 400 *μL* of distillated water resulting in a 10 *μM* solution concentration. In parallel, copper sulfate penthydrate and (+) sodium L-ascorbate were calculated in excess respect to the alkyne-ferrocene solution. The mixture was stirred and dropcasted onto the reactive film surface. Samples were placed on an ice bath during reaction. After 2 hours the film was rinsed and sonicated for a short time (<1 minute) for the removal of adsorbed/trapped species on/in graphene film.

Taking advantage of redox properties of ferrocene containing species, cyclic voltammetries were run in a Phosphate buffered saline solution (PBS) to investigate the efficacy of the performed reaction (see figure 11).

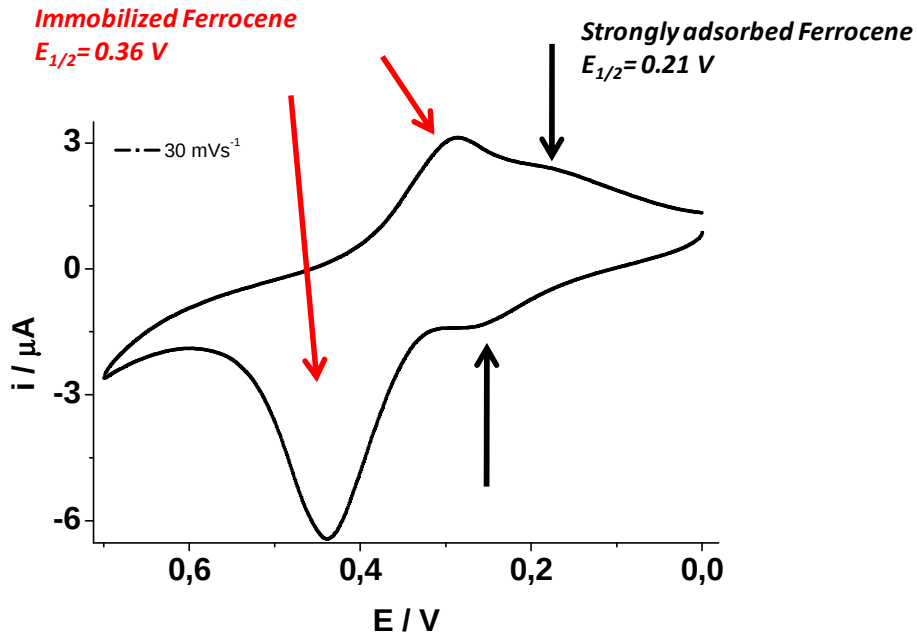

Fig. 11: Analysis of the voltammetric curve of click-modified graphene-based electrodes with ferrocene containing moieties. CV measured in PBS at a scan rate of 30 mV s^{-1}.

The CV curve shows two oxidation processes, both attributed to the ferrocene moieties. The main anodic peak at 0.43 V corresponds to the oxidation of the ferrocene species whose corresponding cathodic peak is located at 0.29 *V* ($E_{1/2}$=0. 36 *V*). The peak separation of 140 *mV* is indicative of slow electron transfer kinetics associated to the presence of the poly aryl film.

The anodic peak at 0.26 *V* and its cathodic partner at 0.18 *V* were also attributed to ferrocene species in a different environment. The peak separation in this case (80 *mV*) is closer to the theoretical value.

In order to attribute the two redox processes a model compound (FcMeOH) was investigated with pristine graphene films (see figure 12a).

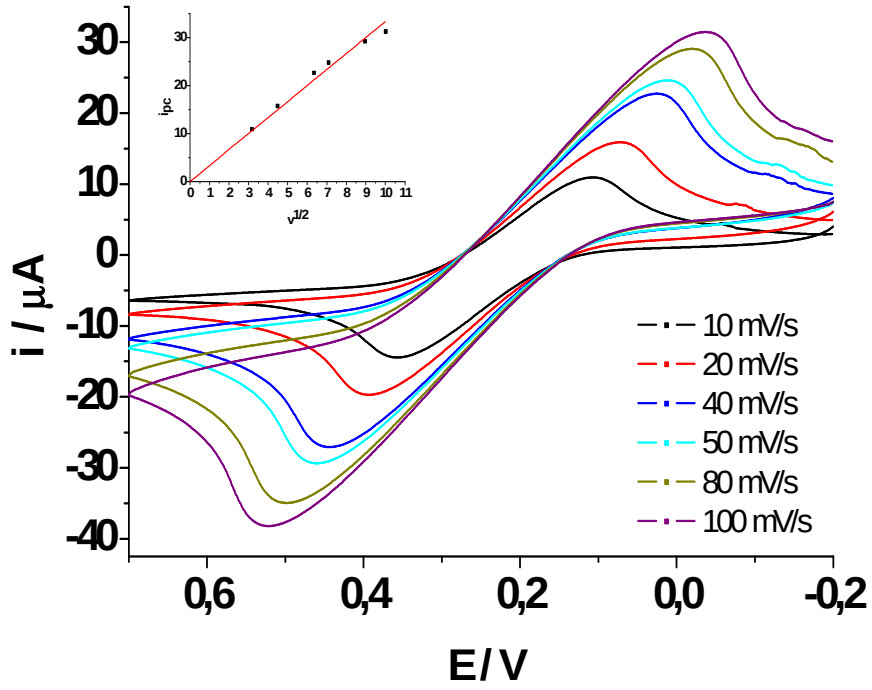

Fig. 12a: Analysis of the scan rate dependence with the voltammetric current of 1 mM FcMeOH in PBS on graphene-based electrode. The inset figure shows linear response of peak currents vs. $v^{1/2}$.

The cyclic voltammetry shows one reversible oxidation process with $E_{1/2}$= 0.36 *V* attributed to diffusion controlled oxidation of FcMeOH. In agreement with

this attribution peak currents were proportional to the square root of the scan rate.

Signal associated to ferrocene species was still observed after rinsing the electrode and placing it in a fresh PBS solution (see figure 12b).

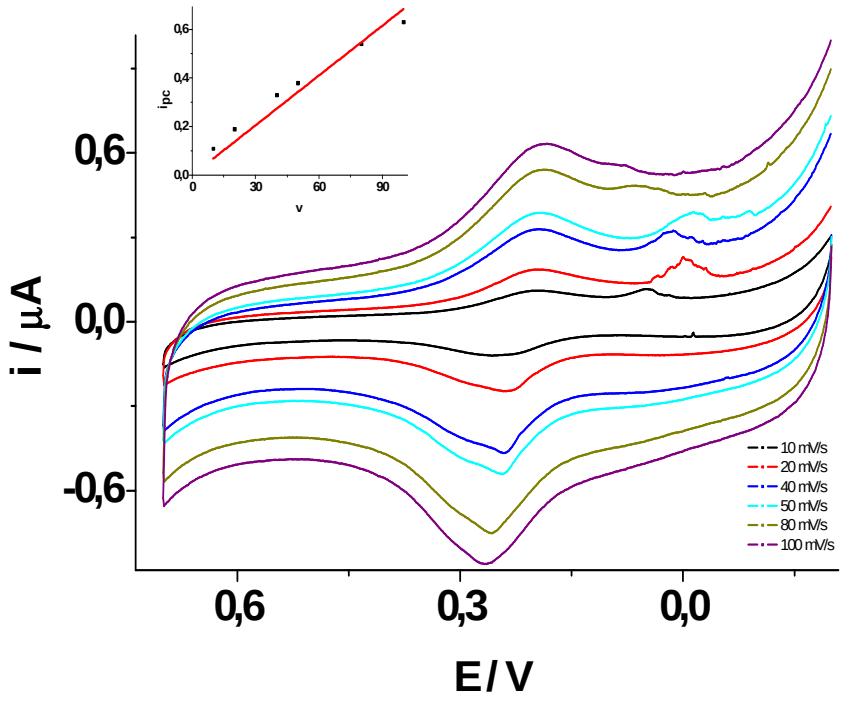

Fig. 12b: Analysis of the scan rate dependence with the voltammetric current of rinsed graphene-based electrode (figure 12a) in PBS. The inset figure shows linear response of peak currents vs. scan rate.

In this case however the signal is much lower, more reversible ($E_{1/2}$= 0.21 *V* and peak separation is 40 *mV*), and the linear dependence on the scan rate

suggests that an immobilized species is involved. Even after sonication, a signal associated with these species is visible.

The comparison of the CV curves in figure 11a with those of the model compound allows to formulate a hypothesis for the two redox processes observed:

1. The main peak with $E_{1/2}$= 0.36 *V* is related to the ferrocene probe covalently anchored to the film surface upon the click reaction. Its redox potential is compatible with that of FcMeOH in solution (vs. Ag/AgCl reference electrode) $E_{1/2}$=0.34 *V*.
2. The minor peak at $E_{1/2}$=0.21 *V* is instead related to ferrocene moieties strongly interacting with graphene (physically adsorved). This explains the anticipation of the redox process with respect to the model. This is in agreement with figure 12b. Furthermore, the faster kinetics associated to this peak is in line with the strong interaction between ferrocene and graphene film (π-π stacking).

5.3.2. SURFACE MODIFICATION THROUGH ELECTROPHYLIC ADDITION OF 1, 3- BDYT

The electrochemical adsorption of 1, 3- BDYT moieties on graphene film, was performed following studies done for SWCNT films.

The graphene film was placed in the electrochemical cell and introduced inside the glove box. The reference electrode was prepared inside the box before the measurement being Ag/AgCl wire in 0.1 *M* tetrabutylammonium hexafluorophosphate (TBA^+PF6^-) acetonitrile solution. The electrodeposition

was carried out in 5 *mM* 1, 3-BDYT acetonitrile solution with 0.1 M $TBA^{+}PF6^{-}$ by performing a variable number of potential cycles between 2 and 20.

As shown in figure 13 the radical species is formed starting at ~0.15 *V*. The efficiency of the process, measured by the passivation of the electrode surface, is lower than in the case of SWCNTs.

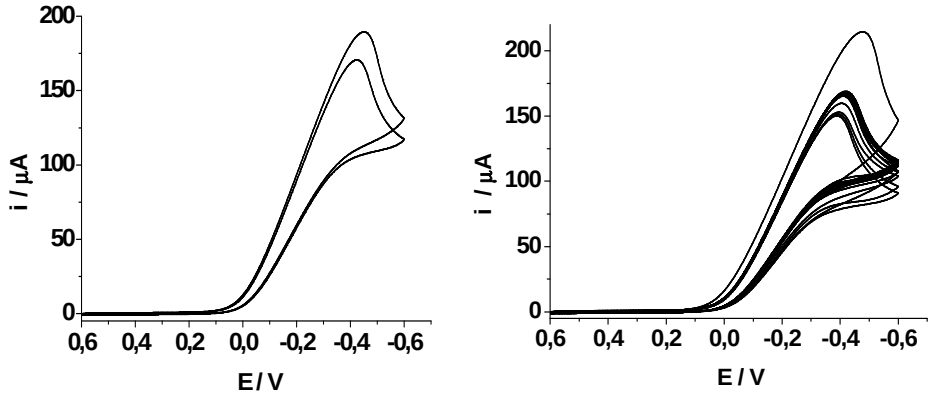

Fig. 13: Cyclic voltammetry for the electrochemical surface modification of graphene film with 5 mM 1, 3- BDYT in acetonitrile. Left: 2 cycles. Right: 20 cycles. Scan rate: 50 *mV* s^{-1}.

After 15 cycles of potential the system leads to an increase of current values, and after twenty, the process leads to a steady state values. The resulting surfaces were analyzed by Raman spectroscopy, atomic force microscopy (AFM) and photoelectron spectroscopy (XPS).

Raman spectra after normalization by the G-band would show an increase of the D-band intensity, as expected in the case of covalent functionalization. However, the strong increase of fluorescence makes this observation less conclusive with respect to the previous systems (figure 14).

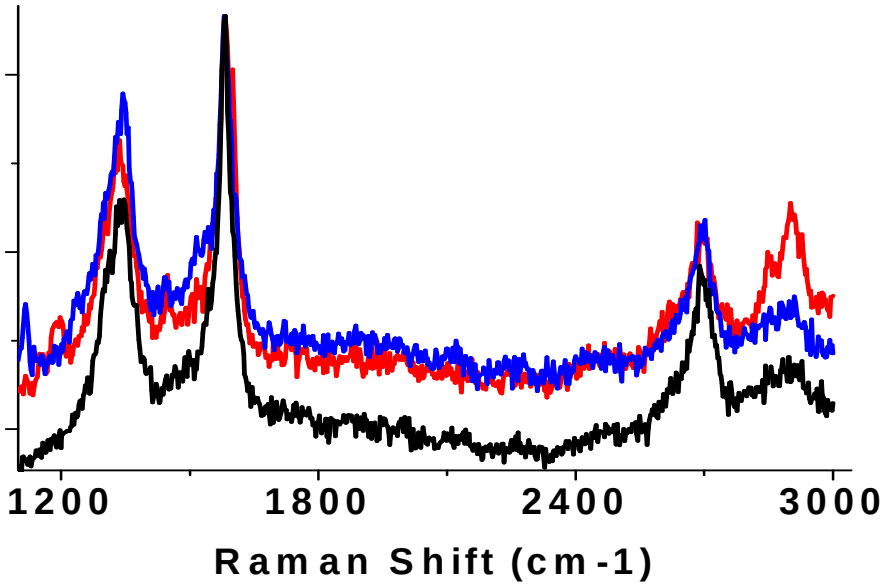

Fig. 14: Raman spectra of graphene film before (black) and after (red and blue lines: 2 and 20 potential cycles) surface modification normalized to the G-band.

XPS spectra (see figure 15) shows the presence of 1.5% of sulfur atoms not present in the surface of the pristine film. That indicates the adsorption of BDYT on the surface has occurred. Besides, the amount of oxygen atoms (peak around 290-295 *eV*) diminished from 3.47% to 2.85% indicative of the elimination of oxygen species present on the surface of the pristine film (see figure 15 and table 2).

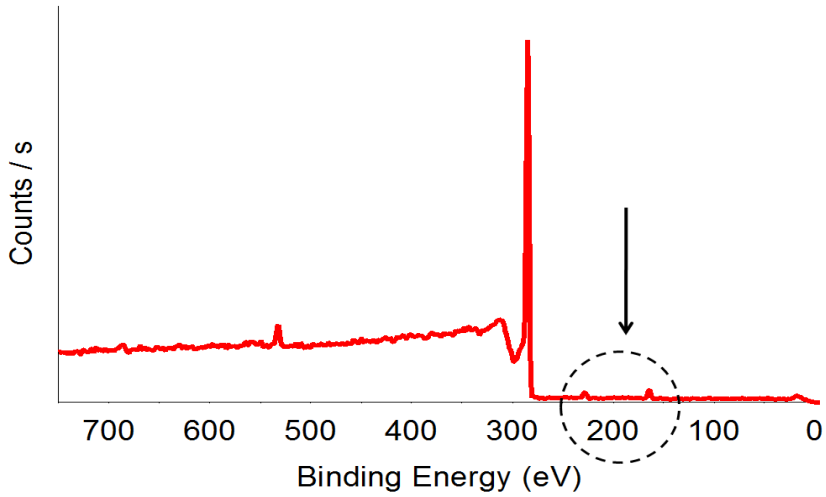

Fig. 15: XPS spectra of BDYT surface modified graphene film. The arrow shows peaks detected after surface modification attributed to sulfur atoms (2p and 2s).

Name	Peak BE	Height Counts	FWHM eV	Area (P) CPS.eV	Area (N)	At. %
S2p	163,77	496,9	1,99	1104,27	0,01	1,5
C1s	284,46	27455,37	1,08	40290,75	0,66	94,52
O1s	532,26	1077,83	2,76	3285,83	0,02	2,85
F1s	686,1	492,24	3,15	1840,54	0,01	1,13

Table 2: Atomic values found for surface modified graphene-based film with BDYT.

These oxygen species could be related to the formation of oxygenated groups on graphene flakes (probably edges) during film re-oxidation. Fluorine atoms were also present on the film surface in amounts of ~1% related to the

supporting electrolyte (tetrabutylammonium hexafluorophosphate) present during the performance of the reaction. Analogously, traces of fluorine and phosphor were also found in SWCNT-BDYT functionalized films. Atomic Force Microscopy images of the graphene film were obtained before and after electrochemical modification with BDYT moieties (see figure 16a and 16b).

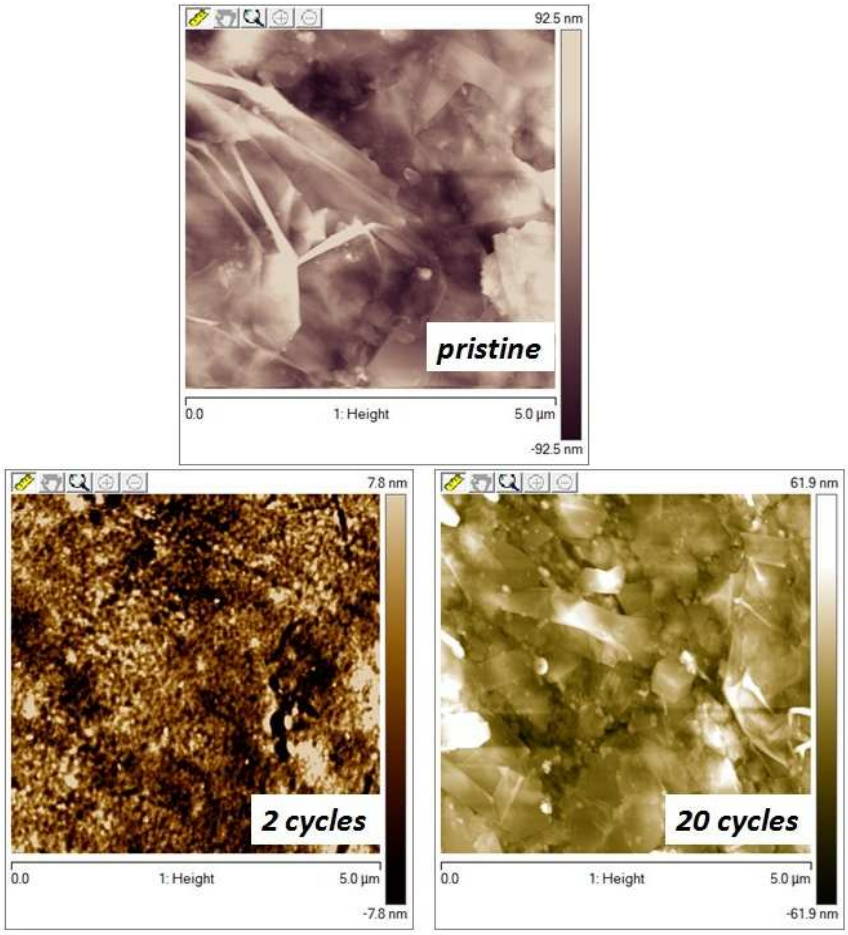

Fig. 16a: AFM images of graphene film before and after electrochemical surface modification with BDYT.

In figure 16a, pristine graphene film shows highest point at ~92 *nm*. After electrochemical reaction with BDYT (2 cycles), the value diminishes to ~8 *nm* and the surface topography has noticeably changed. The electrochemical surface modification upon 20 potential cycles shows values ~62 *nm* and the appearance has also changed with growth of ball-shaped material.

Scanning smaller zones (see figure 16b, 1 μm^2) is possible to observe the formation of ball-shaped material after 2 potential cycles in comparison with the pristine material.

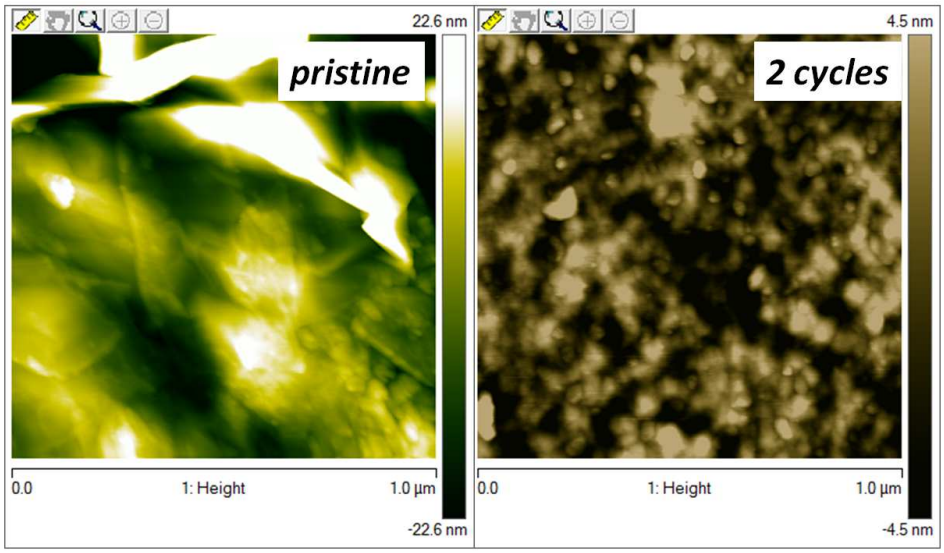

Fig. 16b: AFM images of graphene film before and after electrochemical surface modification.

In this case, the pristine material shows highest point at ~23 *nm* while the modified material appears to be at ~4.5 *nm*. The topography is noticeably changed in comparison with the pristine graphene film.

However, no presence of twisted ropes formation, as in the case of SWCNT films, was observed. An explanation for such an observation may be the lower reactivity of graphene films in comparison with SWCNT films, lacking of any intrinsic curvature of the pristine material.

5.4. CONCLUSIONS

We have presented the synthesis and dissolution of some prepared GICs. Its deposition on glass has been investigated by SEM. Only for solutions prepared with CPME graphene flakes were observed.

Graphene films[e] are transparent conductive films that can be used as electrode devices (as seen for SWCNTs in chapter 4). AFM shows well-defined, folded, and corrugated graphene flakes. XPS analysis shows clean surfaces with the presence of carbon and oxygen mostly. Raman spectra showed well defined bands related to graphitic material.

The electrochemical surface modification of graphene films have been achieved following two different routes (i) electrografting of aryl diazonium salts and (ii) electrophylic addition of BDYT on the graphene film surface.

The electrochemical surface modification with PhDA, transformation of the remaining amino groups and click-reaction leads to the formation of new triazolic rings containing ferrocene moieties which were detected by cyclic voltammetry. The immobilized species through a polymeric aryl film show slower electron transfer with higher peak separation; the strong interaction of ferrocene with electron rich systems, as graphene films, leads to a strong

[e] *Prepared by Ph.D. student Y. Wang, CRPP-CRNS, Pessac.*

adsorption of material on the film surface; thus is detected as a fast electron transfer where the oxidation of ferrocene species is facilitated by the graphene film surface.

Likewise, BDYT moieties were electrochemically investigated to react with graphene films as studied with SWCNT films. Its characterization by Raman spectroscopy, XPS and AFM has been shown. In contrast to SWCNT films, no formation of twisted ropes was observed.

BIBLIOGRAPHY

(1) *Feynman, R. There Is Plenty of Room at the Bottom.* Engrineering Sci. ***1960**, 22–36.*

(2) *Kroto, H.; Heath, J.; O'Brien, S.; Curl, R.; Smalley, R. C60: Buckminsterfullerene.* Lett. to Nat. ***1985**,* 318*, 162–163.*

(3) *Iijima, S. Helical Microtubules of Graphitic Carbon.* Nature ***1991**,* 354*, 56–58.*

(4) *Rivas, G. a; Rubianes, M. D.; Rodríguez, M. C.; Ferreyra, N. F.; Luque, G. L.; Pedano, M. L.; Miscoria, S. a; Parrado, C. Carbon Nanotubes for Electrochemical Biosensing.* Talanta ***2007**,* 74*, 291–307.*

(5) *Dai, H. Carbon Nanotubes: Synthesis, Integration, and Properties.* Acc. Chem. Res. ***2002**,* 35*, 1035–1044.*

(6) *Kataura, H.; Kumazawa, Y.; Maniwa, Y.; Umezu, I. Optical Properties of Single-Wall Carbon Nanotubes.* Synth. Met. ***1999**,* 103*, 2555–2558.*

(7) *Ajayan, P. M. Nanotubes from Carbon.* Chem. Rev. ***1999**,* 99*, 1787–1800.*

(8) *Bronikowski, M. J.; Willis, P. a.; Colbert, D. T.; Smith, K. a.; Smalley, R. E. Gas-Phase Production of Carbon Single-Walled Nanotubes from Carbon Monoxide via the HiPco Process: A Parametric Study.* J. Vac. Sci. Technol. A Vacuum, Surfaces, Film. ***2001**,* 19*, 1800–1805.*

(9) *Bachilo, S. M.; Balzano, L.; Herrera, J. E.; Pompeo, F.; Resasco, D. E.; Weisman, R. B. Narrow (n,m)-Distribution of Single-Walled Carbon*

Nanotubes Grown Using a Solid Supported Catalyst. J. Am. Chem. Soc. ***2003***, 125, *11186–11187.*

(10) *Collins, P. G.; Smalley, R. Nanotube Nanodevice.* Science (80-.). ***1997***, 278, *100–102.*

(11) *McCreery, R. L. Advanced Carbon Electrode Materials for Molecular Electrochemistry.* Chem. Rev. ***2008***, 108, *2646–2687.*

(12) *Dresselhaus, M. Graphene: A Journey through Carbon Nanoscience.* MRS Bull. ***2012***, 37, *1319–1320.*

(13) *Novoselov, K.; Geim, A.; Morozov, S. Electric Field Effect in Atomically Thin Carbon Films.* Science (80-.). ***2004***, 306, *666–669.*

(14) *Stankovich, S.; Piner, R. D.; Chen, X.; Wu, N.; Nguyen, S. T.; Ruoff, R. S. Stable Aqueous Dispersions of Graphitic Nanoplatelets via the Reduction of Exfoliated Graphite Oxide in the Presence of Poly(sodium 4-Styrenesulfonate).* J. Mater. Chem. ***2006***, 16, *155–158.*

(15) *Lee, Y.; Bae, S.; Jang, H.; Jang, S.; Zhu, S.-E.; Sim, S. H.; Song, Y. Il; Hong, B. H.; Ahn, J.-H. Wafer-Scale Synthesis and Transfer of Graphene Films.* Nano Lett. ***2010***, 10, *490–493.*

(16) *Xu, Y.; Liu, Z.; Zhang, X.; Wang, Y. A Graphene Hybrid Material Covalently Functionalized with Porphyrin: Synthesis and Optical Limiting Property.* Adv. Mater. ***2009***, 21, *1275–1279.*

(17) *Novoselov, K.; Geim, A.; Morozov, S. Two-Dimensional Gas of Massless Dirac Fermions in Graphene.* Nature ***2005***, *1–6.*

(18) *Niyogi, S.; Bekyarova, E.; Itkis, M. E.; McWilliams, J. L.; Hamon, M. a; Haddon, R. C. Solution Properties of Graphite and Graphene.* J. Am. Chem. Soc. ***2006***, 128*, 7720–7721.*

(19) *Park, S.; Ruoff, R. S. Chemical Methods for the Production of Graphenes.* Nat. Nanotechnol. ***2009***, 4*, 217–224.*

(20) *Gengler, R. Y. N.; Spyrou, K.; Rudolf, P. A Roadmap to High Quality Chemically Prepared Graphene.* J. Phys. D. Appl. Phys. ***2010***, 43*, 374015–374034.*

(21) *Coleman, J. N.; Lotya, M.; O'Neill, A.; Bergin, S. D.; King, P. J.; Khan, U.; Young, K.; Gaucher, A.; De, S.; Smith, R. J.; et al. Two-Dimensional Nanosheets Produced by Liquid Exfoliation of Layered Materials.* Science ***2011***, 331*, 568–571.*

(22) *Niyogi, S.; Hamon, M. a.; Hu, H.; Zhao, B.; Bhowmik, P.; Sen, R.; Itkis, M. E.; Haddon, R. C. Chemistry of Single-Walled Carbon Nanotubes.* Acc. Chem. Res. ***2002***, 35*, 1105–1113.*

(23) *Margine, E. R.; Bocquet, M.-L.; Blase, X. Thermal Stability of Graphene and Nanotube Covalent Functionalization.* Nano Lett. ***2008***, 8*, 3315–3319.*

(24) *Bekyarova, E.; Itkis, M. E.; Ramesh, P.; Berger, C.; Sprinkle, M.; de Heer, W. a; Haddon, R. C. Chemical Modification of Epitaxial Graphene: Spontaneous Grafting of Aryl Groups.* J. Am. Chem. Soc. ***2009***, 131*, 1336–1337.*

(25) *Kuila, T.; Bose, S.; Mishra, A. K.; Khanra, P.; Kim, N. H.; Lee, J. H. Chemical Functionalization of Graphene and Its Applications.* Prog. Mater. Sci. ***2012***, 57*, 1061–1105.*

(26) *Pénicaud, A.; Poulin, P.; Derré, A.; Anglaret, E.; Petit, P. Spontaneous Dissolution of a Single-Wall Carbon Nanotube Salt.* J. Am. Chem. Soc. ***2005***, 127*, 8–9.*

(27) *Catheline, A.; Vallés, C.; Drummond, C.; Ortolani, L.; Morandi, V.; Marcaccio, M.; Iurlo, M.; Paolucci, F.; Pénicaud, A. Graphene Solutions.* Chem. Commun. (Camb). ***2011***, 47*, 5470–5472.*

(28) *Pénicaud, A.; Drummond, C. Deconstructing Graphite: Graphenide Solutions.* Acc. Chem. Res. ***2013***, 46*, 129–137.*

(29) *Dresselhaus, M. S. Fifty Years in Studying Carbon-Based Materials.* Phys. Scr. ***2012***, T146*, 014002.*

(30) *Cohen, M. L. Nanotubes, Nanoscience, and Nanotechnology.* Mater. Sci. Eng. C ***2001***, 15*, 1–11.*

(31) *Zhao, W.; Tan, P.; Liu, J.; Ferrari, A. Intercalation of Few-Layer Graphite Flakes with FeCl3: Raman Determination of Fermi Level, Layer by Layer Decoupling, and Stability.* J. Am. Chem. Soc. ***2011***, *2–7.*

(32) *Delamar, M.; Hitmi, R. Covalent Modification of Carbon Surfaces by Grafting of Functionalized Aryl Radicals Produced from Electrochemical Reduction of Diazonium Salts.* Am. Chem. Soc. ***1992***, 114*, 5884–5886.*

(33) *Allongue, P.; Delamar, M. Covalent Modification of Carbon Surfaces by Aryl Radicals Generated from the Electrochemical Reduction of Diazonium Salts.* J. Am. Chem. Soc. ***1997***, 119*, 201–207.*

(34) *Bahr, J. L.; Yang, J.; Kosynkin, D. V; Bronikowski, M. J.; Smalley, R. E.; Tour, J. M. Functionalization of Carbon Nanotubes by Electrochemical Reduction of Aryl Diazonium Salts: A Bucky Paper Electrode.* J. Am. Chem. Soc. ***2001***, 123*, 6536–6542.*

(35) *Marcoux, P.; Hapiot, P.; Batail, P.; Pinson, J. Electrochemical Functionalization of Nanotube Films: Growth of Aryl Chains on Single-Walled Carbon Nanotubes.* New J. Chem. ***2004***, 28*, 302–307.*

(36) *Kongsfelt, M.; Vinther, J. Combining Aryltriazenes and Electrogenerated Acids To Create Well-Defined Aryl-Tethered Films and Patterns on Surfaces.* J. … ***2011***, *3788–3791.*

(37) *Joyeux, X.; Mangiagalli, P.; Pinson, J. Localized Attachment of Carbon Nanotubes in Microelectronic Structures.* Adv. Mater. ***2009***, 21*, 4404–4408.*

(38) *Be, D. Direct Modification of a Gold Electrode with Aminophenyl Groups by Electrochemical Reduction of in Situ Generated Aminophenyl Monodiazonium Cations.* ***2006***, *4755–4763.*

(39) *Clavé, G.; Campidelli, S. Efficient Covalent Functionalisation of Carbon Nanotubes: The Use of "click Chemistry."*Chem. Sci. ***2011***, 2*, 1887–1896.*

(40) *Palacin, T.; Khanh, H. Le; Jousselme, B.; Jegou, P.; Filoramo, A.; Ehli, C.; Guldi, D. M.; Campidelli, S. Efficient Functionalization of Carbon*

Nanotubes with Porphyrin Dendrons via Click Chemistry. J. Am. Chem. Soc. ***2009***, 131*, 15394–15402.*

(41) Wang, H.-X.; Zhou, K.-G.; Xie, Y.-L.; Zeng, J.; Chai, N.-N.; Li, J.; Zhang, H.-L. Photoactive Graphene Sheets Prepared by "Click" Chemistry. Chem. Commun. ***2011***, 47*, 5747–5749.*

(42) Balasubramanian, K.; Burghard, M. Biosensors Based on Carbon Nanotubes. Anal. Bioanal. Chem. ***2006***, 385*, 452–468.*

(43) Chen, B.; Flatt, A. K.; Jian, H.; Hudson, J. L.; Tour, J. M. Molecular Grafting to Silicon Surfaces in Air Using Organic Triazenes as Stable Diazonium Sources and HF as a Constant Hydride-Passivation Source. Chem. Mater. ***2005***, 17*, 4832–4836.*

(44) Hauquier, F.; Pastorin, G.; Hapiot, P.; Prato, M.; Bianco, A.; Fabre, B. Carbon Nanotube-Functionalized Silicon Surfaces with Efficient Redox Communication. Chem. Commun. ***2006***, *4536–4538.*

(45) Such, G. K.; Johnston, A. P. R.; Liang, K.; Caruso, F. Synthesis and Functionalization of Nanoengineered Materials Using Click Chemistry. Prog. Polym. Sci. ***2012***, 37*, 985–1003.*

(46) Kolb, H. C.; Finn, M. G.; Sharpless, K. B. Click Chemistry: Diverse Chemical Function from a Few Good Reactions. Angew. Chemie Int. Ed. ***2001***, 40*, 2004–2021.*

(47) Rostovtsev, V. V; Green, L. G.; Fokin, V. V; Sharpless, K. B. A Stepwise Huisgen Cycloaddition Process: copper(I)-Catalyzed Regioselective

"Ligation" of Azides and Terminal Alkynes. Angew. Chem. Int. Ed. Engl. ***2002***, 41, *2596–2599.*

(48) *Rodionov, V. O.; Fokin, V. V.; Finn, M. G. Mechanism of the Ligand-Free CuI-Catalyzed Azide-Alkyne Cycloaddition Reaction.* Angew. Chemie ***2005***, 117, *2250–2255.*

(49) *Bock, V. D.; Hiemstra, H.; van Maarseveen, J. H. CuI-Catalyzed Alkyne-Azide "Click" Cycloadditions from a Mechanistic and Synthetic Perspective.* European J. Org. Chem. ***2006***, 2006, *51–68.*

(50) *Kabalah-Amitai, L.; Mayzel, B.; Kauffmann, Y.; Fitch, A. N.; Bloch, L.; Gilbert, P. U. P. a; Pokroy, B. Vaterite Crystals Contain Two Interspersed Crystal Structures.* Science ***2013***, 340, *454–457.*

(51) *Worrell, B. T.; Malik, J. a; Fokin, V. V. Direct Evidence of a Dinuclear Copper Intermediate in Cu(I)-Catalyzed Azide-Alkyne Cycloadditions.* Science ***2013***, 340, *457–460.*

(52) *Binder, W. H.; Sachsenhofer, R. "Click" Chemistry in Polymer and Materials Science.* Macromol. Rapid Commun. ***2007***, 28, *15–54.*

(53) *Lutz, J.-F. 1,3-Dipolar Cycloadditions of Azides and Alkynes: A Universal Ligation Tool in Polymer and Materials Science.* Angew. Chem. Int. Ed. Engl. ***2007***, 46, *1018–1025.*

(54) *Ganesh, V.; Sudhir, V. S.; Kundu, T.; Chandrasekaran, S. 10 Years of Click Chemistry: Synthesis and Applications of Ferrocene-Derived Triazoles.* Chem. Asian J. ***2011***, 6, *2670–2694.*

(55) *Lallana, E.; Sousa-Herves, A.; Fernandez-Trillo, F.; Riguera, R.; Fernandez-Megia, E. Click Chemistry for Drug Delivery Nanosystems.* Pharm. Res. ***2012***, 29*, 1–34.*

(56) *Hein, C.; Liu, X.; Wang, D. Click Chemistry, a Powerful Tool for Pharmaceutical Sciences.* Pharm. Res. ***2008***, 25*, 2216–2230.*

(57) *Lutz, J.-F.; Zarafshani, Z. Efficient Construction of Therapeutics, Bioconjugates, Biomaterials and Bioactive Surfaces Using Azide-Alkyne "Click" Chemistry.* Adv. Drug Deliv. Rev. ***2008***, 60*, 958–970.*

(58) *Campidelli, S.; Sooambar, C.; Lozano Diz, E.; Ehli, C.; Guldi, D. M.; Prato, M. Dendrimer-Functionalized Single-Wall Carbon Nanotubes: Synthesis, Characterization, and Photoinduced Electron Transfer.* J. Am. Chem. Soc. ***2006***, 128*, 12544–12552.*

(59) *Gehan, H.; Fillaud, L.; Felidj, N.; Aubard, J.; Lang, P.; Chehimi, M. M.; Mangeney, C. A General Approach Combining Diazonium Salts and Click Chemistries for Gold Surface Functionalization by Nanoparticle Assemblies.* Langmuir ***2010***, 26*, 3975–3980.*

(60) *Boudou, T.; Crouzier, T.; Ren, K.; Blin, G.; Picart, C. Multiple Functionalities of Polyelectrolyte Multilayer Films: New Biomedical Applications.* Adv. Mater. ***2010***, 22*, 441–467.*

(61) *Ran, Q.; Peng, R.; Liang, C.; Ye, S.; Xian, Y.; Zhang, W.; Jin, L. Direct Electrochemistry of Horseradish Peroxidase Immobilized on Electrografted 4-Ethynylphenyl Film via Click Chemistry.* Anal. Chim. Acta ***2011***, 697*, 27–31.*

(62) *Sohee, P.; Ki-jeong, K.; Hye-Mi, S.; Jeong-O, L.; Hyunju, C. Adsorption of 1,3-Benzodithiolylium Tetrafluoroborate (1,3-BDYT) on the Carbon Nanotubes.* J. Korean Phys. Soc. ***2010***, 57, *1–4.*

(63) *So, H.-M.; Kim, B.-K.; Park, D.-W.; Kim, B. S.; Kim, J.-J.; Kong, K.-J.; Chang, H.; Lee, J.-O. Selective Suppression of Conductance in Metallic Carbon Nanotubes.* J. Am. Chem. Soc. ***2007***, 129, *4866–4867.*

(64) *Gualandi, A.; Emer, E.; Guiteras Capdevila, M.; Cozzi, P. G. Highly Enantioselective A Alkylation of Aldehydes with 1,3-Benzodithiolylium Tetrafluoroborate: A Formal Organocatalytic A Alkylation of Aldehydes by the Carbenium Ion.* Angew. Chem. Int. Ed. Engl. ***2011***, 50, *7842–7846.*

(65) *Blodgett, K. Films Built by Depositing Successive Monomolecular Layers on a Solid Surface.* J. Am. Chem. Soc. ***1935***, 57, *1007–1022.*

(66) *Bendikov, M.; Wudl, F.; Perepichka, D. F. Tetrathiafulvalenes, Oligoacenenes, and Their Buckminsterfullerene Derivatives: The Brick and Mortar of Organic Electronics.* Chem. Rev. ***2004***, 104, *4891–4946.*

(67) *Naraso, N.; Nishida, J.-I.; Ando, S.; Yamaguchi, J.; Itaka, K.; Koinuma, H.; Tada, H.; Tokito, S.; Yamashita, Y. High-Performance Organic Field-Effect Transistors Based on Pi-Extended Tetrathiafulvalene Derivatives.* J. Am. Chem. Soc. ***2005***, 127, *10142–10143.*

(68) *Gao, X.; Wu, W.; Liu, Y.; Qiu, W.; Sun, X.; Yu, G.; Zhu, D. A Facile Synthesis of Linear Benzene-Fused Bis(tetrathiafulvalene) Compounds and Their Application for Organic Field-Effect Transistors.* Chem. Commun. ***2006***, *2750–2752.*

(69) *Raman, C. The Molecular Scattering of Light.* Proc. Indian Acad. Sci. ***1953**, 267–275.*

(70) *Pimenta, M.; Marucci, A.; Empedocles, S.; Bawendi, M.; Hanlon, E.; Rao, A.; Eklund, P.; Smalley, R.; Dresselhaus, G.; Dresselhaus, M. Raman Modes of Metallic Carbon Nanotubes.* Phys. Rev. B. ***1998**,* 58*, 16016–16019.*

(71) *Jorio, a; Pimenta, M. a; Filho, a G. S.; Saito, R.; Dresselhaus, G.; Dresselhaus, M. S. Characterizing Carbon Nanotube Samples with Resonance Raman Scattering.* New J. Phys. ***2003**,* 5*, 139–139.*

(72) *Burghard, M. Electronic and Vibrational Properties of Chemically Modified Single-Wall Carbon Nanotubes.* Surf. Sci. Rep. ***2005**,* 58*, 1–109.*

(73) *Graupner, R. Raman Spectroscopy of Covalently Functionalized Single-wall Carbon Nanotubes.* J. Raman Spectrosc. ***2007**,* 38*, 673–683.*

(74) *Fantini, C.; Pimenta, M. a.; Strano, M. S. Two-Phonon Combination Raman Modes in Covalently Functionalized Single-Wall Carbon Nanotubes.* J. Phys. Chem. C ***2008**,* 112*, 13150–13155.*

(75) *Saito, R.; Hofmann, M.; Dresselhaus, G.; Jorio, A. Advances in Physics Raman Spectroscopy of Graphene and Carbon Nanotubes.* Adv. Phys. ***2011**, 37–41.*

(76) *Dresselhaus, M.; Dresselhaus, G. Raman Spectroscopy on Isolated Single Wall Carbon Nanotubes.* Carbon N. Y. ***2002**,* 40*, 2043–2061.*

(77) Strano, M. S. Probing Chiral Selective Reactions Using a Revised Kataura Plot for the Interpretation of Single-Walled Carbon Nanotube Spectroscopy. J. Am. Chem. Soc. ***2003****,* 125*, 16148–16153.*

(78) Sharma, R.; Baik, J. H.; Perera, C. J.; Strano, M. S. Anomalously Large Reactivity of Single Graphene Layers and Edges toward Electron Transfer Chemistries. Nano Lett. ***2010****,* 10*, 398–405.*

(79) Galvani, L. Viribus Electricitatis in Motu Musculari*; 1791.*

(80) Marcus, R. A. Electrostatic Free Energy and Other Properties of States Having Nonequilibrium Polarization. I. J. Chem. Phys. ***1956****,* 24*, 979–989.*

(81) Marcus, R. A. On the Theory of Oxidation-Reduction Reactions Involving Electron Transfer. II. Applications to Data on the Rates of Isotopic Exchange Reactions. J. Chem. Phys. ***1957****,* 26*, 867–871.*

(82) Marcus, R. A. On the Theory of Oxidation-Reduction Reactions Involving Electron Transfer. III. Applications to Data on the Rates of Organic Redox Reactions. J. Chem. Phys. ***1957****,* 26*, 872–877.*

(83) Marcus, R. A. Exchange Reactions and Electron Transfer Reactions Including Isotopic Exchange. Theory of Oxidation-Reduction Reactions Involving Electron Transfer. Part 4.—A. Discuss. Faraday Soc. ***1960****, 21–31.*

(84) Marcus, R. A. On the Theory of Oxidation-Reduction Reduction Reactions Involving Electron Transfer. V. Comparision and Properties of Electrochemical and Rate Constants. J. Phys. Chem. ***1963****,* 67*, 853–857.*

(85) *Marcus, R. A. On the Theory of Electron-Transfer Reactions. VI. Unified Treatment for Homogeneous and Electrode Reactions.* J. Chem. Phys. ***1965***, 43, *679–701.*

(86) *Evans, D. .; O'Connell, M.; Petersen, R. A.; Kelly, M. J. Cyclic Voltammetry.* J. Chem. Educ. ***1983***, 60, *290–293.*

(87) *Baughman, R. H.; Zakhidov, A. a; de Heer, W. a. Carbon Nanotubes--the Route toward Applications.* Science ***2002***, 297, *787–792.*

(88) *Pénicaud, A.; Dragin, F.; Pécastaings, G.; He, M.; Anglaret, E. Concentrated Solutions of Individualized Single Walled Carbon Nanotubes.* Carbon N. Y. ***2014***, 67, *360–367.*

(89) *Petit, P.; Mathis, C.; Journet, C.; Bernier, P. Tuning and Monitoring the Electronic Structure of Carbon Nanotubes.* Chem. Phys. Lett. ***1999***, 305, *370–374.*

(90) *Paolucci, D.; Franco, M. M.; Iurlo, M.; Marcaccio, M.; Prato, M.; Zerbetto, F.; Pénicaud, A.; Paolucci, F. Singling out the Electrochemistry of Individual Single-Walled Carbon Nanotubes in Solution.* J. Am. Chem. Soc. ***2008***, 130, *7393–7399.*

(91) *Chen, E. H.; Walter, S. R.; Nguyen, S. T.; Geiger, F. M. Arylsilanated SiOx Surfaces for Mild and Simple Two-Step Click Functionalization with Small Molecules and Oligonucleotides.* J. Phys. Chem. C ***2012***, 116, *19886–19892.*

(92) *Yamakoshi, H.; Dodo, K.; Palonpon, A.; Ando, J.; Fujita, K.; Kawata, S.; Sodeoka, M. Alkyne-Tag Raman Imaging for Visualization of Mobile*

Small Molecules in Live Cells. J. Am. Chem. Soc. ***2012***, 134, *20681–20689.*

(93) Henstridge, M. C.; Batchelor-McAuley, C.; Gusmão, R.; Compton, R. G. Marcus–Hush–Chidsey Theory of Electron Transfer to and from Species Bound at a Non-Uniform Electrode Surface: Theory and Experiment. Chem. Phys. Lett. ***2011***, 517, *108–112.*

(94) Peng, X.; Wong, S. S. Functional Covalent Chemistry of Carbon Nanotube Surfaces. Adv. Mater. ***2009***, 21, *625–642.*

(95) Evrard, D.; Lambert, F.; Policar, C.; Balland, V.; Limoges, B. Electrochemical Functionalization of Carbon Surfaces by Aromatic Azide or Alkyne Molecules: A Versatile Platform for Click Chemistry. Chem. Eur. J. ***2008***, 14, *9286–9291.*

(96) Hayat, A.; Marty, J.-L.; Radi, A.-E. Novel Amperometric Hydrogen Peroxide Biosensor Based on Horseradish Peroxidase Azide Covalently Immobilized on Ethynyl-Modified Screen-Printed Carbon Electrode via Click Chemistry. Electroanalysis ***2012***, 24, *1446–1452.*

(97) Cosnier, S.; Lambert, F.; Stoytcheva, M. A Composite Clay Glucose Biosensor Based on an Electrically Connected HRP. Electroanalysis ***2000***, 12, *356–360.*

(98) Shan, D.; Cosnier, S.; Mousty, C. HRP/[Zn-Cr-ABTS] Redox Clay-Based Biosensor: Design and Optimization for Cyanide Detection. Biosens. Bioelectron. ***2004***, 20, *390–396.*

(99) *Tertis, M.; Florea, A.; Sandulescu, R.; Cristea, C. Carbon Based Electrodes Modified with Horseradish Peroxidase Immobilized in Conducting Polymers for Acetaminophen Analysis.* Sensors (Basel). ***2013***, 13, *4841–4854.*

(100) *Shul'ga, Y. Core Level X-Ray Photoelectron Spectroscopy Study of a Series of Crystalline Fullerene-Organic Donor Compounds.* Phys. LOW- … ***1997***, *103–110.*

(101) *Nishida, J.; Ando, S.; Yamaguchi, J.; Itaka, K.; Tada, H.; Tokito, S. Supporting Information High Performance Organic Field-Effect Transistors Based on Pi -Extended Tetrathiafulvalene Derivatives.* Mater. Struct.

(102) *Brillante, A.; Bilotti, I.; Della Valle, R. G.; Venuti, E.; Milita, S.; Dionigi, C.; Borgatti, F.; Lazar, A. N.; Biscarini, F.; Mas-Torrent, M.; et al. The Four Polymorphic Modifications of the Semiconductor Dibenzo-Tetrathiafulvalene.* Cryst.Eng.Comm. ***2008***, 10, *1899–1909.*

(103) *Mas-Torrent, M.; Hadley, P.; Bromley, S. T.; Crivillers, N.; Veciana, J.; Rovira, C. Single-Crystal Organic Field-Effect Transistors Based on Dibenzo-Tetrathiafulvalene.* Appl. Phys. Lett. ***2005***, 86, *012110.*

(104) *Mas-Torrent, M.; Masirek, S.; Hadley, P.; Crivillers, N.; Oxtoby, N. S.; Reuter, P.; Veciana, J.; Rovira, C.; Tracz, a. Organic Field-Effect Transistors (OFETs) of Highly Oriented Films of Dithiophene-Tetrathiafulvalene Prepared by Zone Casting.* Org. Electron. ***2008***, 9, *143–148.*

(105) *Konarev, D. V. New Complexes of Fullerenes C60 and C70 with Organic Donor DBTTF :synthesis, Some Properties and Crystal Structure of DBTTF C60 C6H6 (DBTTF=dibenzotetrathiafulvalene).* ***1998****,* 92*, 1–6.*

(106) *Saad, A.; Jeannin, O.; Fourmigué, M. Helical Organization of Chiral Binaphthyl Tetrathiafulvalene Primary Amides through Hydrogen Bonding Interactions.* Cryst.Eng.Comm. ***2010****,* 12*, 3866–3874.*

(107) *Matsumoto, R.; Hoshina, Y.; Akuzawa, N. Thermoelectric Properties and Electrical Transport of Graphite Intercalation Compounds.* Mater. Trans. ***2009****,* 50*, 1607–1611.*

(108) *Pumera, M. Graphene-Based Nanomaterials and Their Electrochemistry.* Chem. Soc. Rev. ***2010****,* 39*, 4146–4157.*

(109) *Collman, J. P.; Devaraj, N. K.; Chidsey, C. E. D. "Clicking" Functionality onto Electrode Surfaces.* Langmuir ***2004****,* 20*, 1051–1053.*

(110) *Manuscript, A. NIH Public Access.* ***2008****,* 72*, 2794–2802.*

(111) *Lü, P.; Feng, Y.; Zhang, X.; Li, Y.; Feng, W. Recent Progresses in Application of Functionalized Graphene Sheets.* Sci. China Technol. Sci. ***2010****,* 53*, 2311–2319.*

(112) *Quintana, M.; Spyrou, K.; Grzelczak, M.; Browne, W. R.; Rudolf, P.; Prato, M. Functionalization of Graphene.* ***2010****,* 4*, 3527–3533.*

SUMMARY

Since the discovery of the new allotropes of carbon, modified carbon nanotubes and graphene surfaces have been proposed for several technological applications. Carbon nanotubes and graphene have been already proposed as excellent candidates to improve (bio) sensor performances as they display remarkable electronic properties and the ability to act as individual nanoelectrodes, display an excellent low-dimensional charge carrier transport, and promote surface electrocatalysis. Films are made from such nanomaterials that show chemical and electrochemical inertness, physical robustness as well as adjustable transparency and optical features. Their high surface area and wide versatility in functionalization can be exploited to covalently bind biomolecules, enzymes, antibodies and DNA fragments onto the nanostructured surface.

The mild and spontaneous dissolution of SWCNTs or GICs in polar aprotic solvents without any sonication step allows the preparation of transparent conductive films made only and exclusively of SWCNTs (and graphene in the case of GIC solutions). Their deposition as a continuous film on polystyrene or any other substrate makes them handle and allows their use as electrodes.

This thesis describes the electrochemical surface modification of SWCNT and graphene transparent hybrid films by two routes (i) the electrografting of aryl diazonium salts, and (ii) the electrophylic addition of BDYT moieties. Their post-modification by click-chemistry reactions finally leads to the immobilization at the electrode surface of any desired functional group such as redox probes/shuttles (e.g., a ferrocenyl group) or catalytic moieties (e.g., an enzyme).

Summary

In Chapter 1, an introduction of SWCNTs, graphene, and carbon-related materials is described. The chemical and electrochemical procedures used for the surface modification of the carbon/graphene films with diazonium salts, is explained. Furthermore, a new type of functionalization, namely the electrophylic addition of BDYT, capable in principle of introducing a single carbon atom linker onto the nanocarbon surface, has been introduced.

In Chapter 2 the characterization techniques used in this work have been described. Raman spectroscopy is described as an important technique for SWCNTs and graphene characterization; especially for characterizing the carbonaceous surface before and after electrochemical modification.

In Chapter 3 the preparation and characterization of SWCNT-based electrodes starting from a solution of pristine SWCNTs is described. Films were characterized by AFM and SEM showing clean and homogeneous surfaces. Conductivity measurements showed interesting results for both films. Raman spectrum of HiPCO-based electrode showed small intensities of the D-band in relation to the G-band, characteristic of ordinate sp^2 systems.

In Chapter 4, the electrochemical surface modification of SWCNT films is described. Two routes have been investigated and the resulting modified surfaces were in both cases fully characterized. Both routes lead to the creation of novel covalent carbon-carbon bonds between the tube surface and the anchored moiety. In the first case, the well-known electrochemical grafting of aryl diazonium salts was exploited to anchor functional groups onto the SWCNT film surface suitable for their subsequent click-reaction with ferrocene-containing moieties.

In the second case, the electrophylic addition of electrogenerated BDYT radicals was investigated for the first time.

The aryl-modified SWCNT surface was successfully reacted with an enzyme (HRP), to prove the viability of bioconjugation routes with the present modified nanocarbon surfaces.

In Chapter 5 the electrochemical surface modification of graphene films produced from GIC solutions are described. Earlier GIC synthesis, dissolution and deposition are described at the beginning of the chapter. The electrochemical surface modification of graphene films[f], following the two routes explained for the electrochemical surface modification of SWCNT-based electrodes, is finally described.

[f] Prepared by Y, Wang, CRPP-CNRS, Pessac.